Topological Solitons of the Nonlinear Dirac Equation in 2+1 Dimensional Space Time

Realeboga Dikole

supervised by

Prof. Igor Barashenkov

Thesis presented for the degree of
Master of Science in Applied Mathematics

Department of Mathematics and Applied Mathematics
University of Cape Town
South Africa

Contents

List of Figures

Plagiarism declaration

I, Realeboga Gratitude Dikole , hereby declare that the work on which this thesis is based is my original work (except where acknowledgements indicate otherwise) and that neither the whole work nor any part of it has been, is being, or is to be submitted for another degree in this or any other university. I authorise the University to reproduce for the purpose of research either the whole or any portion of the contents in any manner whatsoever.

Signature: Dikole R.G.

Abstract

The work of this thesis is a presentation of nonlinear Dirac-type models with the primary focus being on planar, $(2+1)$ dimensional nonlinear Dirac models.We study a $(2+1)$ dimensional extension of the $(2+0)$ dimensional reduction the complex sine-Gordon. This is a *tachyonic* nonlinear Dirac equation whose linear part can be reduced to the imaginary mass Klein-Gordon equation. Although this model is *tachyonic* it can be restored into a real and non-hypothetical version by considering it in nonvanishing backgrounds. We investigate the stability of the single vortex solution by considering perturbation about the single vortex solution. Perturbations include the radially symmetric perturbations ($m = 0$) and angular perturbations ($m \in \{\pm 1, \pm 2\}$). The single vortex was found to be stable for both the radially symmetric and angular perturbations $m = \{0, \pm 1, \pm 2\}$, with the real part of the eigenvalues having a negligible nonzero real part of order 10^{-3}. The eigenvalues presented were obtained by use of the sine series expansion and Chebyshev spectral method, where the author is the first to present this work. The Chebyshev spectral method was found to outperform the sine series expansion in terms of computation times. However, the drawback of Chebyshev differentiation matrices is that they contain spurious eigenvalues that grow proportional to the number of modes N. We also present the planar Soler model, both *tachyonic* and *tardyonic* and find that the planar *tachyonic* Soler model does not admit stationary vortex solutions. On the other hand, the *tardyonic* Soler model possesses stable vortex solutions as shown by Cuevas-Maraver *et al.* We also study the numerical solution of another planar nonlinear Dirac model i.e. the nonlinear Dirac equation with Kerr nonlinearity. The $(2+1)$ dimensional nonlinear Dirac equation with Kerr nonlinearity admits stationary vortex solutions as was shown in the work of Smirnova *et al.* Moreover, the $(2+1)$ dimensional nonlinear Dirac equation with Kerr nonlinearity supports topological edge states.

Acknowledgements

The work of in this thesis would never have been possible with our the patience and incredible supervision of prof. Igor Barashenkov. I want to express my gratitude to him, Dr. Alexeeva for her input and for availing herself to all the consultations I had with her regarding the numerical work done in this thesis. I want to also express my gratitude to Mr. Alain Dika for being and warm and welcoming office companion, and Mr. Themba Malusi for offering his numerical assistance in some of the work presented in this thesis. Lastly, wish to thank the *Council for Scientific and Industrial Research (CSIR)* for all the financial aid they have provided since the start of my undergraduate studies.

Chapter 1

Introduction

A common practice in physics is such that for a given Hamilton admitting planar wave solutions, the Hamiltonian must be associated with a dispersion relation whose roots are always real. This is to preserve the physicality of whatever model is being considered. By "physicality" it is meant that the model is physical rather than hypothetical. In recent years, however, there has been an interest in such models whose zero background dispersion relation is associated with complex roots. One such model is the famous ϕ^4 theory with a dispersion relation of the form $\omega^2 = -k^2 + m^2$, where ω is the angular frequency, k is the wave number and m is the mass. This dispersion relation admits complex roots at the moment when $m \neq k$. However, the physicality of this model can be recovered by considering the model over a non-vanishing constant background. In this case of the ϕ^4 theory, this is done by considering small excitations over the zero vacuum solution m/λ.

It is worth mentioning that the ϕ^4 partial differential equation is associated with the imaginary mass (i.e. $m \to im$) Klein-Gordon equation with an additional nonlinear correction term. The linear Klein-Gordon equation, however, when considered by itself factorises into a form of the Dirac equation formerly known as the *tachyonic* Dirac equation. As one might expect, the *tachyonic* Dirac equation is also associated with a dispersion relation whose roots are complex when considered over a zero background. In this thesis, we shall consider such a Dirac equation which is a $(2+1)$ dimensional extension of the spinor version of the $(2+0)$ dimensional complex sine-Gordon equation. We will show that when the $(2+1)$ dimensional extension of the $(2+0)$ dimensional complex sine-Gordon equation is considered over a non-vanishing background its dispersion relation has real roots for all values of the wave number k. The $(2+0)$ dimensional complex sine-Gordon equation was first considered in [2] and was shown in [3, 4] to admit topological vortex solutions. The stability of these vortex solutions, however, was not presented. In this thesis, we shall consider these stationary vortex solutions and study their stability, with the primary focus being on the single vortex solution. The Dirac equation in two spatial dimensions is applicable in two-dimensional lattice structures like graphene. This connection shall be demonstrated shortly.

The Dirac equation has gained much attention recently due to its connection with graphene [1] and a newly discovered class of solids known as topological insulators. These are materials which exhibit special scattering resisting states [5] on the surfaces called topological edge

states [5, 6]. Topological edge states and realisable in condensed matter electronic systems, and photonic crystals in optics [7, 8]. Edge states have been predicted and realised in a large number of photonic systems including arrays of coupled optical resonators, helical waveguide arrays and gyromagnetic photonic crystals [5]. Topological edge states bear the name "topology" because they possess topological invariants. Topological invariants are quantities that remain unaffected by continuous deformation of an object. Examples of topological invariants in lattice models include the Berry phase and Chern number. Topological invariants can be used to describe band structures if certain periodic crystalline materials [5]– deformations in the particular context are such that all symmetries are preserved and band gaps remain open.

The simplest model that exhibits topological properties is the Su-Schrieffer-Heeger mode which describes a one-dimensional dimer chain with alternating strong and weak nearest-neighbour couplings $\kappa_{1,2}$. The model was introduced by Su, Schrieffer and Heeger to study soliton formation in polyacetylene [9]. In the language of the second quantisation, the Su-Schrieffer-Heeger model takes the form

$$\hat{H}_{\mathrm{SSH}} = -\sum_{n=1}^{N} \left(\kappa_1 \hat{a}_n^\dagger \hat{b}_n^\dagger + \kappa_2 \hat{a}_{n+1}^\dagger \hat{b}_n^\dagger + h.c. \right), \tag{1.1}$$

where $\hat{a}_n^\dagger$, $\hat{b}_n^\dagger$, $\hat{a}_n$ and $\hat{b}_n$ are creation and annihilation operators at A or B sublattices of the n-th unit cell. The Fourier transformation of (1.1) is a single-particle Bloch Hamiltonian in momentum space [10]

$$\hat{H}_{\mathrm{SSH}} = -\left(\kappa_1 + \kappa_2 \cos(kd)\right) \sigma_1 - \kappa_2 \sin(kd)\sigma_2, \tag{1.2}$$

where $\sigma_{1,2}$ are the Pauli spin matrices and d is the lattice spacing. This Hamiltonian (1.2) reduces to the one dimensional Dirac Hamiltonian in the vicinity of the Brillouin zone edge $kd = \pi$ [10]. By Brillouin zone it is meant the primitive cell in reciprocal space i.e. the Fourier transform of real space. The two energy bands $\mathscr{E}_\pm$ are separated by a gap when $\kappa_1 \neq \kappa_2$ with a band closure occurring at $\kappa_1 = \kappa_2$ [5, 11]. Edges states of the Su-Schrieffer-Heeger model occur in the middle of the bandgap when coupling is weak, that is $\kappa_2 < \kappa_1$. These edge states have a localisation in one of the sublattices and decay exponentially far away from the edge of the lattice. The edge states are topologically protected in the sense that their frequency is fixed to zero and they cannot be destroyed by chiral symmetry-preserving perturbations. Edge states also emerge in two-dimensional lattices such as hexagonal lattices, which are two-dimensional generalisations of the Su-Schrieffer-Heeger lattices. These include photonic graphene, staggered graphene and the Haldane model. Under consideration of nonlinear effects like the Kerr nonlinearity, for example, these planar models can exhibit topological solitons and vortices, with photonic graphene being the classic example. In what follows we study closely the tight-binding approximation of single-layer graphene.

1.1 Monolayer graphene crystal structure

Monolayer graphene is composed of carbon atoms with electrons organised into a hexagonal (honeycomb) lattice structure in two dimensions. The hexagonal structure can be seen as a

combination of triangular sub-lattices called A sub-lattice and B sub-lattice with a basis of two atoms per unit cell. The lattice vectors of the hexagonal lattice are

$$\mathbf{a}_1 = \frac{a}{2}\left(3, \sqrt{3}\right), \qquad \mathbf{a}_2 = \frac{a}{2}\left(3, -\sqrt{3}\right), \tag{1.3}$$

with $a = |\mathbf{a}_1|^2 = |\mathbf{a}_2|^2$ being the lattice constant, that is a measure of the atomic distance which equals 1.42Å for carbon [1, 12, 13].

The corresponding reciprocal lattice vectors are

$$\mathbf{b}_1 = \frac{2\pi}{3a}\left(1, \sqrt{3}\right), \qquad \mathbf{b}_2 = \frac{2\pi}{3a}\left(1, -\sqrt{3}\right), \tag{1.4}$$

where the real space vectors $\mathbf{a}_1$, $\mathbf{a}_2$ and the reciprocal space vectors $\mathbf{b}_1$ and $\mathbf{b}_2$ satisfy the

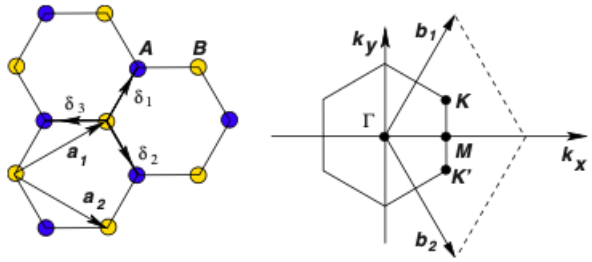

Figure 1.1: The graphene hexagonal lattice on the left with its Brillouin zone on the right. The graphene lattice is made up of two triangular sub-lattices $\mathbf{a}_1$ and $\mathbf{a}_2$ which are the lattice unit vectors. The three vectors $\boldsymbol{\delta}_1, \boldsymbol{\delta}_2, \boldsymbol{\delta}_3$ are the nearest neighbour vectors. The reciprocal lattice vectors $\mathbf{b}_1$, $\mathbf{b}_2$ are shown with points K and K', which locate the Dirac cones. The points $\mathbf{\Gamma} = (0, 0)$ and $\mathbf{M} = (2\pi/\sqrt{3}a, 0)$ are the symmetry points in the Brillouin zone. This image is obtained from Ref. [1].

relation

$$\mathbf{a}_i \cdot \mathbf{b}_j = 2\pi\delta_{ij}. \tag{1.5}$$

Each carbon atom in the lattice has three nearest neighbours and six other second-nearest neighbours.

The three nearest neighbour vectors in real space are

$$\boldsymbol{\delta}_1 = \frac{a}{2}\left(1, \sqrt{3}\right), \qquad \boldsymbol{\delta}_2 = \frac{a}{2}\left(1, -\sqrt{3}\right), \qquad \boldsymbol{\delta}_3 = -a(1, 0), \tag{1.6}$$

the other remaining six second-nearest neighbour vectors are $\boldsymbol{\delta}'_1 = \pm\mathbf{a}_1$, $\boldsymbol{\delta}'_2 = \pm\mathbf{a}_2$, $\boldsymbol{\delta}'_3 = \pm(\mathbf{a}_2 - \mathbf{a}_1)$. The points $\mathbf{K}$ and $\mathbf{K}'$ on the Brillouin zone shown in Fig. 1.1 are known as the Dirac points since graphene can be modelled by the $2+1$-dimensional Dirac equation exactly at those points. Their position is k-space are given by

$$\mathbf{K} = \left(\frac{2\pi}{3a}, \frac{2\pi}{3\sqrt{3}a}\right), \qquad \mathbf{K}' = \left(\frac{2\pi}{3a}, -\frac{2\pi}{3\sqrt{3}a}\right). \tag{1.7}$$

A single carbon atom consists of six electrons with an electronic configuration of $1s^2 2s^2 2p^2$, two of the electrons in this configuration are core and the remaining four are valence electrons. The valence electrons occupy the $2s$, $2p_x$, $2p_y$ and $2p_z$ orbitals [12, 13]. Graphene orbitals are sp^2 hybridized, that is the $2s$ orbital can mix with the $2p_x$ and $2p_y$ orbitals to generate three new orbitals per atom (each with one electron) lying in the graphene plane at 120° to each other [12, 13]. The overlap of the sp^2 orbitals gives rise to strong σ and σ^* bonds; the σ bonds are located on the plane at an angle of 120° to each other. These bonds (σ) make up the hexagonal structure of graphene. The remaining p_z orbitals are perpendicular to the overlap plane and give rise to the π and π^* bonds [12, 13]. The electronic properties of graphene are attributable to the π bonding (valence band) and π^* bonding (conduction band) due to the overlap of the p_z energy levels [12, 13].

1.2 General derivation of the electronic dispersion

To begin with the tight-binding description of graphene we assume that the system possesses translational invariance. This means that we can write the atomic wave function as a linear superposition of Bloch wave functions [12, 14]

$$\Psi_j(\mathbf{k},\mathbf{r}) = \sum_{l=1}^{n} \alpha_{j,l}(\mathbf{k})\Phi_l(\mathbf{k},\mathbf{r}), \tag{1.8}$$

where

$$\Phi_j(\mathbf{k},\mathbf{r}) = \frac{1}{\sqrt{N}} \sum_{i=1}^{N} e^{i\mathbf{k}\mathbf{R}_{j,i}} u_j(\mathbf{r}-\mathbf{R}_{j,i}) \tag{1.9}$$

are the Bloch functions. The Bloch functions are a combination of the Wannier functions u_j (atomic orbitals), with the index $j = 1, 2, \ldots, n$, $\mathbf{r}$ is the position vector, $\mathbf{k}$ is the wave vector and $\mathbf{R}_{j,i}$ is the position of the j-th orbital in the i-th unit cell. The atomic wave functions satisfy the equation

$$\mathcal{H}\Psi_j(\mathbf{k},\mathbf{r}) = \mathscr{E}_j(\mathbf{k})\Psi(\mathbf{k},\mathbf{r}), \tag{1.10}$$

where $\mathcal{H}$ is the Hamiltonian. The expression for $\mathscr{E}_j(\mathbf{k})$ can be found by acting with $\Psi_j^*(\mathbf{k},\mathbf{r})$ from the left and integrating with respect to $d\mathbf{r}$

$$\int d\mathbf{r}\ \Psi_j^*(\mathbf{k},\mathbf{r})\mathcal{H}\Psi_j(\mathbf{k},\mathbf{r}) - \mathscr{E}_j(\mathbf{k}) \int d\mathbf{r}\ \Psi_j^*(\mathbf{k},\mathbf{r})\Psi_j(\mathbf{k},\mathbf{r}) = 0.$$

Therefore the energy eigenvalue expression of the j-th band is

$$\mathscr{E}_j(\mathbf{k}) = \frac{\int d\mathbf{r}\ \Psi_j^*(\mathbf{k},\mathbf{r})\mathcal{H}\Psi_j(\mathbf{k},\mathbf{r})}{\int d\mathbf{r}\ \Psi_j^*(\mathbf{k},\mathbf{r})\Psi_j(\mathbf{k},\mathbf{r})}. \tag{1.11}$$

Substituting (1.9) into (1.11) gives

$$\mathscr{E}_j(\mathbf{k}) = \frac{\sum_{i,l}^{n} \alpha_{ji}^*\alpha_{jl} \int d\mathbf{r}\ \Phi_i^*\mathcal{H}\Phi_l}{\sum_{i,l}^{*} \alpha_{ji}^*\alpha_{jl} \int d\mathbf{r}\ \Phi_i^*\Phi_l}$$

$$\mathscr{E}_j(\mathbf{k}) = \frac{\sum_{i,l}^{n} H_{il}\alpha_{ji}^{*}\alpha_{jl}}{\sum_{i,l}^{n} \zeta_{il}\alpha_{ji}^{*}\alpha_{jl}}, \tag{1.12}$$

with

$$H_{il} = \int d\mathbf{r}\ \Phi_i^{*}\mathcal{H}\Phi_l, \qquad \zeta_{il} = \int d\mathbf{r}\ \Phi_i^{*}\Phi_l, \tag{1.13}$$

H_{il} and ζ_{il} are called the transfer integral and overlap integral matrices respectively.

The goal here is to find a simpler expression for $\mathscr{E}_j$, we do so by minimising (1.12) with respect to the coefficient α_{jm}^{*} by calculating the following derivative

$$\frac{\partial \mathscr{E}_j}{\partial \alpha_{jm}^{*}} = \frac{\sum_{l}^{n} H_{ml}\alpha_{jl}}{\sum_{i,l}^{n} \zeta_{il}\alpha_{ji}^{*}\alpha_{jl}} - \frac{\sum_{i,l}^{n} H_{il}\alpha_{ji}^{*}\alpha_{jl}\sum_{l}^{n}\zeta_{ml}\alpha_{jl}}{\left(\sum_{i,l}^{n} \zeta_{il}\alpha_{ji}^{*}\alpha_{jl}\right)^2}.$$

Identifying $\mathscr{E}_j$ in the second term and setting $\partial\mathscr{E}_j/\partial\alpha_{jm}^{*} = 0$ we find

$$\sum_{l=1}^{n} H_{ml}\alpha_{jl} = \mathscr{E}_j \sum_{l=1}^{n} \zeta_{ml}\alpha_{jl}. \tag{1.14}$$

Upon fixing the orbital index j to a particular number, equation (1.14) can be written as

$$H\psi_i = \mathscr{E}_j \zeta \psi_j, \tag{1.15}$$

where

$$H = \begin{pmatrix} H_{11} & H_{12} & \cdots & H_{1n} \\ H_{21} & H_{22} & \cdots & H_{2n} \\ \vdots & \vdots & \ddots & \vdots \\ H_{n1} & H_{n2} & \cdots & H_{nn} \end{pmatrix}, \qquad \zeta = \begin{pmatrix} \zeta_{11} & \zeta_{12} & \cdots & \zeta_{1n} \\ \zeta_{21} & \zeta_{22} & \cdots & \zeta_{2n} \\ \vdots & \vdots & \ddots & \vdots \\ \zeta_{n1} & \zeta_{n2} & \cdots & \zeta_{nn} \end{pmatrix}, \qquad \psi_j = \begin{pmatrix} \alpha_{j1} \\ \alpha_{j2} \\ \vdots \\ \alpha_{jn} \end{pmatrix}. \tag{1.16}$$

The energy eigenvalues are determined by solving the equation

$$\det(H - \mathscr{E}_j\zeta) = 0, \tag{1.17}$$

assuming that the transfer integral matrix H and the overlap integral matrix S are both known.

1.3 Monolayer graphene tight-binding model in the first quantization

We employ the tight-binding model from section 1.2 above to monolayer (single layer) graphene. The aim is to calculate explicitly the elements of the transfer integral matrix H and the overlap integral matrix ζ in order to find the dispersion relation of monolayer graphene via equation (1.17) and show the connection of the graphene tight binding Hamiltonian with the $(2+1)$-dimensional Dirac equation. The dynamics of electrons at the Dirac points in the Brillouin zone is said to be described by the massless $(2+1)$-dimensional Dirac equation exactly. We begin first by approximating the low energy bands of monolayer graphene and then derive Dirac-like Hamiltonian of massless quasiparticles.

1.3.1 Off-diagonal matrix of the transfer and overlap integral matrices

The two atoms per unit cell in the graphene lattice imply that $n = 2$ in (1.8), that is, the model consists two Bloch functions. We replace orbital index $j = 1$ with $j = A$, and $j = 2$ with $j = B$ for simplicity. Substituting the expression of the Bloch functions (1.9) into the transfer integral matrix (1.13) we can write the off diagonal elements of H as [12, 14]

$$H_{AB} = \frac{1}{N}\sum_{i=1}^{N}\sum_{l=1}^{N} e^{i\mathbf{k}\cdot(\mathbf{R}_{B,l}-\mathbf{R}_{A,i})}\int d\mathbf{r}\; u_A^*(\mathbf{r}-\mathbf{R}_{A,i})\mathcal{H}u_B(\mathbf{r}-\mathbf{R}_{B,l}), \tag{1.18}$$

where $\mathbf{k} = (k_x, k_y)$. Equation (1.18) describes the hopping (or tunneling) of electrons between the A and B sub-lattices. We sum over all the A sites in the lattice, (i.e. $i = 1, \ldots, N$) at position $\mathbf{R}_{A,i}$ and all the B sites ($l = 1, \ldots, N$) at positions $\mathbf{R}_{B,l}$. The off-diagonal entries of the transfer integral are assumed to only come from the hopping between nearest neighbours in the lattice. Turning our attention to a single atom in Fig. 1.1 by fixing the index i we can see that a single atom is surrounded by three neighbouring atoms labeled $\boldsymbol{\delta}_1$, $\boldsymbol{\delta}_2$ and $\boldsymbol{\delta}_3$. This means that the index $l = 1, \ldots, 3$. With this in mind we can write the off-diagonal elements of H as nearest neighbour contribution in the following way

$$H_{AB} \approx \frac{1}{N}\sum_{i=1}^{N}\sum_{l=1}^{3} e^{i\mathbf{k}\cdot(\mathbf{R}_{B,l}-\mathbf{R}_{A,i})}\int d\mathbf{r}\; u_A^*(\mathbf{r}-\mathbf{R}_{A,i})\mathcal{H}u_B(\mathbf{r}-\mathbf{R}_{B,l}). \tag{1.19}$$

We also take the integral in (1.19) which is the transfer integral matrix between nearest neighbour atoms to be independent of indices, i.e. it is the same for all neighbouring pairs. This integral can be set equal to a parameter t. It is common to set $\gamma_0 = t$ since t is a negative quantity, that is

$$\gamma_0 = -\int d\mathbf{r}\; u_A^*(\mathbf{r}-\mathbf{R}_{A,i})\mathcal{H}u_B(\mathbf{r}-\mathbf{R}_{B,l}). \tag{1.20}$$

We can now write H_{AB} as

$$\begin{aligned} H_{AB} &\approx -\frac{1}{N}\sum_{i=1}^{N}\sum_{l=1}^{3} e^{i\mathbf{k}\cdot(\mathbf{R}_{B,l}-\mathbf{R}_{A,i})}\gamma_0, \\ &= -\frac{\gamma_0}{N}\sum_{i=1}^{N}\sum_{l=1}^{3} e^{i\mathbf{k}\cdot\boldsymbol{\delta}_l}, \end{aligned}$$

where $\boldsymbol{\delta}_l = \mathbf{R}_{B,l} - \mathbf{R}_{A,i}$ is the position vector of an atom at $\mathbf{R}_{B,l}$ relative to another atom at $\mathbf{R}_{A,i}$. These are nothing but the nearest neighbour vectors given in (1.6). We can simplify H_{AB} as follows

$$H_{AB} \approx -\gamma_0\varphi(\mathbf{k}), \tag{1.21}$$

where

$$\varphi(\mathbf{k}) = \sum_{l=1}^{3} e^{i\mathbf{k}\cdot\boldsymbol{\delta}_l}. \tag{1.22}$$

It is useful to simplify (1.22) as follows

$$\varphi(\mathbf{k}) = e^{-ik_x a} + \left(e^{ik_y\sqrt{3}a/2} + e^{-ik_y\sqrt{3}a/2}\right) e^{ik_x a/2}$$

$$\varphi(\mathbf{k}) = e^{-ik_x a} + 2\cos\left(\frac{\sqrt{3}k_y a}{2}\right) e^{ik_x a/2}. \tag{1.23}$$

The second off-diagonal element H_{BA} of the transfer integral matrix can also be approximated with the main difference being that the position vector of an atom at $\mathbf{R}_{A,i}$ relative to another atom at $\mathbf{R}_{B,l}$ is $\boldsymbol{\delta}_l = \mathbf{R}_{A,i} - \mathbf{R}_{B,l}$. Therefore H_{BA} becomes

$$H_{BA} \approx -\gamma_0 \varphi^*(\mathbf{k}), \tag{1.24}$$

i.e. the complex conjugation of H_{AB}.

Similarly, the off-diagonal entries of the overlap integral matrix ζ_{AB} can be approximated as follows [12, 14]

$$\zeta_{AB} = \frac{1}{N}\sum_{i=1}^{N}\sum_{l=1}^{N} e^{i\mathbf{k}\cdot(\mathbf{R}_{B,l}-\mathbf{R}_{A,i})} \int d\mathbf{r}\; u_A^*(\mathbf{r}-\mathbf{R}_{A,i}) u_B(\mathbf{r}-\mathbf{R}_{B,l}) \tag{1.25}$$

$$\approx \frac{1}{N}\sum_{i=1}^{N}\sum_{l=1}^{3} e^{i\mathbf{k}\cdot(\mathbf{R}_{B,l}-\mathbf{R}_{A,i})} \int d\mathbf{r}\; u_A^*(\mathbf{r}-\mathbf{R}_{A,i}) \mathcal{H} u_B(\mathbf{r}-\mathbf{R}_{B,l}),$$

where we have used the same argument from above, that $l = 1, \ldots, 3$. We also take the matrix element defined by the integral in ζ_{AB} to be independent of indices in order to obtain

$$\zeta_{AB} \approx z_0 \varphi(\mathbf{k}), \tag{1.26}$$

where

$$z_0 = \int d\mathbf{r}\; u_A^*(\mathbf{r}-\mathbf{R}_{A,i}) \mathcal{H} u_B(\mathbf{r}-\mathbf{R}_{B,l}). \tag{1.27}$$

As previously seen in the calculation of H_{BA} we can easily judge what ζ_{BA} should be, and that is

$$\zeta_{BA} \approx z_0 \varphi^*(\mathbf{k}). \tag{1.28}$$

1.3.2 Diagonal entries of the transfer and overlap integral matrices

To calculate the diagonal entries of H corresponding to the A sub-lattice we set $B = A$, doing this yields [12, 14]

$$H_{AA} = \frac{1}{N}\sum_{i=1}^{N}\sum_{l=1}^{N} e^{i\mathbf{k}\cdot(\mathbf{R}_{A,l}-\mathbf{R}_{A,i})} \int d\mathbf{r}\; u_A^*(\mathbf{r}-\mathbf{R}_{A,i}) \mathcal{H} u_A(\mathbf{r}-\mathbf{R}_{A,l}). \tag{1.29}$$

We can assume that the contribution in (1.29) comes from the same site $l = i$. This assumption yields

$$H_{AA} \approx \frac{1}{N}\sum_{i=1}^{N}\int d\mathbf{r}\; u_A^*(\mathbf{r}-\mathbf{R}_{A,i})\mathcal{H}u_A(\mathbf{r}-\mathbf{R}_{A,i}).$$

We can note that the integral term above is the same for all $i = 1, 2, \ldots, N$ i.e. it is the same of every A site and it can therefore be set to a parameter ε_{2p}

$$\varepsilon_{2p} = \int d\mathbf{r}\; u_A^*(\mathbf{r}-\mathbf{R}_{A,i})\mathcal{H}u_A(\mathbf{r}-\mathbf{R}_{A,i}), \tag{1.30}$$

which equals the energy of the $2p_z$ orbital. With this we can simplify H_{AA} as follows

$$H_{AA} \approx \frac{1}{N}\sum_{i=1}^{N}\varepsilon_{2p},$$

$$H_{AA} \approx \varepsilon_{2p}. \tag{1.31}$$

Using the fact that carbon atoms are identical, meaning that the B sub-lattice has the same structure as the A sub-lattice we can argue that $H_{AA} = H_{BB} = \varepsilon_{2p}$. The transfer integral matrix can be written fully as [12, 14]

$$H = \begin{pmatrix} \varepsilon_{2p} & -\gamma_0\varphi(\mathbf{k}) \\ -\gamma_0\varphi^*(\mathbf{k}) & \varepsilon_{2p} \end{pmatrix}. \tag{1.32}$$

The diagonal entries of the overlap matrix can also be computed in a similar way , that is

$$\zeta_{AA} = \frac{1}{N}\sum_{i=1}^{N}\sum_{l=1}^{N} e^{i\mathbf{k}\cdot(\mathbf{R}_{A,l}-\mathbf{R}_{A,i})}\int d\mathbf{r}\; u_A^*(\mathbf{r}-\mathbf{R}_{A,i})u_A(\mathbf{r}-\mathbf{R}_{A,i}) \tag{1.33}$$

$$\approx \frac{1}{N}\sum_{i=1}^{N}\int d\mathbf{r}\; u_A^*(\mathbf{r}-\mathbf{R}_{A,i})u_A(\mathbf{r}-\mathbf{R}_{A,i}) = 1,$$

where we have used then fact that $\int d\mathbf{r}\; u_A^*(\mathbf{r}-\mathbf{R}_{A,i})u_A(\mathbf{r}-\mathbf{R}_{A,i}) = 1$. It is also clear that $\zeta_{AA} = \zeta_{BB} = 1$. Therefore, the overlap integral matrix can be written fully as [12, 14]

$$\zeta = \begin{pmatrix} 1 & z_0\varphi(\mathbf{k}) \\ z_0\varphi^*(\mathbf{k}) & 1 \end{pmatrix}. \tag{1.34}$$

1.3.3 Low energy bands of monolayer graphene

Having calculated the transfer and overlap integral matrices we can now calculate the energy eigenvalues $\mathscr{E}_j(\mathbf{k})$ of monolayer graphene using (1.17). Substituting H and ζ intro (1.17) we find that

$$\det\begin{pmatrix} \varepsilon_{2p}-\mathscr{E} & -(\gamma_0+\mathscr{E}z_0)\varphi(\mathbf{k}) \\ -(\gamma_0+\mathscr{E}z_0)\varphi^*(\mathbf{k}) & \varepsilon_{2p}-\mathscr{E} \end{pmatrix} = 0,$$

$$(\mathscr{E}-\varepsilon_{2p})^2 - (\gamma_0+\mathscr{E}z_0)^2|\varphi(\mathbf{k})|^2 = 0,$$

simplification yields a quadratic equation of the form

$$(1 - z_0^2|\varphi(\mathbf{k})|^2)\mathscr{E}^2 - 2(\varepsilon_{2p} + \gamma_0 z_0|\varphi(\mathbf{k})|^2)\mathscr{E} + \varepsilon_{2p}^2 - \gamma_0^2|\varphi(\mathbf{k})|^2 = 0.$$

The quadratic formula gives

$$\mathscr{E}_{\pm} = \frac{\varepsilon_{2p} + \gamma_0 z_0|\varphi(\mathbf{k})|^2 \pm (\gamma_0 - \varepsilon_{2p} z_0)|\varphi(\mathbf{k})|}{1 - z_0^2|\varphi(\mathbf{k})|^2},$$

alternatively we can write [15]

$$\mathscr{E}_{\pm} = \frac{\varepsilon_{2p} \pm \gamma_0|\varphi(\mathbf{k})|}{1 \mp z_0|\varphi(\mathbf{k})|}, \tag{1.35}$$

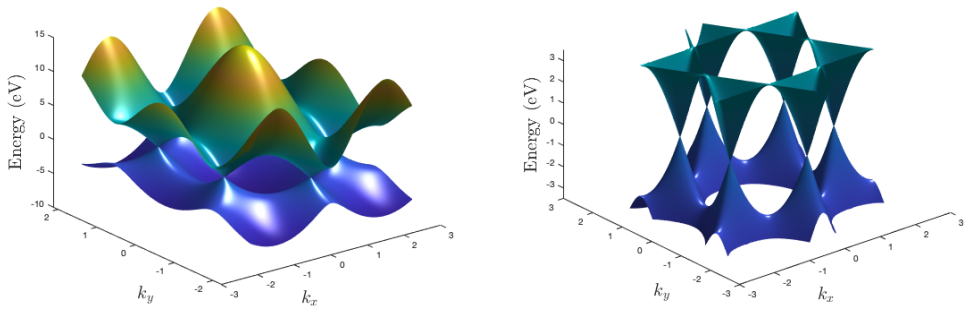

(a) (b)

Figure 1.2: (a) The low energy band structure of monolayer graphene (1.35) with the hopping parameter set to $\gamma_0 = 3.033$eV, and nearest neighbour overlap parameter $z_0 = 0.129$ and the $2p_z$ orbital energy $\varepsilon_{2p} = 0$. (b) On the right is a zoomed-in depiction of the Dirac cones located at the six corners in the Brillouin zone. The conduction and valency bands touch at these points.

where

$$|\varphi(\mathbf{k})|^2 = 1 + 4\cos\left(\frac{3k_x a}{2}\right)\cos\left(\frac{\sqrt{3}k_y a}{2}\right) + 4\cos^2\left(\frac{\sqrt{3}k_y a}{2}\right), \tag{1.36}$$

and $|\varphi(\mathbf{k})|$ is the square root of the above expression. The positive energy spectrum $\mathscr{E}_+$ in (1.35) corresponds to the upper π^* band while the negative energy $\mathscr{E}_-$ corresponds to the lower π band[13]. The upper (conduction) and lower (valency) bands touch at the six corners of the Brillouin zone in such a way that there is no gap between the conduction and valency bands[13]. Fig.1.2 shows a plot of the energy spectrum (1.35) against the wave vector (k_x, k_y), where the $2p_z$ orbital energy ε_{2p} is taken to be zero, with other parameters being $\gamma_0 = 3.003$eV and $z_0 = 0.129$.

1.4 The Dirac-like Hamiltonian in graphene

In the previous section we calculated the explicit form of the monolayer graphene energy spectrum via the tight-binding approximation. Fig.1.2 showed that the conduction (π^*) and valency (π) bands touch in a gapless way at the four corners in the first Brillouin zone. The task now is to derive the Hamiltonian describing the dynamics of electrons at these points. We begin by showing that the coupling between the A and B sub-lattices vanishes exactly at the K and K' points. The coupling is described by the off-dialgonal matrix elements H_{AB}, which is proportional to $\varphi(\mathbf{k})$. Substituting $\mathbf{K}$ into (1.23) gives

$$\begin{aligned}\varphi(\mathbf{K}) =& e^{-2\pi i/3} + 2\cos\left(\frac{\pi}{3}\right) e^{i\pi/3},\\ =& e^{-2\pi i/3} + e^{i\pi/3} = 0.\end{aligned}$$

It is also true that $\varphi(\mathbf{K}') = 0$. This confirms the existence of decoupling in the A and B sub-lattices and thus suggesting the presence of a degeneracy in the energy spectrum at the K and K' point. This cancellation of coupling in the two sub-lattices no longer holds when the wave vector $\mathbf{k}$ does not equal $\mathbf{K}$ or $\mathbf{K}'$ exactly. To demonstrate this we define a new momentum $\delta\mathbf{k} = \mathbf{k} - \mathbf{K}$ measured relative to $\mathbf{K}$. The coupling between the A and B sub-lattices is now proportional to

$$\varphi(\mathbf{k}) = e^{-ia(\delta k_x + K_x)} + 2\cos\left(\frac{\sqrt{3}a(\delta k_y + K_y)}{2}\right) e^{ia(\delta k_x + K_x)/2}. \tag{1.37}$$

Expanding around $\delta\mathbf{k} = 0$ yields

$$\begin{aligned}\varphi(\mathbf{k}) \simeq& 2e^{-iK_x a}\delta\mathbf{k}\cdot\boldsymbol{\nabla}_{\mathbf{k}}\left(e^{3ik_x a/2}\cos\left(\frac{\sqrt{3}k_y a}{2}\right)\right)\Big|_{\mathbf{k}=\mathbf{K}},\\ =& e^{-iK_x a}\frac{3a}{2}(\delta k_x, \delta k_y)\cdot(-i, 1),\\ =& \frac{3a}{2}e^{-iK_x a}(-i\delta k_x + \delta k_y),\end{aligned}$$

$$\varphi(\mathbf{k}) = \frac{3a}{2}(\delta k_x + i\delta k_y) + \mathcal{O}(\delta k/K)^2, \tag{1.38}$$

where we have dropped the phase factor $e^{-iK_x a} = e^{-i\frac{2\pi}{3}}$ since it bears no significance on the physical results (i.e. the energies). Similarly, performing the same expansion $\delta\mathbf{k} = 0$ with $\delta\mathbf{k} = \mathbf{k} - \mathbf{K}'$ yields

$$\varphi(\mathbf{k}) = \frac{3a}{2}(-i\delta k_x - \delta k_y) + \mathcal{O}(\delta k/K)^2. \tag{1.39}$$

The above calculation shows that the coupling between the A and B sublattices vanishes at the Dirac points. Putting all this together the Hamiltonian at the Dirac points can be written as [1, 13, 14]

$$H_{\mathbf{K}',\mathbf{K}} = v_F\begin{pmatrix} 0 & i\delta k_x \pm \delta k_y \\ -i\delta k_x \pm \delta k_y & 0\end{pmatrix}, \tag{1.40}$$

where $v_F = \frac{3\gamma_0 a}{2\hbar} \simeq 10^6 ms^{-1}$ is the Fermi velocity. Replacing δk_x with ∂_x and δk_y with ∂_y the above Hamiltonian corresponds to that of the massless Dirac fermions in $(2+1)$ dimensions. To see this, let us consider

$$H_{\mathbf{K}'} = \begin{pmatrix} 0 & i\partial_x + \partial_y \\ -i\partial_x + \partial_y & 0 \end{pmatrix} = iv_F \boldsymbol{\sigma} \cdot \boldsymbol{\nabla},$$

with $\boldsymbol{\sigma} = (\sigma^1, \sigma^2)$ and $\boldsymbol{\nabla} = (\partial_x, \partial_y)$. $H_{\mathbf{K}}$ is the complex conjugation of $H_{\mathbf{K}'}$.

1.5 Chapter summary

In this chapter showed the applicability of the Dirac equation in one and two spatial dimensions. We showed argued that the Su-Schrieffer-Heeger Hamiltonian reduces to the Dirac Hamiltonian when evaluated at the Brillouin zone. We also introduced the tight-binding model of monolayer graphene in the first quantization and showed that the Taylor expansion of the tight-binding Hamiltonian about the Dirac points coincides with the $(2+1)$ dimensional massless linear Dirac equation. This meant that fermions travelling in a hexagonal lattice, be it a real graphene lattice or a photonic graphene lattice, obey the massless planar Dirac equation as shown in (1.40). This Hamiltonian (1.40) opens us up to the possibility of studying graphene-like structures subject to several nonlinearities, with the common ones being Kerr-like nonlinearities [16]. These nonlinear Dirac equations and their nonlinear wave solutions will be studied in the upcoming chapters.

Chapter 2

The Dirac equation

The previous chapter introduced one-dimensional and two-dimensional lattices namely the Su-Schrieffer-Heeger and tight binding model of monolayer graphene. We showed that there is a close connection between the Dirac equation and these lattice models. In this chapter, we will formally present the Dirac equation and its properties.

2.1 The Klein-Gordon equation

The Klein-Gordon equation serves as a preliminary for the development of a quantum theory consistent with the theory of relativity. This equation resulted from an attempt to generalise the Schrödinger equation so as to incorporate special relativity. The traditional path taken towards a relativistic quantum theory is, to begin with the free, spinless and non-relativistic Schrödinger equation

$$\left(i\partial_t - \frac{(-i\boldsymbol{\nabla}_{\mathbf{x}})^2}{2m}\right)\psi(t,\mathbf{x}) = 0, \tag{2.1}$$

where $(t,\mathbf{x}) \in \mathbb{R}\times\mathbb{R}^3$, $\psi(t,\mathbf{x}) \in \mathbb{C}^4$ in the (3+1)-dimensional case. Equation (2.1) is obtained by replacing classical quantities with operators in

$$E = \frac{\mathbf{p}^2}{2m} \tag{2.2}$$

as follows: $E \to i\hbar\frac{\partial}{\partial t}$, $\mathbf{p} \to \frac{\hbar}{i}\boldsymbol{\nabla}$.

The problem with the linear Schrödinger equation is that it is not Lorentz covariant because of the order of time and spatial derivatives, thus it does not suffice as a candidate for relativistic quantum theory. To derive a relativistic wave equation we recall the relativistic energy-momentum relation

$$p_\mu p^\mu = \frac{E^2}{c^2} - \mathbf{p}^2 = m^2c^2, \tag{2.3}$$

with $p_\mu = g_{\mu\nu}p^\nu = \left(\frac{E}{c}, -\mathbf{p}\right)$. To make a conversion to the relativistic wave equation we note that

$$E = \sqrt{\mathbf{p}^2c^2 + m^2c^4} \tag{2.4}$$

and the four-momentum in operator form becomes $p^\mu \to i\hbar\frac{\partial}{\partial x^\mu}$. Therefore the relativistic wave equation becomes

$$i\frac{\partial}{\partial t}\psi(t,\mathbf{x}) = \sqrt{-\boldsymbol{\nabla}^2 + m^2}\psi(t,\mathbf{x}), \qquad \hbar = c = 1. \tag{2.5}$$

Equation (2.5) has some issues, in particular, the time and spatial derivatives do not appear in a symmetric manner and the square root also presents some problems since its Taylor expansion yields infinite derivatives. In order to reach a successful end we must begin with (2.3) without taking the square root, doing this yields the following relativistic equation with second derivatives in time and space:

$$-\frac{\partial^2}{\partial t^2}\psi(t,\mathbf{x}) = \left(-\boldsymbol{\nabla}^2 + m^2\right)\psi(t,\mathbf{x}). \tag{2.6}$$

This equation can be written more compactly in the Lorentz covariant form as

$$\left(\partial_\mu\partial^\mu + m^2\right)\psi(t,\mathbf{x}) = 0, \qquad \mu = \{0,1,\cdots,N\}, \tag{2.7}$$

where $N \in \mathbb{N}$, $\partial_\mu = \frac{\partial}{\partial x^\mu}$ and $x^\mu = (t,\mathbf{x})$ is the space-time position vector and $\mu = \{0,1,2,3\}$ in the $(3+1)$-dimensional case. Equation (2.7) is known as the Klein-Gordon equation.

2.1.1 Problems with the Klein-Gordon equation

Although the Klein-Gordon equation can describe the dynamics of spinless particles (mesons), it cannot do so for half-integer spin particles (fermions) like the electron. It was thus rejected since at the time the entire project of relativistic quantum mechanics was centered around the quantum mechanics of the electron. Another reason (2.7) was rejected is that it does not possess a positive definite probability density that can lead to a conserved probability current (the continuity equation). To show this we derive an equation in the continuity equation associated with the Klein-Gordon equation and argue that there isn't an object that can be interpreted as a positive definite probability density. We begin by multiplying (2.6) by ψ^* and subtracting the complex conjugate from the resulting expression to obtain:

$$\partial_\mu\left(\psi^*\partial^\mu\psi - \psi\partial^\mu\psi^*\right) = 0.$$

We multiply by $\frac{1}{2mi}$ so that the current density is the same as in the non-relativistic case:

$$\partial_t\left(\frac{i}{2m}\left(\psi^*\partial_t\psi - \psi\partial_t\psi^*\right)\right) + \boldsymbol{\nabla}\cdot\frac{1}{2mi}\left(\psi^*\boldsymbol{\nabla}\psi - \psi\boldsymbol{\nabla}\psi^*\right) = 0.$$

Defining

$$\rho = \frac{i}{2m}\left(\psi^*\partial_t\psi - \psi\partial_t\psi^*\right), \tag{2.8}$$

and

$$\mathbf{j} = \frac{1}{2mi}\left(\psi^*\boldsymbol{\nabla}\psi - \psi\boldsymbol{\nabla}\psi^*\right), \tag{2.9}$$

we obtain

$$\partial_t\rho + \boldsymbol{\nabla}\cdot\mathbf{j} = 0, \tag{2.10}$$

which takes the form of a continuity equation.

The function ρ cannot be interpreted as a probability density because it is not positive definite. To demonstrate this we have to find a solution to (2.6) via the method of separation of variables. Let $\psi(\mathbf{x},t)$ take then form

$$\psi(\mathbf{x},t) = \varphi(t)\phi(\mathbf{x}). \tag{2.11}$$

Substituting (2.11) into (2.6) and dividing the resulting expression by ψ yields

$$-\frac{1}{\varphi}\frac{d^2\varphi}{dt^2} = \frac{1}{\phi}\left(-\boldsymbol{\nabla}^2 + m^2\right)\phi. \tag{2.12}$$

Equation (2.12) holds if both the right and left-hand sides equal a constant, say E^2. We are then left with solving two eigenvalue problems, one ordinary differential equation in time and one partial differential equation in space. The differential equations are

$$\frac{d^2\varphi}{dt^2} = -E^2\varphi, \tag{2.13}$$

$$\boldsymbol{\nabla}^2\phi(\mathbf{x}) = -\mathbf{p}^2\phi(\mathbf{x}), \tag{2.14}$$

where $\mathbf{p}^2 = \mathbf{p}\cdot\mathbf{p} = p_x^2 + p_y^2 + p_z^2 = E^2 - m^2$, where the spatial vector is $\mathbf{x} = (x,y,z)$.

The solution to (2.13) can be written as

$$\varphi(t) = Ae^{-iEt}, \tag{2.15}$$

where A is a constant.

Since (2.14) is a linear differential equation with constant coefficients, we can write down a solution of the form

$$\phi(\mathbf{x}) = Be^{-i\mathbf{k}\cdot\mathbf{x}}, \tag{2.16}$$

with B being a constant. The full solution to the $(3+1)$-dimensional Klein-Gordon equation can be written as

$$\psi(\mathbf{x},t) = \psi_0 e^{-i(Et+\mathbf{k}\cdot\mathbf{x})/\hbar}, \tag{2.17}$$

where $\psi_0 = AB$. Substituting (2.17) into (2.8) we obtain

$$\rho = -\frac{\hbar E}{mc^2}|\psi|^2, \tag{2.18}$$

if $E > 0$, this is negative and so cannot be interpreted as a probability density.

2.2 The Dirac equation

In section 2.1.1 we showed that the Klein-Gordon equation (2.7) does not possess a positive definite probability density function leading to the continuity equation. This fact resulted from the observation that the Klein-Gordon equation is second order in time, this means that the energies can take both positive and negative values and thus resulting in the absurdity shown in (2.18) i.e. a negative probability. The task now is to find a relativistic wave equation in which the time derivatives appear in first order so that we can obtain a positive probability density leading to the continuity equation. The equation of interest must be such that its eigenvalues satisfy the relativistic energy-momentum relation (2.3). In 1928 Dirac proposed an equation of the form[17]:

$$i\hbar\partial_t\psi = \left(\frac{\hbar c}{i}\alpha^k\partial_k + \beta mc^2\right)\psi =: H\psi, \qquad 1 \leq k \leq D, \tag{2.19}$$

where D is the spatial dimensions, α^k and β are anti-commuting matrices and $\partial_k = \frac{\partial}{\partial x^k}$, we sum over repeated indices. Equation (2.19) has the time and spatial derivatives occurring symmetrically. This will solve the negative probability density (2.8) encountered in the Klein-Gordon equation. something to note about the proposition in (2.19) are: (a)α^k cannot be numbers since (2.19) would fail to be invariant even under spatial rotations. (b) α^k and β must be hermitian matrices so that the hermiticity of H can ensure the existence of a conserved probability density. (c) The wave function $\psi = (\psi_1, \cdots, \psi_N)^T$ is an N-component column vector whose components satisfy the Klein-Gordon equation (2.6) so that (2.3) holds. In $(3+1)$-dimensions $N = 4$, $N = 2$ in $(2+1)$ and $N = 2$ in $(1+1)$ dimensions. As we shall see later in Thm (1) that $N = 2^d$ for both cases when the number of dimensions is $\ell = 2d$ (even) and $\ell = 2d+1$ (odd), with $d \in \mathbb{N}$. (d) Equation (2.19) must posses Lorentz invariance.

2.3 The conserved probability density

The Dirac equation possesses a positive definite probability density and a current density that lead to the continuity equation. To derive the continuity equation for the Dirac system we follow a similar procedure as in the case of the Klein-Gordon equation. We first start by writing down the adjoint vector to ψ as $\psi^\dagger = (\psi_1^*, \ldots, \psi_N^*)$. Multiplying (2.19) by $\psi^\dagger$ yields:

$$i\psi^\dagger\partial_t\psi = \frac{1}{i}\psi^\dagger\alpha^j\partial_j\psi + m2\psi^\dagger\beta^\dagger\psi. \tag{2.20}$$

The complex conjugation is given as

$$-i\partial_t\psi^\dagger\psi = -\frac{1}{i}\left(\partial_j\psi^\dagger\right)\alpha^{j\dagger}\psi + \psi^\dagger\beta^\dagger\psi. \tag{2.21}$$

Taking the difference between the two equations gives

$$\partial_t(\psi^\dagger\psi) = -\left(\left(\partial_i\psi^\dagger\right)\alpha^{i\dagger}\psi + \psi^\dagger\alpha^i\partial_i\psi\right) + im\left(\psi^\dagger\beta^\dagger\psi - \psi^\dagger\beta\psi\right).$$

We have used the fact that α^j and β are both hermitian matrices, that is $\alpha^{j\dagger} = \alpha^j$ and $\beta^\dagger = \beta$. We can define the probability density as

$$\rho := \psi^\dagger \psi, \tag{2.22}$$

and a current density

$$j^k := c\psi^\dagger \alpha^k \psi. \tag{2.23}$$

These give rise to the continuity equation

$$\partial_\mu j^\mu = \frac{1}{c}\partial_t j^0 + \partial_k j^k = 0, \tag{2.24}$$

where $j^0 = c\rho$ and $j^\mu = (j^0, j^k)$.
p0d

2.4 Dirac matrices

Making use of all the four facts above, we can consider a two-fold application of the Hamiltonian in (2.19) and obtain

$$-\partial_t^2 \psi = -\sum_{j,k=1}^{3} \frac{1}{2}\left(\alpha^j\alpha^k + \alpha^k\alpha^j\right)\partial_j\partial_k\psi + \frac{m}{i}\sum_{j=1}^{3}\left(\alpha^j\beta + \beta\alpha^j\right)\partial_j\psi + \beta^2 m^2\psi. \tag{2.25}$$

Because we demand that ψ in (2.19) satisfy (2.7), we can make a comparison of (2.25) with the Klein-Gordon equation to obtain the following algebraic relations

$$\{\alpha^i, \alpha^j\} = 2\delta^{ij} I, \qquad \beta^2 = I, \qquad \{\alpha^i, \beta\} = 0, \qquad 1 \le i, j \le n, \tag{2.26}$$

where I is an $N \times N$ identity matrix and δ^{ij} is 1 when $i = j$ and 0 otherwise.

Definition 2.4.1 (Dirac matrices)**.** *We say that the elements of the endomorphism ring of $\mathbb{C}^N$ i.e. $\alpha^i \in \mathrm{End}\,(\mathbb{C}^n)$, $1 \le i \le \ell$, with $\ell \in \mathbb{N}$, are the Dirac matrices if*

$$\left(\alpha^i\right)^\dagger = \alpha^i, \qquad \alpha^i\alpha^j + \alpha^j\alpha^i = 2\delta^{ij} I, \qquad 1 \le i, j \le \ell.$$

Since $(\alpha^i)^2 = I$, one has that the eigenvalues spectrum of α^i is ± 1 i.e. $\sigma(\alpha^i) \subset \{\pm 1\}$. If $\ell \ge 2$, then from the relation

$$\alpha^i = -\alpha^j\alpha^i\alpha^j, \qquad i \ne j,$$

one concludes that $\mathrm{Tr}\,\alpha^i = 0$. It follows that if $\ell \ge 2$, then N is even; without loss of generality, we may then assume that

$$\beta = \alpha^\ell = \begin{pmatrix} I_{N/2} & 0 \\ 0 & -I_{N/2} \end{pmatrix}. \tag{2.27}$$

Then the anticommutation relations $\{\alpha^i, \alpha^\ell\} = 0$, $1 \leq i \leq \ell - 1$, *show that the matrices* $(\alpha^i)_{1\leq i\leq \ell-1}$ *are block-antidiagonal; begin self-adjoint, they have to be of the form*

$$\alpha^i = \begin{pmatrix} 0 & \sigma_i^* \\ \sigma_i & 0 \end{pmatrix}, \qquad 1 \leq i \leq \ell - 1,$$

where the "generalised Pauli matrices" $(\sigma_i)_{1\leq i\leq \ell-1}$ *satisfy*

$$\sigma_i^*\sigma_j + \sigma_j^*\sigma_i = 2\delta_{ij}I, \qquad \sigma_i\sigma_j^* + \sigma_j\sigma_i^* = 2\delta_{ij}I, \qquad 1 \leq i, j \leq \ell - 1. \tag{2.28}$$

Theorem 1, as shall be seen below, shows that there are $\ell = 2d + 1$ Dirac matrices of size $N = 2^d$, $d \in \mathbb{N}$. Let us give an explicit form of these matrices. For $d = 0$, $N = 1$, we can take $\alpha = 1$. For $d = 1$, $N = 2$, we define α^i, $1 \leq i \leq 3$ to be the standard Pauli matrices σ_i. The Dirac matrices can be constructed recursively in higher dimensions, that is, given the Dirac matrices of size $N = 2^d$, α^i, $1 \leq i \leq \ell = 2d + 1$, one can define the Dirac matrices $\hat{\alpha}^i$, $1 \leq i \leq 2d + 3$, of size $2N$, by Kronecker products

$$\begin{aligned} \hat{\alpha}^i =& \sigma_1 \otimes \alpha^i = \begin{pmatrix} 0 & \alpha^i \\ \alpha^i & 0 \end{pmatrix}, \quad 1 \leq i \leq 2d + 1; \\ \hat{\alpha}^{2d+2} =& \sigma_2 \otimes I_N = \begin{pmatrix} 0 & -iI_N \\ iI_N & 0 \end{pmatrix}, \\ \hat{\beta} :=& \hat{\alpha}^{2d+3} = \sigma_3 \otimes I_N = \begin{pmatrix} I_N & 0 \\ 0 & -I_N \end{pmatrix}. \end{aligned} \tag{2.29}$$

There are various choices of Dirac matrices, some of which can be constructed according to (2.29). However, the overall analysis of equations that are of Dirac type is not sensitive to the choice of a Dirac matrix basis set. A practical example of this is the use of the so-called Weyl (spinor) representations of Dirac matrices over the standard Dirac-Pauli matrices. The exact representations of these matrices are shown in appendix A.2. These matrices can also be chosen as shown in Thm. 1. This is done by considering matrices $M_i \in \mathbf{GL}(N, \mathbb{C})$, $1 \leq i \leq \ell$, with $N \in \mathbb{N}$ and $\ell \in \mathbb{N}$, which satisfy the Clifford algebra relations

$$M_iM_j + M_jM_i = 2\delta_{ij}I_N, \qquad 1 \leq i, j \leq \ell, \qquad \ell \in \mathbb{N}. \tag{2.30}$$

A few examples of these include the standard Dirac-Pauli γ-matrices and the Weyl representation of the Dirac matrices; these form the Clifford algebra as shown (2.37) and (2.38). Lemma 1 provides the relevant information about irreducible representations of complex Clifford algebras needed in Thm. 1.

Lemma 1 (Irreducible representations of complex Clifford algebras)**.** *Let* $\ell \in \mathbb{N}$ *and consider the complex Clifford algebra* $\mathbf{Cl}_\ell(\mathbb{C})$*, which is an unital algebra over a field of complex numbers formed by the generators* e_i, $1 \leq i \leq \ell$*, which satisfy the following relations*

$$\{e_i, e_j\} = e_ie_j + e_je_i = 2\delta_{ij}\mathbf{1}, \qquad 1 \leq i, j \leq \ell, \tag{2.31}$$

where $\mathbf{1}$ *is the unit element in* $\mathbf{Cl}_\ell(\mathbb{C})$.

1. *If $\ell = 2d, \ell$, then there is only one irreducible representation of $\mathbf{Cl}_\ell(\mathbb{C})$. This representation is of rank 2^d.*

2. *If $\ell = 2d+1$, $d \in \mathbb{N}_0$, then there are two (non-isomorphic) representations of $\mathbf{Cl}_\ell(\mathbb{C})$. Both these representations are of rank 2^d. These two representations can be distinguished by whether the product of all Clifford algebras (times i),*

$$\boldsymbol{\omega} = ie_1e_2\dots e_{2d+1},$$

acts by multiplication by 1 or -1 (when d is odd) or by i or $-i$ (when d is even).

Theorem 1 (Dirac-Pauli theorem)**.** *Let $\ell \in \mathbb{N}$ and let $\{M_i, 1 \le i \le \ell\}$ and $\{\tilde{M}_i, 1 \le i \le \ell\}$ be two sets of anticommuting matrices of the same size $N \in \mathbb{N}$ which satisfy the anticommutation relations*

$$M_iM_j + M_jM_i = 2\delta_{ij}I, \qquad \tilde{M}_i\tilde{M}_j + \tilde{M}_j\tilde{M}_i = 2\delta_{ij}I; \qquad 1 \le i,j \le \ell.$$

Assume that

$$N = 2^D n_0,$$

with n_0 an odd natural number and $D \in \mathbb{N}_0$ (note that $\ell \le 2D+1$ by Lemma 1).

1. *If $\ell = 2d$, $d \in \mathbb{N}_0$, then there is $S \in \mathbf{GL}(N,\mathbb{C})$ such that*

$$\tilde{M}_i = S^{-1}M_iS, \qquad 1 \le i \le \ell. \tag{2.32}$$

2. *If $\ell = 2d+1$, $d \in \mathbb{N}_0$, then there are $S, \Sigma \in \mathbf{GL}(N,\mathbb{C})$, with $\Sigma^2 = I$, such that*

$$\tilde{M}_i = S^{-1}M_iS, \qquad 1 \le i \le \ell; \qquad \tilde{M}_\ell = \Sigma S^{-1}M_\ell S; \tag{2.33}$$

$$[M_i, \Sigma] = 0, \qquad [\tilde{M}_i, \Sigma] = 0, \qquad 1 \le i \le \ell; \qquad [S, \Sigma] = 0.$$

Moreover $\sigma(\Sigma) = \pm 1$, and the multiplicities of both eigenvalues ± 1 of Σ are multiples of 2^d. One can choose $\Sigma = I$ if and only if

$$\operatorname{Tr} M_1M_2\dots M_\ell = \operatorname{Tr} \tilde{M}_1\tilde{M}_2\dots\tilde{M}_\ell.$$

3. *If $n_0 = 1$ and $D = d$, so that $N = 2^d$ and $\ell = 2d$ or $\ell = 2d+1$, then the choice of S is unique up to a nonzero complex factor; if moreover $\ell = 2d+1$, then $\Sigma = \mu I$ with $\mu \in \{\pm 1\}$.*

4. *If the matrices M_i and $\tilde{M}_i$, $1 \le i \le \ell$, are self-adjoint, then S could be chosen as unitary; if more, moreover, ℓ is odd, the Σ could be chosen as self-adjoint.*

An important consequence of Thm. 1 is that there exist matrices of size $N = 2^d$ for both $\ell = 2d$ and $\ell = 2d+1$. This will be useful later on in identifying the dimensions of the Dirac matrices in odd dimensions, for example in $(2+1)$-dimensions.

2.5 Dirac equation in covariant form

In order to cast the Dirac equation in its covariant form we must write down the Dirac gamma-matrices. To do this we follow the convention, that $0 \leq \mu, \nu \leq n$ and $1 \leq 1, j \leq n$. We let γ^μ, $0 \leq \mu \leq n$, be the $N \times N$ Dirac gamma-matrices; by this we mean that γ^0 is self-adjoint, γ^i, $1 \leq i \leq n$ are anti-self-adjoint. The γ^μ's are said to form the Clifford algebra, that is

$$\gamma^\mu \gamma^\nu + \gamma^\nu \gamma^\mu = 2g^{\mu\nu} I_N, \tag{2.34}$$

where

$$g_{\mu\nu} = g^{\mu\nu} = \text{diag}(1, -1, \ldots, -1), \qquad 0 \leq \mu, \nu \leq n. \tag{2.35}$$

The Dirac equation can now be cast into the covariant form as

$$(-i\gamma^\mu \partial_\mu + m)\, \psi = 0. \tag{2.36}$$

The γ-matrices in then standard Dirac-Pauli representation are given as

$$\gamma^0 = \begin{pmatrix} I_{N/2} & 0 \\ 0 & -I_{N/2} \end{pmatrix}, \qquad \gamma^i = \begin{pmatrix} 0 & \sigma_i^* \\ -\sigma_i & 0 \end{pmatrix} \tag{2.37}$$

and

$$\gamma^0_W = \begin{pmatrix} 0 & I_{N/2} \\ I_{N/2} & 0 \end{pmatrix}, \qquad \gamma^i_W = \begin{pmatrix} 0 & -\sigma^i \\ \sigma^i & 0 \end{pmatrix} \tag{2.38}$$

in the Weyl representation, where the subscript W stands for "Weyl". Both matrices i.e Dirac-Puali and Weyl representations satisfy equation (2.31) and (2.30) according to Lemma 1 and Thm. 1.

2.5.1 Dirac equation in (3+1) dimensions

The $(3+1)$ dimensional Dirac equation is the most common of the Dirac-type equations in (particle) physics. This form ($(3+1)$ dimensions) of the Dirac equation was first introduced by Paul Dirac in his efforts to study the quantum theory of an election [18]. The $(3+1)$ dimensional case implies that the (α^i)'s are 4×4, because $d = 2$, $\ell = 2d$, thus $N = 4$. With this we can write down the Dirac matrices using Def. 2.4 as:

$$\alpha^j = \begin{pmatrix} 0 & \sigma_j^* \\ \sigma_j & 0 \end{pmatrix}, \qquad \beta = \begin{pmatrix} I_4 & 0 \\ 0 & -I_4 \end{pmatrix}, \tag{2.39}$$

where σ_j are the usual Pauli matrices:

$$\sigma_1 = \begin{pmatrix} 0 & 1 \\ 1 & 0 \end{pmatrix}, \qquad \sigma_2 = \begin{pmatrix} 0 & -i \\ i & 0 \end{pmatrix}, \qquad \sigma_3 = \begin{pmatrix} 1 & 0 \\ 0 & -1 \end{pmatrix}. \tag{2.40}$$

See (A.3) for proof that this choice of α^i and β satisfy the algebraic relations in (2.26). The $(3+1)$ dimensional case is one that is most encountered – the Dirac matrices for this case are given in (2.39) as 4×4 matrices. The spinors of the $(3+1)$ dimensional Dirac equation

are represented by a four dimensional vector $\psi = (\psi_1, \psi_2, \psi_3, \psi_4)$. The Dirac equation can thus be written as

$$i\partial_t\psi = -i\alpha^k \frac{\partial\psi}{\partial x^k} + \beta m\psi, \qquad 1 \leq k \leq 3. \tag{2.41}$$

Equation (2.41) can be cast into its covariant form by multiplying both sides by β from the left and calling $\gamma^0 = \beta$ and $\gamma^i = \beta\alpha^i$.

2.5.2 Dirac equation in (2+1) dimensions

In the $(2+1)$ dimensional case we have that $d = 1$, $N = 2$ and α^i, $1 \leq i \leq 3$ are taken to be the standard Pauli matrices. In which case $\alpha^1 = \sigma_1$, $\alpha^2 = \sigma_2$ and $\beta = \sigma_3$. With this, we can write the Dirac equation in $(2+1)$ dimensions as:

$$\begin{aligned} i\partial_t\psi_1 &= -(i\partial_x + \partial_y)\psi_2 + m\psi_1 \\ i\partial_t\psi_2 &= -(i\partial_x - \partial_y)\psi_1 - m\psi_2. \end{aligned} \tag{2.42}$$

There exists. another set of equations found by considering the conjugation of the Pauli matrices, that is, we define $\alpha^1 = \sigma_1^* = \sigma_1$ and $\alpha^2 = \sigma_2^* = -\sigma_2$. With this choice of matrices, the Dirac equation can be written as:

$$\begin{aligned} i\partial_t\psi_1 &= -(i\partial_x - \partial_y)\psi_2 + m\psi_1 \\ i\partial_t\psi_2 &= -(i\partial_x + \partial_y)\psi_1 - m\psi_2. \end{aligned} \tag{2.43}$$

2.5.3 Dirac equation in (1+1) dimensions

There are a few ways of choosing the Dirac matrices in the $(1+1)$ dimensional case, the first one is seen in Ref. [19], where $\alpha^1 = -\sigma_2^* = -\sigma_2$ and $\beta = \sigma^3$. This choice of matrices yields the following system of equations:

$$\begin{aligned} i\partial_t\psi_1 &= \partial_x\psi_2 + m\psi_1, \\ i\partial_t\psi_2 &= -\partial_x\psi_1 - m\psi_2. \end{aligned} \tag{2.44}$$

Another set of $(1+1)$ dimensional Dirac equations can be obtained by conjugating the Pauli matrices used in (2.44). Doing this yields:

$$\begin{aligned} i\partial_t\psi_1 &= \partial_x\psi_2 + m\psi_1, \\ i\partial_t\psi_2 &= -\partial_x\psi_1 - m\psi_2. \end{aligned} \tag{2.45}$$

These choices of the Pauli matrices can be seen in Ref.[20].

One can still choose a different combination of the Dirac matrices to find a different system of equations. We can choose $\alpha^1 = -\sigma_3$ and $\beta = \sigma_1$, this choice is used in Ref.[21] where "spinor solitons and their $\mathcal{PT}$-symmetric offspring" are studied. This choice of Dirac matrices yields

$$\begin{aligned} i\partial_t\psi_1 &= i\partial_x\psi_1 - \psi_2, \\ i\partial_t\psi_2 &= -i\partial_x\psi_2 - \psi_1 \end{aligned} \tag{2.46}$$

normally referred to as the spinor representation of the Dirac equation.

2.6 The tachyonic Dirac equation

The standard Dirac equation (2.36) which appears in most physics texts is such that the two-fold application of the Hamiltonian operator is required to match the standard Klein-Gordon equation, that is, the Klein-Gordon equation which satisfies the energy-momentum relation $E^2 = \mathbf{p}^2 + m^2$. A Dirac equation of this type is often referred to as the *tardyonic* Dirac equation [22, 23, 24]. It is possible to construct another energy-momentum relation

$$E^2 = \mathbf{p}^2 - m^2 \tag{2.47}$$

by replacing $m \mapsto im$ [22]. Such a relation (2.47) represents the so-called superluminal propagation of matter waves. The Klein-Gordon equation for the superluminal waves is [25]

$$\partial_t^2\psi - \boldsymbol{\nabla}^2\psi - m^2\psi = 0. \tag{2.48}$$

Despite (2.48) describing superluminal particles it can be reverted to its original *tardyonic* form by including a nonlinear term and considering excitations over a nontrivial vacuum state. To show this, consider a Klein-Gordon equation of the form

$$\partial_t^2\psi - \nabla^2\psi - m^2\psi + \lambda^2\psi^3 = 0, \tag{2.49}$$

(the so-called ϕ^4 theory). For small ψ (2.49) becomes the *tachyonic* Klein-Gordon equation (2.48). However, if you consider a small excitation ϕ of the vacuum solution $\psi_{vac} = m/\lambda$, you obtain

$$\partial_t^2\phi - \nabla^2\phi + 2m^2\phi = 0, \tag{2.50}$$

a perfectly *tardyonic* Klein-Gordon equation. A Dirac equation corresponding to (2.48) can be written as

$$i\partial_t\psi = H\psi, \qquad H = -i\alpha^k\partial_k + i\beta m, \tag{2.51}$$

where we have replaced $m \to im$ in the standard Dirac proposition (2.19). The Dirac equation consisting of an imaginary mass term is called the *tachyonic* Dirac equation since it describes the quantum mechanics of hypothetical particles known as *tachyons* [25, 26].

Alternatively, instead of explicitly replacing the mass term as $m \mapsto im$ one can choose a Hamiltonian of the form

$$H = -i\alpha^k\partial_k + \beta\gamma^5 m, \tag{2.52}$$

with relation (2.47) still being satisfied [23, 27, 28, 29, 30], and

$$\gamma^5 = \begin{pmatrix} 0 & I_{N/2} \\ I_{N/2} & 0 \end{pmatrix} \tag{2.53}$$

being the matrix representation of the imaginary unit. The Dirac-Pauli theorem 1 ensures that for any given $\ell = D + 1$ dimensional Dirac-type system, where D is the number of spatial dimensions, if $\ell = 2d$ (even), with $d \in \mathbb{N}$ then $N = 2^d$. Similarly, there exist Dirac

matrices with $N = 2^d$ for $\ell = 2d + 1$ (odd).

Similar to the case of the *tardyonic* Dirac equation (2.25), a two-fold application of the Hamiltonian operator on (2.51) and the requirement that imaginary mass energy-momentum relation (2.47) be satisfied yields the following relations:

$$\left\{\alpha^j, \alpha^k\right\} = 2\delta^{jk} I_N, \qquad \left\{\alpha^j, \beta\right\} = 0, \qquad \beta^2 = -I_N. \tag{2.54}$$

The corresponding covariant form of (2.51) in the standard representation of the Dirac matrices is

$$(i\gamma^\mu \partial_\mu - im)\,\psi = 0. \tag{2.55}$$

2.7 Chapter summary

In this chapter, we introduced the Dirac equation, both *tardyonic* (2.5) and *tachyonic* (2.55). The Dirac equation was introduced as a supplement to the Klein-Gordon equation in an attempt to understand fermionic quantum mechanics, namely the quantum theory of the electron. We showed in section 2.1 that the Klein-Gordon equation fails as a candidate for this project because it gives rise to a negative probability density (2.18) (since the energies can be both positive and negative). For this reason there isn't a continuity equation associated with the Klein-Gordon equation, and thus the Klein-Gordon equation was rejected.

In section 2.2 we argued that the new relativistic equation (2.19) must be a spinor equation with $\psi(t, \mathbf{x}) = (\psi_1, \ldots, \psi_N)^T$. This equation consisted of matrices α^i and β whose hermiticity ensured the existence of a conserved probability density. The matrices can be extended to higher dimensions and were computed in Def.2.4 in (2.29) by use of Kronecker products.

Theorem 1 was also used to argue for the independence of the Dirac equation on the choice of matrices. Lemma 1 was also introduced to provide information about the irreducible representations of complex Clifford algebras needed for Thm.1. Through the help of Thm.1 it was argued that there are Dirac matrices of size $N = 2^d$, $d \in \mathbb{N}$ for both cases when the number of dimensions in the Dirac system is either even or odd. This was useful in constructing the dimensions of the α^i, $1 \leq i \leq \ell - 1$ in the $(2+1)$-dimensional case (2.42)-(2.43) since the number of dimensions ℓ is odd. The Dirac equations in the case o of $(3+1)$, $(2+1), (1+1)$ dimensions were given with the suitable choices of Dirac matrices in sections 2.5.1-2.5.3.

Chapter 3

Symmetries of The Dirac Equation

This chapter looks at the symmetries of the linear Dirac equation beginning with discrete symmetries which include *parity transformation(s)*, and *time inversion*. We also look at the Lorentz invariance of the Dirac equation. The Lorentz invariance is a symmetry property of the Dirac equation such that the transformation of a spinor $\psi(t,x) \in \mathbb{C}^N$, $(t,x) \in \mathbb{R} \times \mathbb{R}^D$, with $N = 2^d$, $d \in \mathbb{N}$ does not alter the structure of the Dirac equation, that is, it only results in the original function $\psi(t,x)$ multiplied with a matrix exponential.

3.1 Discrete symmetries

Discrete symmetries in the context of the linear Dirac equation consist of transformations such as: (a) *parity transformation*, which is a reflection of the spatial coordinate(s), (b) *times inversion*, which corresponds to a reflection of the time axis.

Let $\psi(t,x) \in \mathbb{C}^N$ be a solution to the Dirac equation (2.36) with $N = 2^d$ and $x \in \mathbb{R}^D$, where $D = 2d-1$ or $D = 2d$ is the spatial dimension. We assume that there are $2d+1$ Dirac matrices (α^i), $1 \leq i \leq 2d$, and β, such that $\alpha^{2i-1}, 1 \leq i \leq d$ and β are real, while α^{2i} with $1 \leq i \leq d$ are imaginary. This is done to ensure that the matrices are in agreement with the standard case of $D = 3$ with $N = 4$, and the construction of higher dimensional Dirac matrices in (2.29).

Before we begin studying discrete symmetries it is useful to define the free Dirac operator.

Definition 3.1.1 (Dirac operator in $\mathbb{R}^n$)**.** *Let $m \geq 0$, n, $N \in \mathbb{N}$. We define a free Dirac operator*

$$D_m : L^2\left(\mathbb{R}^n, \mathbb{C}^N\right) \to L^2\left(\mathbb{R}^n, \mathbb{C}^N\right), \qquad \mathfrak{D}(D_m) = H^1\left(\mathbb{R}^n, \mathbb{C}^N\right)$$

by

$$D_m : \psi \mapsto D_m\psi = (D_0 + \beta m)\,\psi, \tag{3.1}$$

with

$$D_0 = -i\boldsymbol{\alpha} \cdot \boldsymbol{\nabla} = -i\alpha^i \frac{\partial}{\partial x^i},$$

where the summation in $1 \leq i \leq n$ *is a assumed. The symbol* $\mathfrak{D}(\cdot)$ *denotes the domain of a linear operator.*

3.1.1 Parity transformation

For any spatial dimension $D \in \mathbb{N}$ and $N = 2^d$, $d \in \mathbb{N}$, the linear Dirac equation

$$i\partial_t \psi = D_m \psi = (-i\boldsymbol{\alpha} \cdot \boldsymbol{\nabla} + \beta m)\psi, \qquad \psi(t,x) \in \mathbb{C}^N, \qquad (t,x) \in \mathbb{R} \times \mathbb{R}^D$$

is invariant with respect to the *parity transformation*:

$$\mathcal{P} : \psi(t,x) \mapsto \psi^{\mathcal{P}}(t,x) := \beta\psi(t,-x), \qquad (t,x) \in \mathbb{R} \times \mathbb{R}^D. \tag{3.2}$$

3.1.2 Time inversion

When the number of spatial dimensions is $D = 2d-1$, for spinors with $N = 2^d$, $d \in \mathbb{N}$,the total *time-reversal transformation* is

$$\mathcal{T} : \psi(t,x) \mapsto \psi^{\mathcal{T}}(t,x) := i\gamma^1\gamma^3 K\psi(-t,x), \tag{3.3}$$

where $K : \mathbb{C} \times \mathbb{C}^D \mapsto \mathbb{C} \times \mathbb{C}^D$ is the complex conjugation and $(t,x) \in \mathbb{R} \times \mathbb{R}^D$. Equation (3.3) can further be simplified into the form

$$\begin{aligned} \psi(t,x) \mapsto & i\gamma^1\gamma^3 K\psi(-t,x) \\ = & i\gamma^1\gamma^3\psi^*(-t,x) \\ = & i\gamma^1\gamma^3\gamma^0\bar{\psi}^T(-t,x), \end{aligned}$$

$$\psi(t,x) \mapsto i\gamma^2\gamma^5\bar{\psi}^T(-t,x). \tag{3.4}$$

3.2 Lorentz covariance of the Dirac equation

In this section, we investigate how spinors of the Dirac equation transform under Lorentz transformations. As in special relativity, we expect that the laws of motion to be identical in all inertial frames of reference.

Definition 3.2.1 (Lorentz transformation)**.** *A homogeneous Lorentz transformation of* $\mathbb{R}^4$ *is a linear map* $\Lambda : \mathbb{R}^4 \mapsto \mathbb{R}^4$ *with*

$$\langle \Lambda y, \Lambda x \rangle = \langle y, x \rangle \text{ for all } x, y \in \mathbb{R}^4, \tag{3.5}$$

where $\langle y, x \rangle = y^\mu x_\mu = y_\mu x^\mu$*. The elements of the matrix* Λ *are denoted by* Λ^μ_ν*.*

The task at hand is to demonstrate that the structure of the Dirac equation is identical in both coordinate systems i.e. the primed and unprimed. We construct $\psi'(x^\mu)$ from $\psi(x^\mu)$ as follows

$$\psi'(x'^\mu) = S(\Lambda)\psi(x^\mu), \qquad \psi(x^\mu) = S(\Lambda)^{-1}\psi'(x'^\mu) \tag{3.6}$$

where $S(\Lambda)$ has the same dimensions as the γ_μ matrices and $x'^\mu = \Lambda^\mu_\nu x_\nu$ is the Lorentz transformation between two coordinate systems as per Def.3.5. In $(3+1)$-dimensions $S(\Lambda)$ is a 4×4, and in both $(2+1)$ and $(1+1)$ dimensional case $S(\Lambda)$ is a 2×2 matrix. The $S(\Lambda)$ matrix transforms the spinors linearly. The Lorentz covariance of (2.36) demands that ψ'^μ obey

$$\left(-i\gamma^\mu\partial'_\mu + m\right)\psi' = 0, \qquad (c=\hbar=1) \tag{3.7}$$

the matrices γ^μ are unchanged under the Lorentz transformation. To show the covariance of the Dirac equation we cast (2.36) (with $c=\hbar=1$) into (3.7) using (3.6) as follows

$$\left(-i\gamma^\mu\Lambda^\nu_\mu\partial'_\nu + m\right)S(\Lambda)^{-1}\psi'(x'^\mu) = 0,$$

multiplying by $S(\Lambda)$ from the left yields

$$-iS(\Lambda)\gamma^\mu\Lambda^\nu_\mu\partial'_\nu S(\Lambda)^{-1}\psi' + mS(\Lambda)S(\Lambda)^{-1}\psi' = 0.$$

Comparing the above expression with (3.7) we find that the Dirac equation is invariant if S satisfies the relation

$$S(\Lambda)^{-1}\gamma^\nu S(\Lambda) = \Lambda^\nu_\mu\gamma^\mu. \tag{3.8}$$

Equation (3.8) is true for both the *tardyonic* and *tachyonic* Dirac equations.

3.2.1 The special orthogonal group

The $SO(n)$ group is a group that captures rotations of n dimensional (abstract) objects. The SO simply refers to the fact that this is a *special orthogonal* group. Let us begin by looking at the notion of orthogonality. An $n\times n$ matrix A is said to orthogonal if

$$(A^T)_{ik}A_{kj} = \delta_{ij}, \tag{3.9}$$

where the superscript T denotes the transposition of a matrix and repeated indices are summed over. From (3.9) we can see that if

$$A^T A = I,$$

then since

$$\det A^T = \det A$$

this implies that

$$(\det A)^2 = \det I = 1.$$

We, therefore, have that $\det A = \pm 1$ for all orthogonal matrices. Let us look at some definitions.

Definition 3.2.2 (Orthogonal group)**.** *Let A be an $n\times n$ matrix , where $n\geq 1$. The real orthogonal group $O(n)$ is*

$$O(n) := \{A\in \mathbf{GL}(n,\mathbb{R}) \mid A^T A = I\}, \tag{3.10}$$

where $\mathbf{GL}(n,\mathbb{R})$ is a group of all $n\times n$ invertible matrices with real entries called the general linear group over $\mathbb{R}$.

Definition 3.2.3 (Special orthogonal group)**.** *Let A be an $n \times n$ matrix, the set $SO(n)$ of orthogonal matrices with unit determinant is*

$$SO(n) := \{A \in \mathbf{GL}(n, \mathbb{R}) \mid A^T A = I, \det A = 1\}. \tag{3.11}$$

Theorem 2 (Cayley-Hamilton)**.** *A matrix satisfies its own characteristic equation. That is if the characteristic equation of an $n \times n$ matrix A is*

$$\lambda^n + a_{n-1}\lambda^{n-1} + \cdots + a_1\lambda + a_0 = 0, \tag{3.12}$$

then

$$A^n + a_{n-1}A^{n-1} + \cdots + a_1 A + a_0 I = 0. \tag{3.13}$$

3.2.2 Rotational group in three dimensions

We begin first by looking at the rotation group $SO(3)$, the rotation group $SO(3)$ will be useful in our analysis of the $(2+1)$ and $(3+1)$ dimensional Dirac equation. Rotations of three-dimensional objects are generated by the group $SO(3)$ ($n = 3$ in (3.11)), that is, the orthogonal matrices A are 3×3. In the (present) case of $n = 3$, there exist three planes of rotations, namely

$$(x^1, x^2),\ (x^1, x^3),\ (x^2, x^3).$$

This implies that there are a total of three rotational matrices with three angles of rotation let's call them ω_1, ω_2 and ω_3. Now let $\hat{\mathbf{n}}$ be a unit vector denoting the direction of rotation. An element $A(\hat{\mathbf{n}}, \omega) \in SO(3)$ representing rotations in $\mathbb{R}^3$ in the direction of $\hat{\mathbf{n}}$ satisfies the following relations

$$A(\hat{\mathbf{n}}, \omega + 2\pi) = A(\hat{\mathbf{n}}, \omega) = A(-\hat{\mathbf{n}}, 2\pi - \omega), \tag{3.14}$$

$$A(\hat{\mathbf{n}}, \pi) = A(-\hat{\mathbf{n}}, \pi), \tag{3.15}$$

where ω is taken as the length of a vector defined as $\boldsymbol{\omega} = (\omega_1, \omega_2, \omega_3)$. The rotation matrices in the three planes of rotation stated above can be written as

$$A(e_1, \omega) = \begin{pmatrix} 1 & 0 & 0 \\ 0 & \cos\omega & -\sin\omega \\ 0 & \sin\omega & \cos\omega \end{pmatrix} = e^{-i\omega T_1}, \tag{3.16}$$

$$A(e_2, \omega) = \begin{pmatrix} \cos\omega & 0 & \sin\omega \\ 0 & 1 & 0 \\ -\sin\omega & 0 & \cos\omega \end{pmatrix} = e^{-i\omega T_2}, \tag{3.17}$$

$$A(e_3, \omega) = \begin{pmatrix} \cos\omega & -\sin\omega & 0 \\ \sin\omega & \cos\omega & 0 \\ 0 & 0 & 1 \end{pmatrix} = e^{-i\omega T_3}, \tag{3.18}$$

where

$$T_1 = \begin{pmatrix} 0 & 0 & 0 \\ 0 & 0 & -i \\ 0 & i & 0 \end{pmatrix},\ T_2 = \begin{pmatrix} 0 & 0 & i \\ 0 & 0 & 0 \\ -i & 0 & 0 \end{pmatrix},\ T_3 = \begin{pmatrix} 0 & -i & 0 \\ i & 0 & 0 \\ 0 & 0 & 0 \end{pmatrix} \tag{3.19}$$

are the generators of $SO(3)$. These satisfy the commutation relations

$$[T_j, T_k] = i\epsilon_{jkl}T_l, \tag{3.20}$$

which in physics are interpreted as angular momentum commutation relations.

The exponential $e^{-i\omega\mathbf{n}\cdot\mathbf{T}}$ can be expanded into its real and imaginary parts. To expand the exponential we used the fact that

$$\hat{\mathbf{n}}\cdot\mathbf{T} = \begin{pmatrix} 0 & -in_3 & in_2 \\ in_3 & 0 & -in_1 \\ -in_2 & in_1 & 0, \end{pmatrix} \tag{3.21}$$

where (3.21) has a characteristic equation of the form: $-\lambda^3 + (\hat{\mathbf{n}}\cdot\hat{\mathbf{n}})\lambda = -\lambda^3 + \lambda = 0$, $\lambda \in \mathbb{R}$. Using Thm.2 we find that $(\hat{\mathbf{n}}\cdot\mathbf{T})^3 - \hat{\mathbf{n}}\cdot\mathbf{T} = 0$, which gives the higher powers to be $(\hat{\mathbf{n}}\cdot\mathbf{T})^4 = (\hat{\mathbf{n}}\cdot\mathbf{T})^2$, $(\hat{\mathbf{n}}\cdot\mathbf{T})^5 = (\hat{\mathbf{n}}\cdot\mathbf{T})^3 = \hat{\mathbf{n}}\cdot\mathbf{T}$, $(\hat{\mathbf{n}}\cdot\mathbf{T})^6 = (\hat{\mathbf{n}}\cdot\mathbf{T})^4 = (\hat{\mathbf{n}}\cdot\mathbf{T})^2$ and so on. With this we are able to expand $A(\hat{\mathbf{n}}, \omega)$ as follows:

$$\begin{aligned} A(\hat{\mathbf{n}}, \omega) =& e^{-i\omega\mathbf{n}\cdot\mathbf{T}} \\ =& I - i\omega(\hat{\mathbf{n}}\cdot\mathbf{T}) - \frac{1}{2!}\omega^2(\hat{\mathbf{n}}\cdot\mathbf{T})^2 + \frac{(i\omega)^3}{3!}(\hat{\mathbf{n}}\cdot\mathbf{T})^3 + \dots. \end{aligned}$$

Gathering the even and odd powers separately yields

$$\begin{aligned} A(\hat{\mathbf{n}}, \omega) =& I - (\hat{\mathbf{n}}\cdot\mathbf{T})^2 + (\hat{\mathbf{n}}\cdot\mathbf{T})^2\left(1 - \frac{1}{2!}\omega^2 + \frac{1}{4!} + \dots\right) \\ & - (\hat{\mathbf{n}}\cdot\mathbf{T})\left(\omega - \frac{1}{3!}\omega^3 + \frac{1}{5}\omega^5 + \dots\right), \end{aligned}$$

that is

$$A(\hat{\mathbf{n}}, \omega) = I - (\hat{\mathbf{n}}\cdot\mathbf{T})^2 + (\hat{\mathbf{n}}\cdot\mathbf{T})^2\cos\omega - (\hat{\mathbf{n}}\cdot\mathbf{T})\sin\omega. \tag{3.22}$$

3.2.3 Lorentz transformations in (3+1) dimensional space-time

The nature of space-time as commonly understood is that an event is represented by the coordinates x^0, x^1, x^2, x^3. This means that the space of space-time in special relativity is $\mathbb{R}^4$. The main idea in special relativity is that two inertial frames or rather coordinate systems separated by a uniform velocity are related by a linear transformation called a *proper Lorentz transformation*.

Rotations of the coordinate (x^1, x^2, x^3) around the three planes of rotations are given by the following matrices

$$\tilde{A}(e_1, \omega) = \begin{pmatrix} 1 & 0 & 0 & 0 \\ 0 & 1 & 0 & 0 \\ 0 & 0 & \cos\omega & -\sin\omega \\ 0 & 0 & \sin\omega & \cos\omega \end{pmatrix} = e^{-i\omega J_1}, \tag{3.23}$$

$$\tilde{A}(e_2,\omega) = \begin{pmatrix} 1 & 0 & 0 & 0 \\ 0 & \cos\omega & 0 & \sin\omega \\ 0 & 0 & 1 & 0 \\ 0 & -\sin\omega & 0 & \cos\omega \end{pmatrix} = e^{-i\omega J_2}, \tag{3.24}$$

$$\tilde{A}(e_3,\omega) = \begin{pmatrix} 1 & 0 & 0 & 0 \\ 0 & \cos\omega & -\sin\omega & 0 \\ 0 & \sin\omega & \cos\omega & 0 \\ 0 & 0 & 0 & 1 \end{pmatrix} = e^{-i\omega J_3}, \tag{3.25}$$

where

$$J_1 = \begin{pmatrix} 0 & 0 & 0 & 0 \\ 0 & 0 & 0 & 0 \\ 0 & 0 & 0 & -i \\ 0 & 0 & i & 0 \end{pmatrix}, \; J_2 = \begin{pmatrix} 0 & 0 & 0 & 0 \\ 0 & 0 & 0 & i \\ 0 & 0 & 0 & 0 \\ 0 & -i & 0 & 0 \end{pmatrix}, \; J_3 = \begin{pmatrix} 0 & 0 & 0 & 0 \\ 0 & 0 & -i & 0 \\ 0 & i & 0 & 0 \\ 0 & 0 & 0 & 0 \end{pmatrix}. \tag{3.26}$$

These are the rotation generators seen in section (3.2.2) with an added coordinate x^0. These satisfy the algebra

$$[J_j, J_k] = i\epsilon_{jkl} J_l. \tag{3.27}$$

The matrices of the Lorentz boost are

$$B(e_1,\gamma) = \begin{pmatrix} \cosh\eta & \sinh\eta & 0 & 0 \\ \sinh\eta & \cosh\eta & 0 & 0 \\ 0 & 0 & 1 & 0 \\ 0 & 0 & 0 & 1 \end{pmatrix} = e^{\eta K_1}, \tag{3.28}$$

$$B(e_2,\gamma) = \begin{pmatrix} \cosh\eta & 0 & \sinh\eta & 0 \\ 0 & 1 & 0 & 0 \\ \sinh\eta & 0 & \cosh\eta & 0 \\ 0 & 0 & 0 & 1 \end{pmatrix} = e^{\eta K_2}, \tag{3.29}$$

$$B(e_3,\gamma) = \begin{pmatrix} \cosh\eta & 0 & 0 & \sinh\eta \\ 0 & 1 & 0 & 0 \\ 0 & 0 & 1 & 0 \\ \sinh\eta & 0 & 0 & \cosh\eta \end{pmatrix} = e^{\eta K_3}, \tag{3.30}$$

where

$$\cosh\eta = \gamma = \frac{1}{\sqrt{1-\beta^2}}, \tag{3.31}$$

$$\sinh\eta = \gamma\beta = \frac{\beta}{\sqrt{1-\beta^2}}, \tag{3.32}$$

and the generators K_i are

$$K_1 = \begin{pmatrix} 0 & i & 0 & 0 \\ i & 0 & 0 & 0 \\ 0 & 0 & 0 & 0 \\ 0 & 0 & 0 & 0 \end{pmatrix}, \; K_2 = \begin{pmatrix} 0 & 0 & 0 & i \\ 0 & 0 & 0 & 0 \\ i & 0 & 0 & 0 \\ 0 & 0 & 0 & \end{pmatrix}, \; K_3 = \begin{pmatrix} 0 & 0 & 0 & i \\ 0 & 0 & 0 & 0 \\ 0 & 0 & 0 & 0 \\ i & 0 & 0 & 0 \end{pmatrix}. \tag{3.33}$$

These generators satisfy the following algebra

$$[K_j, K_k] = -i\epsilon_{jkl} J_l. \tag{3.34}$$

3.2.4 Lorentz transformations in (2+1) dimensional space-time

The generators of Lorentz transformations in (2+1)-dimensional space-time can be computed by use of equation (3.43), just to jump ahead a little bit, where $L_0 = \sigma^{12}$ is a generator of rotations on the (x, y) plane and $L_1 = \sigma^{01}$ and $L_2 = \sigma^{02}$ generate Lorentz boost along the x and y axis respectively. These generators can be written explicitly as

$$L_0 := \frac{1}{2}\sigma^3,\ L_1 := \frac{i}{2}\sigma_1,\ L_2 := \frac{i}{2}\sigma_2, \tag{3.35}$$

where the L_i satisfy the following algebraic relations

$$[L_1, L_2] = iL_0, \qquad [L_0, L_2] = iL_1, \qquad [L_0, L_1] = -iL_2. \tag{3.36}$$

3.3 Construction of the S matrix

In section 3.2 we showed that in order for the Dirac equation to be invariant under Lorentz transformations the matrix S must satisfy equation (3.8). The matrix S contains all the information about transformations in the Lorentz group, for example, rotations and Lorentz boosts. In this section, the explicit form of this matrix will be calculated in terms of the Dirac matrices. We begin by considering infinitesimal Lorentz transformations and then proceed to construct the finite transformations considering a series of infinitesimal transformations.

Let us consider first an infinitesimal Lorentz transformation of the form

$$x'^\mu = \Lambda^\mu_\nu x^\nu = (\delta^\mu_\nu + \epsilon^\mu_\nu)x^\nu = x^\mu + \epsilon^\mu_\nu x^\nu, \tag{3.37}$$

where the infinitesimal matrix ϵ satisfies

$$\epsilon^{\mu\nu} = -\epsilon^{\nu\mu}. \tag{3.38}$$

Having written down the infinitesimal transformation, we can now expand the matrix $S(\Lambda)$ in terms of $\epsilon^{\mu\nu}$ as

$$S(\Lambda) = S(\epsilon) = I - \frac{i}{4}\chi_{\mu\nu}\epsilon^{\mu\nu}, \tag{3.39}$$

where the matrices $\chi_{\mu\nu}$ are also assumed to satisfy

$$\chi_{\mu\nu} = -\chi_{\nu\mu}. \tag{3.40}$$

We can also write the inverse of (3.39) as

$$S^{-1}(\epsilon) = I + \frac{i}{4}\chi_{\mu\nu}\epsilon^{\mu\nu}. \tag{3.41}$$

We can show that (3.41) is indeed an inverse, that is its product with $S(\epsilon)$ gives the identity matrix,

$$\begin{aligned} S^{-1}(\epsilon)S(\epsilon) &= \left(I - \frac{i}{4}\chi_{\mu\nu}\epsilon^{\mu\nu}\right)\left(I + \frac{i}{4}\chi_{\mu\nu}\epsilon^{\mu\nu}\right) \\ &= I + \frac{i}{4}\chi_{\mu\nu}\epsilon^{\mu\nu} - \frac{i}{4}\chi_{\mu\nu}\epsilon^{\mu\nu} + \mathcal{O}(\epsilon^2) \\ &= I + \mathcal{O}(\epsilon^2). \end{aligned}$$

This confirms that the leading orders in the product $S^{-1}(\epsilon)S(\epsilon)$ does yield the identity matrix, therefore (3.41) is an inverse of (3.39).

The infinitesimal matrix of Lorentz transformations are required to satisfy equation (3.8). Plugging (3.39) and its inverse into (3.8) yields:

$$\begin{aligned} S^{-1}(\epsilon)\gamma^\mu S(\epsilon) = \Lambda^\mu_\nu\gamma^\nu = (\delta^\mu_\nu + \epsilon^\mu_\nu)\gamma^\mu, \\ \left(I - \frac{i}{4}\chi_{\lambda\rho}\epsilon^{\lambda\rho}\right)\gamma^\mu\left(I + \frac{i}{4}\chi_{\sigma\tau}\epsilon^{\sigma\tau}\right) = \gamma^\mu + \epsilon^\mu_\nu\gamma^\nu \\ \gamma^\mu + \frac{i}{4}\epsilon^{\lambda\rho}\chi_{\lambda\rho}\gamma^\mu - \frac{i}{4}\epsilon^{\lambda\rho}\gamma^\mu\chi_{\lambda\rho} + \mathcal{O}(\epsilon^2) = \gamma^\mu + \epsilon^\mu_\nu\gamma^\nu, \\ -\frac{i}{4}\epsilon_{\lambda\rho}[\gamma^\mu, \chi^{\lambda\rho}] = \epsilon^\mu_\nu\gamma^\nu. \end{aligned} \tag{3.42}$$

The task of establishing the Lorentz covariance of the Dirac equation is now reduced to finding matrices that satisfy the relation in (3.42). To do this, let us define a set of matrices via the commutator

$$\sigma^{\mu\nu} := \frac{i}{2}[\gamma^\mu, \gamma^\nu]. \tag{3.43}$$

It is clear from the definition that $\sigma^{\mu\nu} = -\sigma^{\nu\mu}$. Notice that

$$\begin{aligned} \sigma^{\mu\nu} &= \frac{i}{2}\left(\gamma^\mu\gamma^\nu - \gamma^\nu\gamma^\mu\right) \\ &= \frac{i}{2}\left(2g^{\mu\nu}I - 2\gamma^\nu\gamma^\mu\right), \end{aligned}$$

therefore

$$\sigma^{\mu\nu} = i(g^{\mu\nu}I - \gamma^\nu\gamma^\mu). \tag{3.44}$$

With this we can evaluate the commutator $[\gamma^\mu, \sigma^{\nu\lambda}]$ as follows

$$\begin{aligned} [\gamma^\mu, \sigma^{\mu\nu}] &= [\gamma^\mu, i\left(g^{\nu\lambda} - \gamma^\nu\gamma^\lambda\right)] \\ &= i[\gamma^\mu, \gamma^\nu\gamma^\lambda] \\ &= i\left(\{\gamma^\mu, \gamma^\nu\}\gamma^\lambda - \gamma^\nu\{\gamma^\mu, \gamma^\lambda\}\right), \end{aligned}$$

therefore

$$[\gamma^\mu, \sigma^{\nu\lambda}] = 2i\left(g^{\mu\nu}\gamma^\lambda - g^{\mu\lambda}\gamma^\nu\right). \tag{3.45}$$

We can now identify $\chi^{\lambda\rho}$ in (3.42) with $\sigma^{\nu\lambda}$ in the above commutator. To show that this identification make sense we evaluate

$$\begin{aligned} -\frac{i}{4}\epsilon_{\lambda\rho}[\gamma^\mu, \chi^{\lambda\rho}] &= -\frac{i}{4}\epsilon_{\lambda\rho} \times 2i\left(g^{\mu\lambda}\gamma^\rho - g^{\mu\rho}\gamma^\lambda\right) \\ &= \frac{1}{2}\left(\epsilon^\mu_\rho\gamma^\rho + \epsilon^\mu_\lambda\gamma^\lambda\right) = \epsilon^\mu_\nu\gamma^\nu, \end{aligned}$$

which is the same as the right hand side of (3.42). Finally we can write

$$S(\epsilon) = I - \frac{i}{4}\sigma_{\mu\nu}\epsilon^{\mu\nu}. \tag{3.46}$$

We have successfully calculated the infinitesimal matrix $S(\epsilon)$ as shown in (3.46). The remaining task is to extend this matrix to a finite form. This is done by considering a series of such infinitesimal transformations as and taking the large N limit:

$$S(\Lambda) = \lim_{N\to\infty}\left(I - \frac{i}{4N}\sigma_{\mu\nu}\epsilon^{\mu\nu}\right)^N = e^{-\frac{i}{4}\sigma_{\mu\nu}\epsilon^{\mu\nu}}. \tag{3.47}$$

The factor of $\frac{1}{N}$ in the above expression implies that the finite transformation is decomposed into a sequence of N steps. Equation (3.47) shows that the transformations of spinor amount to a multiplication by a complex matrix exponential.

3.3.1 The S matrix in 3+1 dimensions

Having constructed the $S(\Lambda)$ i.e. the matrix consisting of all the transformations within the Lorentz group, we will show explicitly what this matrix is in the $(3+1)$-dimensional case, and the $(2+1)$ and $(1+1)$ dimensional cases thereafter. Recall that the finite transformation (3.47) was constructed through a consideration of a series of infinitesimal transformations. As an example, let us consider a rotation about the z axis through an angle $\omega/2$:

$$\psi'(x') = S(\Lambda)\psi(x) = \lim_{N\to\infty}\left(1 + \frac{i}{2N}\omega\sigma^{12}\right)^N\psi(x) = e^{\frac{i}{2}\omega\sigma^{12}}\psi(x), \tag{3.48}$$

where σ^{12} can be identified as the generator of a rotation on the z-axis. As in (3.22), we can Taylor expand $e^{\frac{i}{2}\omega\sigma^{12}}$ and write it in terms of sines and cosines. First, notice that $\sigma^{12} = J_3$ since J_3 (in (3.26)) is a generator of a rotation around the z axis. The generator J_3 has a characteristic equation of the form $\lambda^2 - 1 = 0$, $\lambda \in \mathbb{R}$. Using Thm. 2 we find that the higher powers of J_3 are

$$(J_3)^2 = I, \qquad (J_3)^{2n} = I, \qquad (J_3)^{2n+1} = J_3, \qquad n \in \mathbb{N}.$$

With these relations we can write $e^{\frac{i}{2}\omega J_3}$ as

$$
\begin{aligned}
e^{\frac{i}{2}\omega J_3} =& \sum_{k=0}^{\infty} \frac{i^k \left(\frac{\omega}{2} J_3\right)^k}{k!}, \qquad k \in \mathbb{N} \\
=& \sum_{p=0}^{\infty} \frac{(-1)^p \left(\frac{\omega J_3}{2}\right)^{2p}}{(2p!)} + i \sum_{q=0}^{\infty} \frac{(-1)^q \left(\frac{\omega J_3}{2}\right)^{2q+1}}{(2q+1)!}, \qquad p, q \in \mathbb{N}, \\
=& I \sum_{p=0}^{\infty} \frac{(-1)^p \left(\frac{\omega}{2}\right)^{2p}}{(2p!)} + i J_3 \sum_{q=0}^{\infty} \frac{(-1)^q \left(\frac{\omega}{2}\right)^{2q+1}}{(2q+1)!} \\
=& \left(I \cos \frac{\omega}{2} + i J_3 \sin \frac{\omega}{2} \right).
\end{aligned}
$$

We can now write

$$\psi'(x') = \left(I \cos \frac{\omega}{2} + i J_3 \sin \frac{\omega}{2} \right) \psi(x). \tag{3.49}$$

Equation (3.49) is a reduction of (3.48) into a simpler form through sines and cosines. The Lorentz boost of ψ along the x axis is done according to $\psi'(x') = S(\Lambda)\psi(x)$, with S being

$$
\begin{aligned}
S(\Lambda) =& e^{-(i/2)\omega\sigma^{01}} \\
=& I \cosh \frac{\eta}{2} + K_1 \sinh \frac{\eta}{2},
\end{aligned}
$$

where we have expanded $e^{-(i/2)\omega\sigma^{01}}$ as (in the case of rotations) above, we have used the fact that $\sigma^{01} = K_1$, since K_1 (3.33) is the generator of a Lorentz boost along the x axis.

3.3.2 The S matrix in 2+1 dimensions

The generators of Lorentz transformations in (2+1)-dimensional space time can be computed by use of equation (3.43) where $L_0 = \sigma^{12}$ is a generator of rotations on the (x, y) plane and $L_1 = \sigma^{01}$ and $L_2 = \sigma^{02}$ generate Lorentz boost along the x and y axis respectively. These generators can be written explicitly as

$$L_0 := \frac{1}{2}\sigma^3, \; L_1 := \frac{i}{2}\sigma_1, \; L_2 := \frac{i}{2}\sigma_2, \tag{3.50}$$

where the L_i satisfy the following algebraic relations

$$[L_1, L_2] = iL_0, \qquad [L_0, L_2] = iL_1, \qquad [L_0, L_1] = -iL_2. \tag{3.51}$$

With help of these generators (3.50) we can write the S in each case as $S(\Lambda) = e^{-i\omega\sigma^3/2}$ for rotations and $S(\Lambda) = e^{\beta\sigma^1/2}$, $S(\Lambda) = e^{-\alpha\sigma^3/2}$ for Lorentz boosts along x and y respective. These can be written in matrix form as

$$
\begin{aligned}
S(\Lambda) =& e^{-i\omega\sigma^3/2}, \\
=& I \cos \frac{\omega}{2} - i\sigma_3 \sin \frac{\omega}{2},
\end{aligned}
$$

$$S(\Lambda) = \begin{pmatrix} e^{i\omega/2} & 0 \\ 0 & e^{-i\omega/2} \end{pmatrix}, \tag{3.52}$$

for rotations in the (x, y) plane. The matrix representation of S for boosts along x and y becomes

$$S(\Lambda) = \begin{pmatrix} \cosh\frac{\beta}{2} & \sinh\frac{\beta}{2} \\ \sinh\frac{\beta}{2} & \cosh\frac{\beta}{2} \end{pmatrix}, \qquad S(\Lambda) = \begin{pmatrix} \cosh\frac{\alpha}{2} & -i\sinh\frac{\alpha}{2} \\ i\sinh\frac{\alpha}{2} & \cosh\frac{\alpha}{2} \end{pmatrix}. \tag{3.53}$$

The Lorentz invariance of the *tachyonic* Dirac equation means that the transformation of the spinor $\psi \mapsto S(\Lambda)\psi$, with $S(\Lambda)$ being chosen as in (3.52)-(3.53), does not change the structure of (2.55). We can formally write down how the spinor components u and v transform under Lorentz transformation as follows:

1. *Rotations on the* (x, y) *plane*

$$u \mapsto e^{i\omega/2}u, \qquad v \mapsto e^{-i\omega/2}v, \tag{3.54}$$

2. *Boost along* x

$$u \mapsto \cosh\frac{\beta}{2}u + \sinh\frac{\beta}{2}v, \qquad v \mapsto \cosh\frac{\beta}{2}v + \sinh\frac{\beta}{2}u, \tag{3.55}$$

3. *Boost along* y

$$u \mapsto \cosh\frac{\alpha}{2}u - i\sinh\frac{\alpha}{2}v, \qquad v \mapsto \cosh\frac{\alpha}{2}v + i\sinh\frac{\alpha}{2}u. \tag{3.56}$$

3.3.3 Discrete symmetries

Discrete symmetries in the context of the linear Dirac equation consist of transformations such as: (a) *parity transformation*, which reflects the spatial coordinate(s), (b) *times inversion*, which corresponds to a reflection of the time axis. These transformations are [23]:

1. *Parity*

$$\psi(t, \mathbf{x}) \mapsto \psi^{\mathcal{P}}(t, \mathbf{x}) = \beta\psi(t, -\mathbf{x}) \tag{3.57}$$

2. *Time inversion*

$$\psi(t, \mathbf{x}) \mapsto i\gamma^2\gamma^5\bar{\psi}^T(-t, \mathbf{x}), \tag{3.58}$$

where the superscript T denotes matrix transposition and the role of γ^5 above is played by the 2×2 identity matrix. The transformations can be written in terms of the spinor components u and v as

$$u(t, \mathbf{x}) \mapsto u(t, -\mathbf{x}), \qquad v(t, \mathbf{x}) \mapsto -v(t, -\mathbf{x}), \tag{3.59}$$

for parity. For time inversion we have

$$u(t, \mathbf{x}) \mapsto v^*(-t, \mathbf{x}), \qquad v(t, \mathbf{x}) \mapsto u^*(-t, \mathbf{x}), \tag{3.60}$$

where we have used the fact that $\bar{\psi}^T = (\psi^\dagger\beta)^T = \beta^T(\psi^\dagger)^T = \beta(\psi^\dagger)^T$, with $\bar{\psi} = \psi^\dagger\gamma^0$ being the *adjoint spinor*. It is worth noting that the imaginary mass Hamiltonian (2.51) is not in variant under a time inversion since [27]

$$\mathcal{T} : H = -i\alpha^k\partial_k + i\beta m \mapsto -i\alpha^k\partial_k - i\beta m, \tag{3.61}$$

where $\alpha^k \mapsto -\alpha^k$, $-i\partial_k \mapsto i\partial_k$ and $im \mapsto -im$.

3.3.4 The S matrix in 1+1 dimensions

In the $(1+1)$-dimensional the only operations that can be performed are Lorentz boost and discrete transformations on the (t, x) plane, with $(t, x) \in \mathbb{R} \times \mathbb{R}$. The S matrix of a Lorentz boost along the x-axis is:

$$S(\Lambda) = e^{-\frac{\eta}{2}\sigma_1} = \begin{pmatrix} \cosh\frac{\eta}{2} & -\sinh\frac{\eta}{2} \\ -\sinh\frac{\eta}{2} & \cosh\frac{\eta}{2} \end{pmatrix}. \tag{3.62}$$

In order to write the discrete transformations explicitly in $(1+1)$ dimensions we adopt the spinor representation of the γ-matrices, the Dirac equation in this representation was written down in equation (2.46). Discrete transformations in the $(1+1)$ dimensions are

$$u(t, x) \mapsto v^*(-t, x), \qquad v(t, x) \mapsto u^*(-t, x), \tag{3.63}$$

for parity transformation, where we have used (3.2) with $\gamma^0 = \sigma^1$. In the case of time reversal transformation, we adopt the method used by the authors of Ref.[31] by defining the transformation as

$$\mathcal{T} : \ \psi(t, x) \mapsto \mathcal{T}\psi(t, x)\mathcal{T}^{-1} = \gamma^0\psi^*(-t, x). \tag{3.64}$$

Writing this in terms of the spinor components u and v we obtain

$$u(t, x) \mapsto v^*(-t, x), \qquad v(t, x) \mapsto u^*(-t, x). \tag{3.65}$$

3.4 Chapter summary

This chapter looked at the symmetries of the linear Dirac equation, in particular, the construction of the matrix $S(\Lambda)$ which consists of transformations in the Lorentz group. This matrix was constructed by first considering infinitesimal Lorentz transformations and extending those to a finite transformation through a series of infinitesimal transformations. We discovered in (3.47) that the Lorentz transformation of spinors amounts to a multiplication by a complex matrix exponential. For this matrix to render the Dirac equation (both *tardyonic* and *tachyonic*) invariant under Lorentz transformations, it had to satisfy equation (3.8). Next, we studied discrete symmetries in section 3.1. On the subject of discrete symmetries, we looked at *parity transformation(s)* (3.2) and *time reversal transformation* (3.3). Sections 3.3.1-3.3.4 looked at specific Lorentz transformations, in particular: rotations in $(3+1)$, $(2+1)$ and $(1+1)$ dimensional space-time, and Lorentz boosts in the aforementioned dimensions.

Chapter 4

Nonlinear Dirac Models

The previous chapters looked into the formulation of the Dirac equation in the absence of self-interaction. We studied the structure of the Dirac equation, including the Dirac matrices and the Clifford algebra formed by these matrices. We also looked at the Lorentz transformations and symmetry properties of both the *tachyonic* and *tardyonic* Dirac equation. In this chapter, we will study the Dirac equation with self-interaction. The nonlinear Dirac equation was introduced to model self-interacting fermions. The nonlinear Dirac model was introduced by Ivanenko in an attempt to formulate the unified field theory of elementary particles. Ivanenko did this by considering only a scalar self-interaction of fermions. Soler later used the nonlinear Dirac equation with scalar self-interaction to study extended nucleons, while Gross and Neveu used the one-dimensional version of the Soler model to study quack confinement in quantum chromodynamics[21, 32].

Another self-interaction type potential was introduced by Thirring– this potential is based on the vector self-interaction of a spinor field [33]. The massive Thirring model has been shown to be completely integrable via the inverse scattering transform [34]– the one-dimensional version of the massive Thirring model possesses solitary wave solutions and its fundamental solutions can be transformed to solitons of the sine-Gordon theory via bosonisation. Recent years have seen a growing interest in the study of near relativistic phenomena in two-dimensional materials like graphene, Bose-Einstein condensates, and photorefractive lattices or the so-called photonic graphene. In these materials atoms (or light) are arranged in a hexagonal lattice such that the near-Dirac-point expansion of the tight binding Hamiltonian of such an arrangement reduces to the Dirac Hamiltonian. It is for this reason that the nonlinear Dirac equation has seen much utility in recent years.

In optics the recurrent nonlinearity is the Kerr nonlinearity, this is a cubic-type nonlinearity which does not couple with the spinor components and thus breaks the Lorentz symmetry i.e. the nonlinearity is not invariant under Lorentz transformations[35]. Although there is a broken symmetry in the optical version of the nonlinear Dirac equation, studies have shown that these models have solitary wave solutions, vortices [10, 36] and topologically protected states and topological edge states [10, 37]. Topological edge states are found in one-dimensional lattice equations like the nonlinear Su-Schrieffer-Heeger (SSH) where the Dirac Hamiltonian is obtained by Fourier transforming the tight-binding Hamiltonian of the

SSH model. Photonic graphene and staggered graphene have also been shown to support solitons of this kind [10].

In this chapter we will consider the nonlinear Dirac equation with self-interaction in one, two and three spatial dimensions. The nonlinearities considered are the Thirring and Soler nonlinearities. We present exact solitary wave solutions of the massive Thirring model in one spatial dimension and quote the results obtained in Refs. [38, 39] in the case of the standard Soler model. Both the $(1+1)$ dimensional massive Thirring and Soler models admit stable solitary wave solutions. In two spatial dimensions, we will consider a $(2+1)$ dimensional extension of the $(2+0)$ dimensional complex sine-Gordon equation. This is a nonlinear Dirac equation with Thirring-type nonlinearity. We will study the stability of the single vortex solution of the aforementioned. Next, we will look at the Soler model in the context of the imaginary mass Dirac equation (*tachyonic*) in a constant background and see whether this version of the Soler model admits vortex solutions or not. We also consider the standard Soler model in $(2+1)$ dimensions and reproduce results obtained by Cuevas-Maraver *et al* in Ref. [40]. Lastly, we consider the $(3+1)$ dimensional Soler model and reproduce the numerical results by Soler in Ref. [41].

4.1 The massive Thirring model

The massive Thirring model considers a vector-type self-interaction of a spinor field where the Lagrangian includes the scalar product $J_\mu J^\mu$, with $J_\mu = \bar{\psi}\gamma^\mu\psi$ [42]. The product $J_\mu J^\mu$ couples with the spinor components in the Dirac equation, thus the product is invariant under Lorentz transformations (3.47). This model arose in the context of quantum field theory where theories of elementary particles were being proposed. The massive Thirring model also occurs in the context of optical gratings in which Bragg-resonant wave propagation in a Kerr medium is described [43]. The one-dimensional version of this model is completely integrable since it possesses an infinite number of conserved quantities or commuting charges [44]. The standard (*tardyonic*) Lagrangian of the massive Thirring model is

$$\mathscr{L} = \bar{\psi}\left(i\gamma^\mu\partial_\mu - m\right)\psi - \frac{1}{2}\left(\bar{\psi}\gamma^\mu\psi\right)\left(\bar{\psi}\gamma_\mu\psi\right), \qquad \mu = 0, 1, \tag{4.1}$$

where m and g are the mass and coupling constant, respectively. The equations of motion associated with (4.1) are

$$i\gamma^\mu\partial_\mu\psi + \psi + \frac{1}{2}\gamma^\mu J_\mu\psi = 0, \qquad \mu = 0, 1. \tag{4.2}$$

4.2 Massive Thirring model in 1+1 dimensions

In the spinor representation (see A.2) the $(1+1)$ dimensional massive Thirring model is

$$i(u_t + u_x) + v + |v|^2 u = 0 \tag{4.3}$$

$$i(v_t - v_x) + u + |u|^2 v = 0, \tag{4.4}$$

where the Dirac matrices in (4.2) are chosen as $\gamma^0 = \sigma^1$ and $\gamma^1 = \sigma^3$ and $\psi = (u, v)^T$, with u and v being spinor components. We are looking for the quiescent (non-propagating) wave solutions to the Thirring model. To find these types of waves we consider a solution ansatz of the form $u(x,t) = e^{-i\omega t} f(x)$ and $v(x,t) = -e^{-i\omega t} g(x)$, where the minus sign in v is chosen for convenience. Under the aforementioned assumptions, we obtain the following system of nonlinear ordinary differential equations :

$$if_x + \omega f - g + |g|^2 f = 0, \tag{4.5}$$

$$-ig_x + \omega g - f + |f|^2 g = 0. \tag{4.6}$$

The system (4.5) - (4.6) can be solved by the use of the conservation laws of the massive Thirring model, namely the conservation of charge and conservation of energy.

4.2.1 Charge conservation

The massive Thirring model admits conservation of charge law. To see this we multiply (4.5) by $\bar{f}$ and subtract the complex conjugate of the resulting equation. Carrying this operation yields

$$i\left(\bar{f} f_x - f \bar{f}_x\right) - \bar{f} g - f \bar{g} = 0. \tag{4.7}$$

Similarly, we can do the same for (4.6); doing that yields

$$-i\left(\bar{g} g_x + g \bar{g}_x\right) - f \bar{g} + \bar{f} g = 0. \tag{4.8}$$

Equations (4.7) and (4.8) can be added so that

$$i\frac{d}{dx}\left(f\bar{f}\right) - i\frac{d}{dx}\left(g\bar{g}\right) = 0.$$

Applying the boundary conditions $|u|^2, |v|^2 \to 0$ as $|x| \to \infty$ yields the charge conservation law

$$|f| = |g|. \tag{4.9}$$

4.2.2 Energy conservation

The massive Thirring model also exhibits the conservation of energy. To see this we multiply (4.5) and multiply it with $\bar{g}_x$ and add the complex conjugate of the resulting expression. Doing that yield the following equation:

$$\omega\frac{d}{dx}\left(f\bar{f}\right) - g\bar{f}_x - \bar{g} f_x + |g|^2 \frac{d}{dx}\left(f\bar{f}\right) = 0. \tag{4.10}$$

Similarly, we multiply (4.6) by $\bar{g}_x$ and subtract the complex conjugate of the resulting equation. The operation yields

$$\omega\frac{d}{dx}\left(g\bar{g}\right) - f\bar{g}_x - \bar{f} g_x + |f|^2 \frac{d}{dx}\left(g\bar{g}\right) = 0. \tag{4.11}$$

Adding (4.10) and (4.11) gives

$$\omega\frac{d}{dx}\left(|f|^2+|g|^2\right)-\frac{d}{dx}\left(\bar{f}g+f\bar{g}\right)+\frac{d}{dx}|fg|^2=0,$$

therefore

$$\omega\left(|f|^2+|g|^2\right)-\left(\bar{f}g+f\bar{g}\right)+|fg|^2=0. \tag{4.12}$$

Our task is to find soliton solutions to (4.5) and (4.6), we do this by requiring $f(x)$ and $g(x)$ to take the form $f(x)=a(x)e^{i\theta(x)}$ and $g(x)=a(x)e^{i\varphi(x)}$. Substituting $g(x)$ and $g(x)$ into (4.12)

$$2\omega a^2-2a^2\cos(\varphi-\theta)+a^4=0. \tag{4.13}$$

We are particularly interested in solutions with $|f|=|g|\neq 0$ so that we can divide the above expression by a to obtain the following identity:

$$2\omega-2\cos(\varphi-\theta)+a^2=0. \tag{4.14}$$

Substituting the Ansatz for $f(x)$ and $g(x)$ into (4.5) and (4.6) yields a coupled system of ordinary differential equations in $a(x)$, $\theta(x)$ and $\varphi(x)$. The system reads

$$-ia_x-a\theta_x+\omega a-ae^{i(\varphi-\theta)}+a^3=0, \tag{4.15}$$

$$-ia_x+a\varphi_x+\omega a-ae^{i(\theta-\varphi)}+a^3=0. \tag{4.16}$$

The above equations (4.15) and (4.16) can further be broken down into their real and imaginary parts to give the following equations

$$-a\theta_x+\omega a-a\cos(\varphi-\theta)+a^3=0, \tag{4.17}$$

$$-a_x+\sin(\varphi-\theta)=0, \tag{4.18}$$

$$a\varphi_x+\omega a-a\cos(\theta-\varphi)+a^3=0, \tag{4.19}$$

$$-a_x-a\cos(\theta-\varphi)=0. \tag{4.20}$$

We can subtract (4.19) from (4.17) to produce

$$-a(\theta_x+\varphi_x)=0,$$

from whence we notice that

$$\theta=-\varphi. \tag{4.21}$$

What is now left is to solve either (4.17) or (4.19) with the knowledge that (4.21) holds. By making a^2 the subject in (4.14), (4.17) can be re-written as

$$\theta_x=\cos 2\theta-\omega,$$

where the solution for the newly written θ_x equation can be obtained from the standard table of integrals as

$$x=\frac{1}{\sqrt{1-\omega^2}}\arctan\left\{\frac{(\omega+1)\tan\left(\frac{\theta}{2}\right)}{\sqrt{1-\omega^2}}\right\}. \tag{4.22}$$

Returning to the identity in (4.14), notice that

$$\begin{aligned}\omega - \cos 2\theta < 0,\\ \omega < \cos 2\theta,\end{aligned}$$

therefore,

$$|\omega| < 1.$$

We can call $\omega = \cos\alpha$ so that when $w > 0$ we have that $0 < \alpha < \frac{\pi}{2}$ and $\frac{\pi}{2} < \alpha < \pi$ when $\omega < 0$. Let us now direct our attention at equation (4.22) and re-write it as

$$\begin{aligned}\tan\left(\frac{\theta}{2}\right) = \frac{\sqrt{1-\omega^2}}{\omega+1}\tanh\left(\sqrt{1-\omega^2}x\right),\\ (\omega+1)\left|\tan\left(\frac{\theta}{2}\right)\right| < \sqrt{1-\omega^2},\\ |\tan(\varphi)| < \tan\left(\frac{\alpha}{2}\right),\end{aligned}$$

therefore

$$|\varphi(x)| < \alpha/2.$$

We are now able to further simplify (4.22) as

$$\tan(\varphi) = -\tan(\alpha/2)\tanh(\sin(\alpha)x). \tag{4.23}$$

We are now in a good position to find the form of $a(x)$ and write out the full solution of system (4.5)-(4.6). From (4.14) we write

$$\begin{aligned}\frac{a^2}{2} =& \cos 2\varphi - \cos\alpha\\ =& \frac{1-\tan^2\varphi}{1+\tan^2\varphi} - \cos\alpha,\\ =& \frac{2\sin^2(\alpha/2) - 2\cos^2(\alpha/2)\tan^2(\alpha/2)\tanh^2(\sin(\alpha)x)}{\cos^{-2}(\varphi)},\\ =& 2\sin^2(\alpha/2)\cos^2\varphi\left(1-\tanh^2(\sin(\alpha)x)\right),\end{aligned}$$

therefore

$$a(x) = 2\sin(\alpha/2)\cos\varphi\,\mathrm{sech}(\sin(\alpha)x). \tag{4.24}$$

We can now compute the product $a(x)e^{i\varphi(x)}$

$$\begin{aligned}a(x)e^{i\varphi(x)} =& 2\sin(\alpha/2)\cos\varphi\,\mathrm{sech}(\sin(\alpha)x)e^{i\varphi},\\ =& 2\sin(\alpha/2)\,\mathrm{sech}(\sin(\alpha)x)\cos^2\varphi\,(1+i\tan\varphi),\\ =& 2\sin(\alpha/2)\,\mathrm{sech}(\sin(\alpha)x)\frac{1+i\tan\varphi}{1+\tan^2\varphi},\end{aligned}$$

$$a(x)e^{i\varphi(x)} = \frac{\sin(\alpha)}{\cosh(\sin(\alpha)x + \alpha)}. \tag{4.25}$$

Finally, we can write the exact solution to (4.5) and (4.6) as

$$f(x) = \frac{\sin\alpha}{\cosh(\sin(\alpha)x - i\alpha)}, \tag{4.26}$$

and

$$g(x) = -\frac{\sin\alpha}{\cosh(\sin(\alpha)x + i\alpha)}, \tag{4.27}$$

where $0 < \alpha < \pi$.

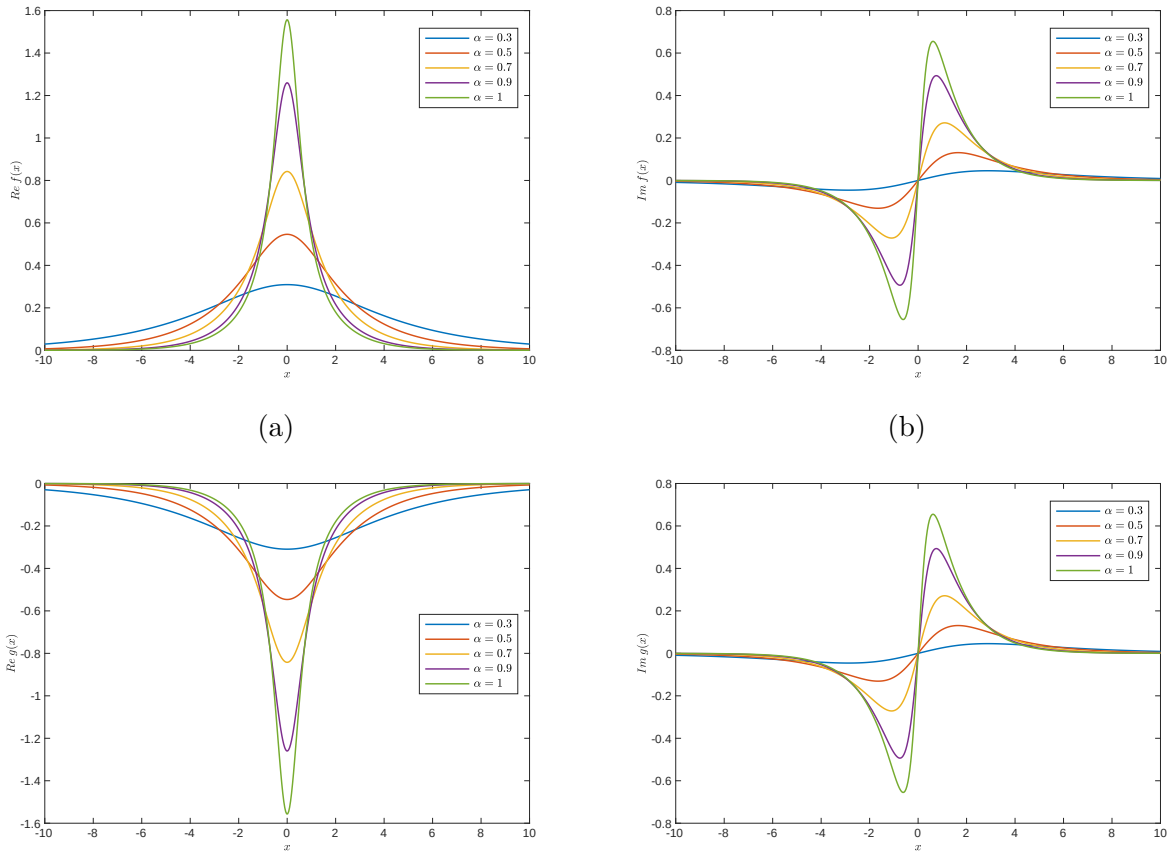

(a) (b)

(c) (d)

Figure 4.1: The stationary soliton solution of the (1+1) dimensional massive Thirring model (4.3) for various values of α, namely $\alpha = 0.3,\ 0.5,\ 0.7,\ 0.9,\ 1$. The top left image (a) is the real part of (4.26) while (b) is its imaginary part. The real and imaginary parts of (4.27) are shown in (c) and (d) respectively.

Figures 4.1a-4.1d show the graphs of solutions (4.26) and (4.27) for several values of the free parameter α. Fig. 4.1a-4.1b show the real (left) and imaginary (right) parts of f respectively, while Fig. 4.1c-4.1d depict the real (left) and imaginary (right) parts of g.

The solutions describe solitons whose width becomes smaller for increasing values of α. The soliton amplitude increases with an increase in α. Fig. 4.2a-4.2b show the evolution of initial wave profiles f and g according to the massive Thirring model (4.3). These are quiescent waves that oscillate up and down with zero velocity. Solitons of the massive Thirring model are known to always be stable due to the Lorentz invariant nature of the nonlinear term. These solutions were obtained by Barashenkov *et al* [21] in their $\mathcal{PT}$-symmetric form. The multisoliton solution was also obtained by Barashenkov *et al* in Ref.[2]. The analysis performed above is done with no $\mathcal{PT}$-symmetry, that is, the gain-loss parameter γ is set to zero, taking advantage of the conservation laws present in the system.

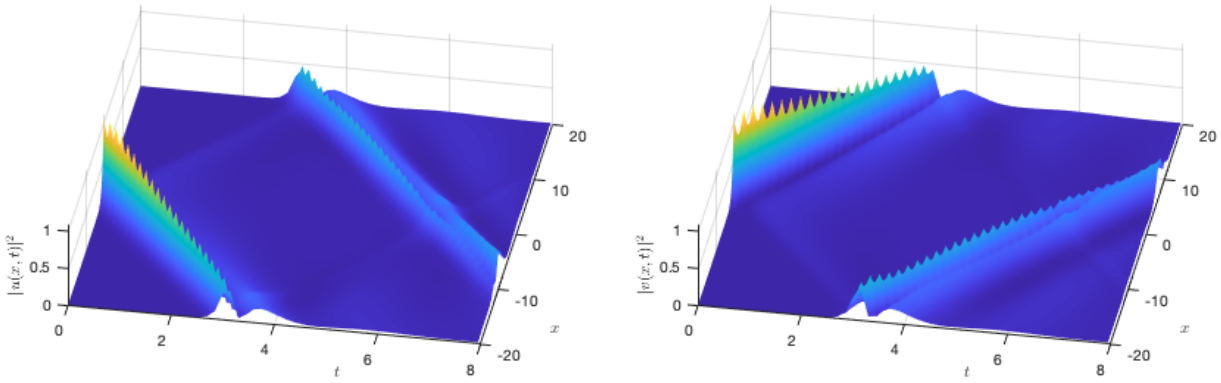

(a) (b)

Figure 4.2: The evolution of initial soliton profiles (4.26) and (4.27) according to the massive Thirring model (4.3). The numerical solution is generated via the Fourier split-step method with $\alpha = \frac{\pi}{4}$ on the interval $x \in [-20, 20]$. Shown in (a) is the square modulus of u while (b) shows the square modulus of v.

4.3 Standard Soler model in 1+1 dimensions

The one-dimensional *tardyonic* Soler model has a Lagrangian density of the form

$$\mathscr{L} = \bar{\psi}\left(i\gamma^{\mu}\partial_{\mu} - m\right)\psi + \frac{1}{2}\left(\bar{\psi}\psi\right)^{2}, \qquad 0 \leq \mu \leq 1. \tag{4.28}$$

The equations of motion associated with the above Lagrangian density are

$$i\gamma^{\mu}\partial_{\mu}\psi = m\psi - \left(\bar{\psi}\psi\right)\psi, \qquad \mu = 0, 1, \tag{4.29}$$

or in component form

$$\begin{aligned} i\partial_t u - \partial_x v - \left(1 - \left(|u|^2 - |v|^2\right)\right) u = 0, \\ i\partial_t v + \partial_x u + \left(1 - \left(|u|^2 - |v|^2\right)\right) v = 0, \end{aligned} \tag{4.30}$$

where the Dirac matrices are chosen as $\gamma^0 = \sigma^3$ and $\gamma^1 = i\sigma^1$. The above system possesses stationary solutions of the form $u(t,x) = e^{-i\omega t}f(x)$ and $u(t,x) = e^{-i\omega t}g(x)$. Substituting this solution ansatz into (4.30) yields a system of ordinary nonlinear differential equations

$$\begin{aligned} \partial_x f + \left(1 - \left(f^2 - g^2\right)\right) g + \omega g = 0, \\ \partial_x g + \left(1 - \left(f^2 - g^2\right)\right) f - \omega f = 0. \end{aligned} \tag{4.31}$$

Equation (4.31) has been shown in Refs. [38, 39] to have a solution of the form

$$\begin{aligned} f(x) = \cosh(\beta x)\frac{\beta\sqrt{2(\omega+1)}}{1+\cosh(2\beta x)}, \\ g(x) = \sinh(\beta x)\frac{\beta\sqrt{2(1-\omega)}}{1+\cosh(2\beta x)}, \end{aligned} \tag{4.32}$$

where $\beta = \sqrt{1-\omega^2}$, not to be confused with the Dirac matrix in (2.27). The solutions were shown to be stable in Ref. [45].

4.4 2+1 dimensional nonlinear Dirac models

The planar Dirac equation has generated a lot of interest in recent years due to the fact that it coincides with hexagonal lattices like graphene, photonic graphene and Bose-Einstein condensates when studied at the K points. This was shown in equation (1.40) in section 1.4. In this section we present nonlinear Dirac models on a plane, beginning with the spinor reduction of the $(2+0)$ dimensional complex sine-Gordon model and its spatiotemporal extension. We also look at the Soler model in the *tardyonic* and *tachyonic* representations and study the vortex solutions (if any) associated with these models. Lastly, we also look at a photonic graphene model, i.e. a nonlinear Dirac equation with Kerr nonlinearity.

4.4.1 Lorentz transformation of quadratic nonlinear terms

Before considering planar nonlinear Dirac equation(s) it is useful to consider how quadratic terms (or bilinear forms) in $(2+1)$ dimensions behave under Lorentz transformations. The transformations of bilinears are important since they inform us which nonlinear terms can preserve the Lorentz invariance of the Dirac equation.

4.4.2 The not-so-Lorentz scalar

To begin we consider the scalar product

$$\psi^\dagger\psi = |u|^2 + |v|^2, \tag{4.33}$$

and Lorentz transform it, that is,

$$\psi^\dagger\psi \longrightarrow S^\dagger\psi^\dagger S\psi = \psi^\dagger S^\dagger S\psi.$$

Since $S^\dagger S \neq I$, where I is a 2×2 identity matrix, the quantity $\psi^\dagger\psi$ is not a Lorentz scalar and thus not invariant under Lorentz transformations.

4.4.3 The Lorentz scalar

Since (4.33) is not invariant, we construct another quadratic product of the form

$$\bar{\psi}\psi = \psi^\dagger\gamma^0\psi = |u|^2 - |v|^2, \qquad \gamma^0 = \sigma^3, \tag{4.34}$$

and check how it behaves under Lorentz transformations. Let us begin by checking how (4.34) behaves under rotations:

$$|u|^2 - |v|^2 \mapsto e^{i\omega/2}ue^{-i\omega/2}\bar{u} - e^{-i\omega/2}ve^{i\omega/2}\bar{v} = |u|^2 - |v|^2. \tag{4.35}$$

In the case of a boost along the x direction we have

$$\begin{aligned}|u|^2-|v|^2 \mapsto & \left(\cosh\frac{\beta}{2}u+\sinh\frac{\beta}{2}v\right)\left(\cosh\frac{\beta}{2}\bar{u}+\sinh\frac{\beta}{2}\bar{v}\right)\\ & -\left(\cosh\frac{\beta}{2}v+\sinh\frac{\beta}{2}u\right)\left(\cosh\frac{\beta}{2}\bar{v}+\sinh\frac{\beta}{2}\bar{u}\right),\\ & =\cosh^2\frac{\beta}{2}\left(|u|^2-|v|^2\right)-\sinh^2\left(|u|^2-|v|^2\right),\end{aligned}$$

therefore

$$|u|^2-|v|^2 \mapsto \left(\cosh^2\frac{\beta}{2}-\sinh^2\frac{\beta}{2}\right)\left(|u|^2-|v|^2\right)=|u|^2-|v|^2. \tag{4.36}$$

For a Lorentz boost along the y direction the quantity $|u|^2-|v|^2$ transforms as

$$\begin{aligned}|u|^2-|v|^2 \mapsto & \left(\cosh\frac{\alpha}{2}u-i\sinh\frac{\alpha}{2}v\right)\left(\cosh\frac{\alpha}{2}\bar{u}+i\sinh\frac{\alpha}{2}\bar{v}\right)\\ & -\left(\cosh\frac{\alpha}{2}v+i\sinh\frac{\alpha}{2}u\right)\left(\cosh\frac{\alpha}{2}\bar{v}-i\sinh\frac{\alpha}{2}\bar{u}\right),\end{aligned}$$

therefore

$$|u|^2-|v|^2 \mapsto \left(\cosh^2\frac{\alpha}{\beta}-\sinh^2\frac{\alpha}{2}\right)|u|^2+\left(\sinh^2\frac{\alpha}{2}-\cosh^2\frac{\alpha}{2}\right)|v|^2=|u|^2-|v|^2. \tag{4.37}$$

The quadratic quantity $\bar{\psi}\psi$ is indeed a Lorentz scalar since it is unaltered under rotations and Lorentz boosts. Another candidate that one might consider is the quantity $\bar{\psi}\gamma^5\psi$, however, in $(2+1)$ dimensions $\bar{\psi}\gamma^5\psi$ coincides with $\bar{\psi}\psi$ due to the fact that $\gamma^5=i\gamma^0\gamma^1\gamma^2=I_2$, with $\gamma^0=\sigma^2$, $\gamma^1=i\sigma^2$ and $\gamma^2=-i\sigma^1$.

4.5 The complex sine-Gordon model

The complex sine-Gordon equation was introduced as a model for the description of relativistic vortices in superfluids by Lund and Regge [46, 47]. This model can be thought of as an integrable generalisation of the sine-Gordon theory. The complex sine-Gordon theory has found a wide range of use including in optics where it provides a more accurate description of optical pulses[48], the model is also capable of incorporating effects such as frequency modulation. The complex sine-Gordon equation in $(2+0)$ dimensions was first considered in Ref. [2] and takes the form

$$\partial\bar{\partial}\Psi+\frac{\bar{\Psi}\partial\Psi\bar{\partial}\Psi}{1-|\Psi|^2}+\Psi\left(1-|\Psi|^2\right)=0, \tag{4.38}$$

where $\partial=\partial_z$, $\bar{\partial}=\partial_{\bar{z}}$, $z=\frac{x+iy}{2}$ and $\bar{z}=\frac{x-iy}{2}$. The above system (4.38) can be reduced back to the usual sine-Gordon theory by letting

$$\Psi = \sin\varphi, \tag{4.39}$$

with φ being a real field. The complex sine-Gordon (4.38) has been shown to have topological vortices $\Psi = f_n e^{in\theta}$[3, 4], where $f_n \to 1$ as $r \to 0$, with vorticity $n \in \mathbb{Z}$. The system in (4.38) has been shown to be reducible to a spinor representation in terms of a Euclidean spinor field $\Psi = (u, v)^T$ [49, 2]. The authors of Ref. [2] have identified this reduction as the Euclidean version of the massive Thirring model, which takes the form

$$\begin{aligned} \bar{\partial}u + v\left(1 - |u|^2\right) &= 0, \\ \partial v - u\left(1 - |v|^2\right) &= 0. \end{aligned} \tag{4.40}$$

The above is clearly a nonlinear Dirac-type equation with cubic nonlinearity, with the components u and v satisfying (4.38). Equation (4.40) has a Lagrangian of the form

$$L = \int \left(i\bar{u}\partial v + i\bar{v}\partial u + |u|^2 + |v|^2 - |uv|^2 - 1 + \text{c.c.}\right) dz. \tag{4.41}$$

Since the complex sine-Gordon equation (4.38) possesses topological vortices, it is natural to expect its equivalent representation (4.40) to have these vortices. This section is devoted to studying the vortex solutions of (4.40). The stability of these solutions is studied by extending (4.40) to its $(2+1)$-dimensional version and studying its perturbation about the vortex solution, in particular, the single vortex solution.

4.5.1 The 2+1 dimensional extension of the 2+0 dimensional complex sine-Gordon

Extending stationary nonlinear Dirac equation (4.40) to $(2+1)$ dimension requires first noticing that it reduces to the imaginary mass Klein-Gordon equation. Thus, its temporal extension must also reduce to the imaginary mass Klein-Gordon equation. This was done in chapter 2, therefore what we have to do is simply choose the right Dirac γ-matrices. Choosing the Dirac matrices as $\gamma^0 = \sigma^3$, $\gamma^1 = i\sigma^2$ and $\gamma^2 = -i\sigma^1$ the $(2+1)$ dimensional extension of the $(2+0)$ dimensional complex sine-Gordon equation takes the form:

$$\begin{aligned} u_t + (\partial_x + i\partial_y)\, v - u\left(1 - |v|^2\right) &= 0, \\ v_t + (\partial_x - i\partial_y)\, u + v\left(1 - |u|^2\right) &= 0. \end{aligned} \tag{4.42}$$

4.5.2 Dispersion relation in a nonvanishing background

When the differential equation (4.42) is studied under vanishing boundary conditions it possesses a dispersion relation with complex roots. This problem of the complexity of the roots can be overcome by studying the system over a nonvanishing background. Equation (4.42) has a constant solution $u = 1$, $v = e^{i\alpha}$. Linearising (4.42) about this solution gives

$$\begin{aligned} \delta\dot{u} + (\partial_x + i\partial_y)\, \delta v + \left(e^{i\alpha}\delta\bar{v} + e^{-i\alpha}\delta v\right) &= 0, \\ \delta\dot{v} + (\partial_x - i\partial_y)\, \delta u - e^{i\alpha}\left(\delta u + \delta\bar{u}\right) &= 0. \end{aligned} \tag{4.43}$$

A change of variables $\delta u = a(t,x,y) + ib(t,x,y)$ and $\delta v = p(t,x,y) + iq(t,x,y)$ yields:

$$\begin{aligned}(\dot{a} + i\dot{b}) + (\partial_x + i\partial_y)(p + iq) + 2(p\cos\alpha + q\sin\alpha),\\ (\dot{p} + i\dot{q}) + (\partial_x - i\partial_y)(a + ib) - 2e^{i\alpha}a = 0,\end{aligned} \tag{4.44}$$

where the overdot is shorthand for the time derivative. Splitting (4.44) into its real and imaginary parts yields the following system of equations:

$$\dot{b}\partial_x q + \partial_y p = 0, \tag{4.45}$$

$$\dot{a} + \partial_x q - \partial_y q + 2(p\cos\alpha + q\sin\alpha) = 0, \tag{4.46}$$

$$\dot{q} + \partial_x b - \partial_y a - 2\sin\alpha a = 0, \tag{4.47}$$

$$\dot{p} + \partial_x a + \partial_y b - 2\cos\alpha a = 0. \tag{4.48}$$

To obtain the dispersion relation for (4.45)–(4.48) we restrict ourselves to solutions of the form $(a,b,p,q)^T = (A,B,P,Q)^T e^{i(\omega t - \mathbf{k}\cdot\mathbf{x})}$ with $\mathbf{k} = (k_1,k_2)$ and $\mathbf{x} = (x,y)$, where the superscript T denoting matrix transposition. Plugging this ansatz into (4.45)–(4.48) yields

$$e^{i(\omega t - k_1 x - k_2 x)} \begin{pmatrix} 0 & i\omega & -ik_2 & -ik_1 \\ i\omega & 0 & -ik_1 + 2\cos\alpha & ik_2 + 2\sin\alpha \\ ik_2 - 2\sin\alpha & -ik_1 & 0 & i\omega \\ -ik_1 - 2\cos\alpha & -ik_2 & i\omega & 0 \end{pmatrix} \begin{pmatrix} A \\ B \\ P \\ Q \end{pmatrix} = \begin{pmatrix} 0 \\ 0 \\ 0 \\ 0 \end{pmatrix}. \tag{4.49}$$

Equation (4.49) has a solution if the determinant of the matrix above is zero, i.e.

$$\det \begin{pmatrix} 0 & i\omega & -ik_2 & -ik_1 \\ i\omega & 0 & -ik_1 + 2\cos\alpha & ik_2 + 2\sin\alpha \\ ik_2 - 2\sin\alpha & -ik_1 & 0 & i\omega \\ -ik_1 - 2\cos\alpha & -ik_2 & i\omega & 0 \end{pmatrix} = 0. \tag{4.50}$$

evaluating this yields a fourth-order polynomial of the form:

$$\omega^4 - 4\omega^2 + 2(k_1^2 - k_2^2)\cos 2\alpha + 8k_1k_2\sin\alpha\cos\alpha + (k_1^2 + k_2^2)(k_1^2 + k_2^2 - 2\omega^2 + 2) = 0. \tag{4.51}$$

The above expression (4.51) can be simplified by writing

$$\omega^4 - 2\omega^2(|\mathbf{k}|^2 + 2) + 2(k_1^2 - k_2^2)\cos 2\alpha + 8k_1k_2\sin\alpha\cos\alpha + |\mathbf{k}|^2(|\mathbf{k}|^2 + 2) = 0, \tag{4.52}$$

where $|\mathbf{k}|^2 = k_1^2 + k_2^2$. The dispersion relation (4.52) is bi-quadratic and is real when its discriminant is greater than zero, i.e.

$$(|\mathbf{k}|^2 + 2)^2 - 2(k_1^2 - k_2^2)\cos 2\alpha - 8k_1k_2\sin\alpha\cos\alpha - |\mathbf{k}|^2\left(|\mathbf{k}|^2 + 2\right) > 0. \tag{4.53}$$

Simplification of the above expression yields

$$k_1^2(1 - \cos 2\alpha) + k_2^2(1 + \cos 2\alpha) + 1 - 2k_1k_2\sin\alpha\cos\alpha > 0,$$

therefore

$$(k_2 \cos\alpha - k_1 \sin\alpha)^2 + 1 > 0. \tag{4.54}$$

Equation (4.54) is always positive, thus the roots of (4.52) are real for all values $\alpha \in \mathbb{R}$. For the roots ω_1^2, ω_2^2, Vieta's formulae are

$$\omega_1^2 + \omega_2^2 = 2\left(|\mathbf{k}|^2 + 2\right), \tag{4.55}$$

$$\omega_1^2\omega_2^2 = |\mathbf{k}|^4 + 4(k_1\cos\alpha + k_2\sin\alpha)^2. \tag{4.56}$$

The above equations (4.55)–(4.56) are always positive thus both ω_1^2 and ω_2^2 are positive. The absence of complex roots in the dispersion relation of this model implies that the model can be interpreted physically when studied in a nonvanishing and constant background.

4.6 Stability analysis of the vortex solution

To study the stability of the perturbed vortex ansatz it is useful to first cast the nonlinear Dirac equation (4.42) into polar coordinates. Equation (4.42) in polar coordinates is

$$\begin{aligned} \partial_t u + e^{-i\theta}\left(\partial_r - i\frac{\partial_\theta}{r}\right)v - u\left(1-|v|^2\right) = 0, \\ \partial_t v + e^{i\theta}\left(\partial_r + i\frac{\partial_\theta}{r}\right)u + v\left(1-|u|^2\right) = 0, \end{aligned} \tag{4.57}$$

where r is the radial coordinate and θ is the angle. . To examine the stability of the vortex solutions of (4.57) we consider a perturbed vortex solution of the form

$$u(t,r,\theta) = e^{i(n-1)\theta}\left(f(r) + \delta u(t,r,\theta)\right), \qquad v(t,r,\theta) = e^{in\theta}\left(g(r) + \delta v(t,r,\theta)\right), \tag{4.58}$$

with $f, g \in \mathbb{R}$ and δu and δv are small perturbations near the stationary vortex solution. The substitution of (4.58) into (4.57) gives

$$\begin{aligned} \partial_t(f+\delta u)e^{i(n-1)\theta} + e^{-i\theta}\left(\partial_r + i\frac{\partial_\theta}{r}\right)(g+\delta v)e^{in\theta} - e^{i(n-1)\theta}(f+\delta u)\left(1-|g+\delta v|^2\right) = 0, \\ \partial_t(g+\delta v)e^{in\theta} + e^{i\theta}\left(\partial_r - i\frac{\partial_\theta}{r}\right)(f+\delta u)e^{i(n-1)\theta} + (g+\delta v)\left(1-|f+\delta u|^2\right)e^{in\theta} = 0. \end{aligned}$$

Letting $\delta u(t,r,\theta) = a(t,r,\theta) + ib(t,r,\theta)$ and $\delta v(t,r,\theta) = p(t,r,\theta) + iq(t,r,\theta)$ and substituting into the above system gives:

$$\begin{aligned} \partial_t(f+a+ib)e^{i(n-1)\theta} + e^{-i\theta}\left(\partial_r + i\frac{\partial_\theta}{r}\right)(g+p+iq)e^{in\theta} \\ -e^{i(n-1)\theta}(f+a+ib)\left(1-|g+p+iq|^2\right) = 0, \\ \partial_t(g+p+iq)e^{in\theta} + e^{i\theta}\left(\partial_r - i\frac{\partial_\theta}{r}\right)(f+a+ib)e^{i(n-1)\theta} \\ +(g+p+iq)\left(1-|f+a+ib|^2\right)e^{in\theta} = 0, \end{aligned}$$

whence

$$\begin{aligned}\partial_t(f+a+ib)+\left(\partial_r+\frac{n}{r}-i\frac{\partial_\theta}{r}\right)(g+p+iq)-(1-g^2)f-2pfg\\ +(a+ib)(1-g^2)+\mathcal{O}(ap+bp)=0,\\ \partial_t(g+p+iq)+\left(\partial_r-\frac{n-1}{r}+i\frac{\partial_\theta}{r}\right)(f+a+ib)+(1-f^2)g-2afg\\ +(p+iq)(1-f^2)+\mathcal{O}(ap+aq)=0.\end{aligned}$$

Equating terms of order $\mathcal{O}(a^0+b^0)$ and $\mathcal{O}(p^0+q^0)$ yields a system of equations for $f(t,r)$ and $g(t,r)$:

$$\begin{aligned}\partial_t f+\left(\partial_r+\frac{n}{r}\right)g-(1-g^2)f=0,\\ \partial_t g+\left(\partial_r+\frac{n-1}{r}\right)f+(1-f^2)g=0.\end{aligned}\tag{4.59}$$

On the other hand equating terms of order $\mathcal{O}(a+b)$ and $\mathcal{O}(p+q)$ and splitting the resulting equations into their real and imaginary parts yields:

$$\partial_t a+\left(\partial_r+\frac{n}{r}\right)p+\frac{1}{r}\partial_\theta q-\left(1-g^2\right)a+2fgp=0,\tag{4.60}$$

$$\partial_t b+\left(\partial_r+\frac{n}{r}\right)q-\frac{1}{r}\partial_\theta p-\left(1-g^2\right)b=0\tag{4.61}$$

$$\partial_t p+\left(\partial_r-\frac{n-1}{r}\right)a-\frac{1}{r}\partial_\theta b+\left(1-f^2\right)p-2fga=0,\tag{4.62}$$

$$\partial_t q+\left(\partial_r-\frac{n-1}{r}\right)b+\frac{1}{r}\partial_\theta a+\left(1-f^2\right)q=0.\tag{4.63}$$

The time derivatives can be replaced by $\partial_t a\to\lambda a$, $\partial_t b\to\lambda b$, $\partial_t p\to\lambda p$ and $\partial_t q\to\lambda q$ to yield:

$$\mathcal{L}_m\Phi(t,r,\theta)=-\lambda\mathcal{J}\Phi(t,r,\theta),\tag{4.64}$$

where $\Phi(t,r,\theta)=(a,b,p,q)^T$ and

$$\mathcal{L}_m=\begin{pmatrix}\partial_r-\frac{n-1}{r}-2fg & -\frac{1}{r}\partial_\theta & 1-f^2 & 0\\ \frac{1}{r}\partial_\theta & \partial_r-\frac{n-1}{r} & 0 & 1-f^2\\ -(1-g^2) & 0 & \partial_r+\frac{n}{r}+2fg & \frac{1}{r}\partial_\theta\\ 0 & -(1-g^2) & -\frac{1}{r}\partial_\theta & \partial_r+\frac{n}{r}\end{pmatrix},\tag{4.65}$$

and

$$\mathcal{J}=\begin{pmatrix}0&0&1&0\\0&0&0&1\\1&0&0&0\\0&1&0&0\end{pmatrix}.\tag{4.66}$$

It is worth noting that the matrix $\mathcal{J}$ is its own inverse, thus (4.64) reduces to

$$\mathcal{J}\mathcal{L}_m\Phi(t,r,\theta)=-\lambda\Phi(t,r,\theta).\tag{4.67}$$

The operation of $\mathcal{J}$ on $\mathcal{L}$ is simply to swap the rows of $\mathcal{L}_m$.
We can impose a further simplification by letting

$$(a, b, p, q)^T = (A(r)\sin m\theta, B(r)\cos m\theta, P(r)\sin m\theta, Q(r)\cos m\theta)^T, \tag{4.68}$$

with $m \in \mathbb{Z}$ being the angular momentum number, so that (4.67) reduces to a one dimensional problem in the radial coordinate r. Substituting (4.68) into (4.60)–(4.63) simplifies (4.65) to

$$\mathcal{L}_m = \begin{pmatrix} \partial_r - \frac{n-1}{r} - 2fg & \frac{m}{r} & 1-f^2 & 0 \\ \frac{m}{r} & \partial_r - \frac{n-1}{r} & 0 & 1-f^2 \\ -(1-g^2) & 0 & \partial_r + \frac{n}{r} + 2fg & -\frac{m}{r} \\ 0 & -(1-g^2) & -\frac{m}{r} & \partial_r + \frac{n}{r} \end{pmatrix}. \tag{4.69}$$

4.6.1 The radially symmetric perturbations about the single vortex

To study radially symmetric perturbations about the single vortex we let $n = 1$ and $m = 0$ and consider only the large r limit so that the product of $\mathcal{J}$ and $\mathcal{L}$ becomes

$$\mathcal{J}\mathcal{L}_0 = \begin{pmatrix} 0 & 0 & \partial_r + 2 & 0 \\ 0 & 0 & 0 & \partial_r \\ \partial_r - 2 & 0 & 0 & 0 \\ 0 & \partial_r & 0 & 0 \end{pmatrix}. \tag{4.70}$$

The above matrix is an anti-hermitian matrix whose entries are derivatives with constant coefficients. The eigenvalues of (4.70) can be obtained by taking an ansatz of the form

$$(A, B, P, Q) = (\tilde{A}, \tilde{B}, \tilde{P}, \tilde{Q})e^{ikr}, \tag{4.71}$$

where $\tilde{A}, \tilde{B}, \tilde{P}, \tilde{Q}$ are constants. Ansatz (4.71) transforms (4.70) into

$$\mathcal{J}\mathcal{L}_0 = \begin{pmatrix} 0 & 0 & ik + 2 & 0 \\ 0 & 0 & 0 & ik \\ ik - 2 & 0 & 0 & 0 \\ 0 & ik & 0 & 0 \end{pmatrix}. \tag{4.72}$$

With this (4.67) has a solution if

$$\det\left(\mathcal{J}\mathcal{L}_0 + \lambda I\right) = 0,$$

$$\det \begin{pmatrix} \lambda & 0 & ik+2 & 0 \\ 0 & \lambda & 0 & ik \\ ik-2 & 0 & \lambda & 0 \\ 0 & ik & 0 & \lambda \end{pmatrix} = \left(\lambda^2 + k^2\right)\left(\lambda^2 + k^2 + 4\right) = 0.$$

The above has solutions $\lambda_{1,2} = \pm ik$ and $\lambda_{3,4} = \pm i\sqrt{k^2+4}$. As expected (4.70) has pure imaginary eigenvalues since it is an anti-hermitian operator.

4.6.2 Stationary single vortex solution

Equation (4.59) admits stationary vortex solutions, these can be obtained by setting the partial derivatives to zero so that the resulting system is

$$\begin{aligned}\left(\partial_r + \frac{n}{r}\right) g - (1-g^2) f = 0,\\ \left(\partial_r + \frac{n-1}{r}\right) f + (1-f^2) g = 0.\end{aligned} \tag{4.73}$$

For the purpose of this thesis we are only interested in the single vortex solution. Thus, setting $n = 1$ and $f = 1$ yields a nonlinear ordinary differential equation of the form

$$\frac{dg}{dr} + \frac{1}{r} g = 1 - g^2. \tag{4.74}$$

The above differential equation can be linearised through a change of variables $g = \frac{S'}{S}$. This change of variables yields

$$S'' + \frac{1}{r} S' - S = 0. \tag{4.75}$$

This is nothing but the modified Bessel equation of the zeroth order whose solution, $S(r)$, is given in terms of the Bessel functions of the zeroth and first order. Therefore $g(r)$ takes the form:

$$g = \frac{I_1(r)}{I_0(r)}, \tag{4.76}$$

where $I_0(r)$ and $I_1(r)$ are the modified Bessel functions of the zeroth and first order respectively. Figure 4.3a shows the radial part of the single vortex solution which approaches one as $r \to \infty$. The radially symmetric function $|v(x,t)|^2$ is shown in Fig. 4.3b. The solution is an inverted hump centered at the origin with an asymptotic maximum of one.

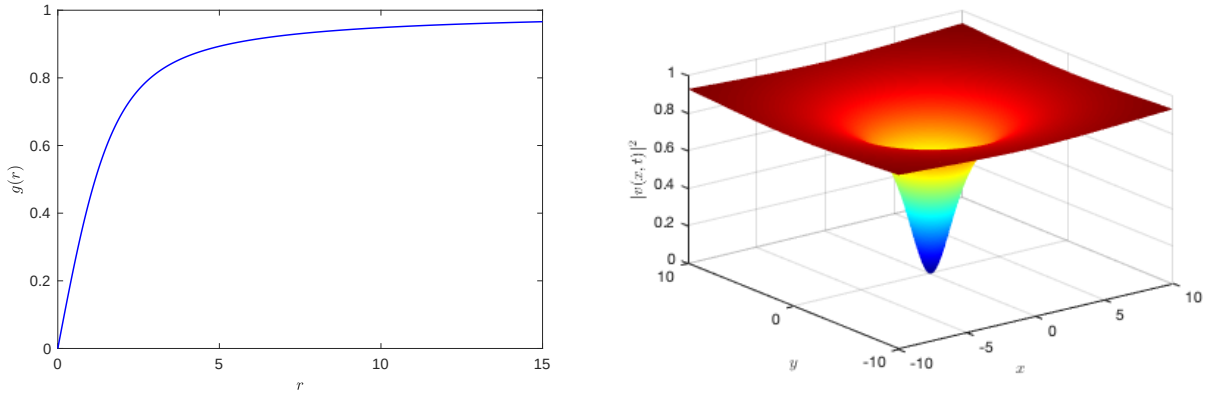

(a) (b)

Figure 4.3: The radial part of the stationary single vortex solution (4.76)(a) with the square modulus of v shown in (b) as the $n = 1$ vortex centered at the origin.

4.7 Searching for the eigenvalues via sine series expansion

The eigenvalue problem (4.67) can be solved via the sine series expansion as an alternative– the sine series makes use of the sine function which is well-behaved at the endpoints, i.e. it has zero endpoints. We write the components of $\Phi(r)$ as:

$$\begin{aligned} A(r) &= \sum_{\alpha=1}^{N} \tilde{A}_\alpha \sin\left(\frac{\pi\alpha r}{R}\right), \qquad B(r) = \sum_{\alpha=1}^{N} \tilde{B}_\alpha \sin\left(\frac{\pi\alpha r}{R}\right), \\ P(r) &= \sum_{\alpha=1}^{N} \tilde{P}_\alpha \sin\left(\frac{\pi\alpha r}{R}\right), \qquad Q(r) = \sum_{\alpha=1}^{N} \tilde{Q}_\alpha \sin\left(\frac{\pi\alpha r}{R}\right), \end{aligned} \tag{4.77}$$

with $A_\alpha, B_\alpha, P_\alpha, Q_\alpha$ being constants weights. Substitution of (4.77) with $n = 1, m = 0$ yields

$$\begin{aligned} \sum_{\alpha=1}^{N} \tilde{A}_\alpha \left(g^2 - 1\right) \sin\left(\frac{\pi\alpha r}{R}\right) + \sum_{\alpha=1}^{N} \tilde{P}_\alpha \frac{\pi\alpha}{R} \cos\left(\frac{\pi\alpha r}{R}\right) + \sum_{\alpha=1}^{N} \tilde{P}_\alpha \left(\frac{1}{r} + 2g\right) \sin\left(\frac{\pi\alpha r}{R}\right) \\ - \frac{m}{r} \sum_{\alpha=1}^{N} \sin\left(\frac{\pi\alpha r}{R}\right) \tilde{Q} = -\lambda \sum_{\alpha=1}^{N} \tilde{A}_\alpha \sin\left(\frac{\pi\alpha r}{R}\right), \\ \sum_{\alpha=1}^{N} \tilde{B}_\alpha \left(g^2 - 1\right) \sin\left(\frac{\pi\alpha r}{R}\right) - \frac{m}{r} \sum_{\alpha=1}^{N} \sin\left(\frac{\pi\alpha r}{R}\right) \tilde{P} + \sum_{\alpha=1}^{N} \tilde{Q}_\alpha \frac{\pi\alpha}{R} \cos\left(\frac{\pi\alpha r}{R}\right) + \sum_{\alpha=1}^{N} \tilde{Q}_\alpha \frac{1}{r} \sin\left(\frac{\pi\alpha r}{R}\right) \\ = -\lambda \sum_{\alpha=1}^{N} \tilde{B}_\alpha \sin\left(\frac{\pi\alpha r}{R}\right), \\ \sum_{\alpha=1}^{N} \tilde{A}_\alpha \frac{\pi\alpha}{R} \cos\left(\frac{\pi\alpha r}{R}\right) - 2 \sum_{\alpha=1}^{N} g \sin\left(\frac{\pi\alpha r}{R}\right) + \frac{m}{r} \sum_{\alpha=1}^{N} \tilde{B}_\alpha \sin\left(\frac{\pi\alpha r}{R}\right) \\ = -\lambda \sum_{\alpha=1}^{N} \tilde{P}\alpha \sin\left(\frac{\pi\alpha r}{R}\right) \\ \frac{m}{r} \sum_{\alpha=1}^{N} \sin\left(\frac{\pi\alpha r}{R}\right) \tilde{A} + \sum_{\alpha=1}^{N} \tilde{B}_\alpha \frac{\pi\alpha}{R} \cos\left(\frac{\pi\alpha r}{R}\right) = -\lambda \sum_{\alpha=1}^{N} \tilde{Q}\alpha \sin\left(\frac{\pi\alpha r}{R}\right). \end{aligned} \tag{4.78}$$

To simplify (4.78) we multiply $\sin\left(\frac{\pi\beta r}{R}\right)$ and integrate over the interval $r \in [0, R]$ yields the following systems of equations

$$\begin{aligned} \sum_{\alpha=1}^{N} S_{\beta\alpha}\tilde{A}_\alpha + \sum_{\alpha:\alpha+\beta=\text{odd}}^{N} \frac{2\beta\alpha}{\beta^2 - \alpha^2} \tilde{P}_\alpha + \sum_{\alpha=1}^{N} \left(I_{\beta\alpha} + 2V_{\beta\alpha}\right) \tilde{P}_\alpha - m \sum_{\alpha=1}^{N} I_{\beta\alpha}\tilde{Q}_\alpha = -\lambda \frac{R}{2} A_\beta, \\ \sum_{\alpha=1}^{N} S_{\beta\alpha}\tilde{B}_\alpha + \sum_{\alpha=1}^{N} \left(I_{\beta\alpha} + 2V_{\beta\alpha}\right) \tilde{P}_\alpha - m \sum_{\alpha=1}^{N} I_{\beta\alpha}\tilde{P}_\alpha + \sum_{\alpha:\alpha+\beta=\text{odd}}^{N} \frac{2\beta\alpha}{\beta^2 - \alpha^2} \tilde{Q}_\alpha = -\lambda \frac{R}{2} \tilde{B}_\beta, \\ \sum_{\alpha:\alpha+\beta=\text{odd}}^{N} \frac{2\beta\alpha}{\beta^2 - \alpha^2} \tilde{A}_\alpha + m \sum_{\alpha=1}^{N} I_{\beta\alpha}\tilde{B}_\alpha - 2 \sum_{\alpha=1}^{N} V_{\beta\alpha}\tilde{A}_\alpha = -\lambda \frac{R}{2} \tilde{P}_\beta, \\ m \sum_{\alpha=1}^{N} I_{\beta\alpha}\tilde{A}_\alpha + \sum_{\alpha:\alpha+\beta=\text{odd}}^{N} \frac{2\beta\alpha}{\beta^2 - \alpha^2} \tilde{B}_\alpha = -\lambda \frac{R}{2} \tilde{Q}_\beta, \end{aligned} \tag{4.79}$$

where we have used the fact that

$$\int_0^R dr\ \sin\left(\frac{\pi\beta r}{R}\right)\sin\left(\frac{\pi\alpha r}{R}\right) = \frac{1}{2}\int_0^R dr\ \left(\cos\frac{\pi(\alpha-\beta)r}{R} - \cos\frac{\pi(\alpha+\beta)r}{R}\right) = \frac{R}{2}\delta_{\alpha\beta}, \tag{4.80}$$

and

$$\int_0^R dr\ \sin\left(\frac{\pi\beta r}{R}\right)\sin\left(\frac{\pi\alpha r}{R}\right) = \begin{cases} \frac{2R\beta}{\pi(\beta^2-\alpha^2)}, & \text{if } \alpha+\beta = \text{odd} \\ 0, & \text{if } \alpha+\beta = \text{even.} \end{cases} \tag{4.81}$$

The matrix elements $S_{\beta\alpha}, V_{\beta\alpha}, I_{\beta\alpha}$ are defied as

$$\begin{aligned} \int_0^R dr\ \left(g^2-1\right)\sin\left(\frac{\pi\beta r}{R}\right)\sin\left(\frac{\pi\alpha r}{R}\right) &:= S_{\beta\alpha} \\ \int_0^R dr\ g\sin\left(\frac{\pi\beta r}{R}\right)\sin\left(\frac{\pi\alpha r}{R}\right) &:= V_{\beta\alpha} \\ \int_0^R dr\ \frac{1}{r}\sin\left(\frac{\pi\beta r}{R}\right)\sin\left(\frac{\pi\alpha r}{R}\right) &:= I_{\beta\alpha}. \end{aligned} \tag{4.82}$$

4.7.1 Results

The sine series expansion requires one to compute a total of $(4N)^2$ integrals $S_{\beta\alpha}$, $V_{\beta\alpha}$ and $I_{\beta\alpha}$. These integrals require approximations of a higher accuracy like *MATLAB*'s `integral()` and quadrature rule (`quadgk()`) whose error tolerance can go to 10^{-13}. This is one advantage that *MATLAB*'s `integral()` and quadrature rule have over standard numerical integration techniques like Simpson's rule and trapezoidal rule since these compromise the accuracy of the eigenvalues due to a larger error compared to *MATLAB*'s `integral()` and `quadgk()` . The disadvantage of these high-accuracy techniques is that they possess longer computation times which grow proportional to N. Therefore, much of the time is spent approximating $3\times(4N)^2$ of the integrals stated in (4.82) before the actual eigenvalues can be computed. The figures below were computed using the sine series expansion code written in *MATLAB* with $N = 600$ so that the resulting matrix eigenvalue problem (4.79) is $4N\times 4N = 2400\times 2400$. This choice of N proved to be the largest my computer can handle without heating up badly.

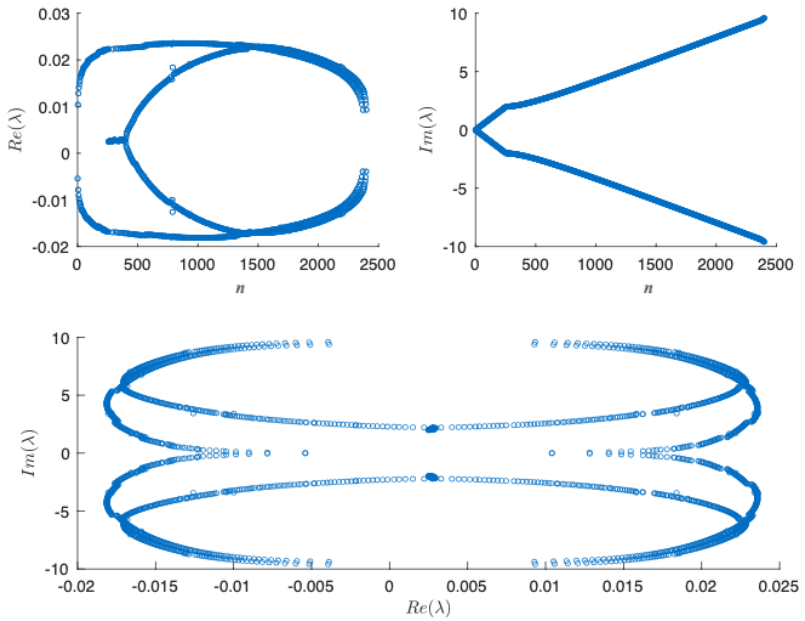

Figure 4.4: The sine series expansion evaluation of the eigenvalues of $\mathcal{J}\mathcal{L}_m$ (4.69) with $m = 0$.

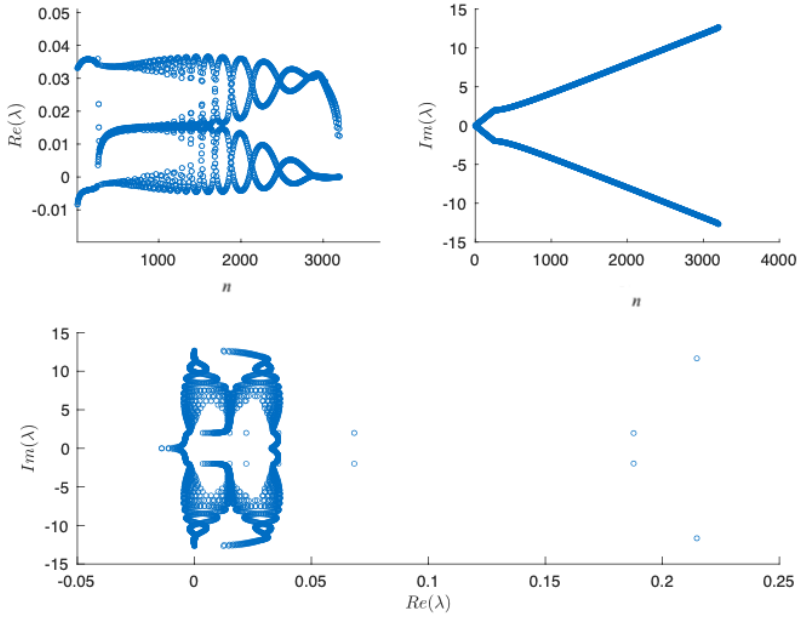

Figure 4.5: The sine series expansion evaluation of the eigenvalues of $\mathcal{J}\mathcal{L}_m$ (4.69) with $m = -1$.

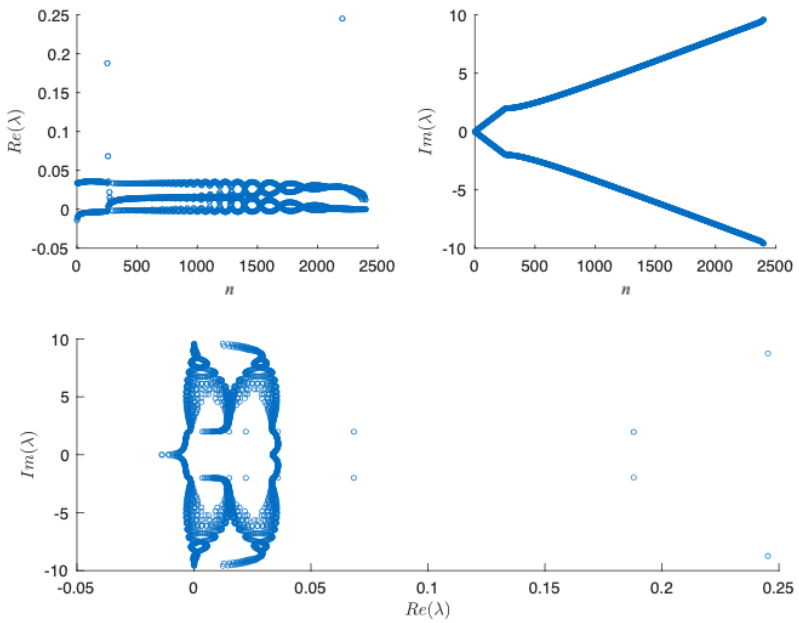

Figure 4.6: The sine series expansion evaluation of the eigenvalues of $\mathcal{J}\mathcal{L}_m$ (4.69) with $m = 1$.

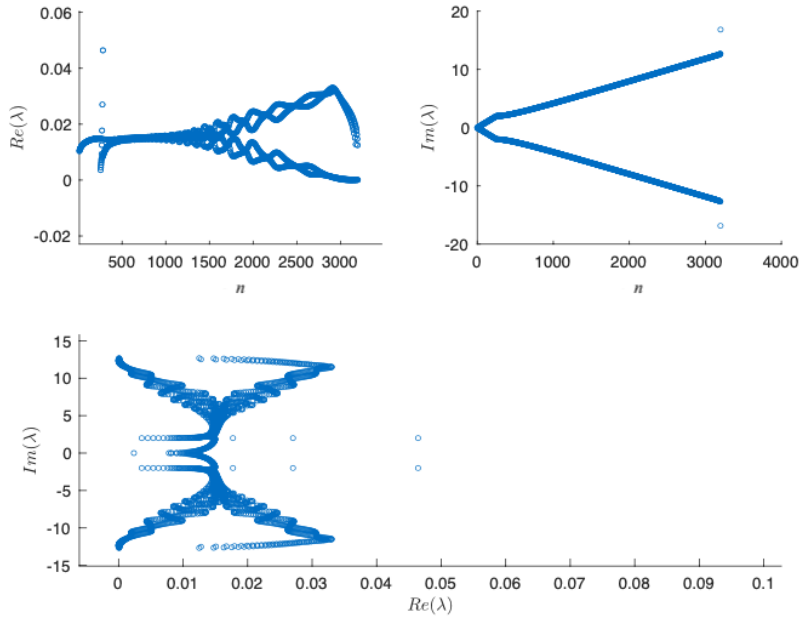

Figure 4.7: The sine series expansion evaluation of the eigenvalues of $\mathcal{J}\mathcal{L}_m$ (4.69) with $m = -2$.

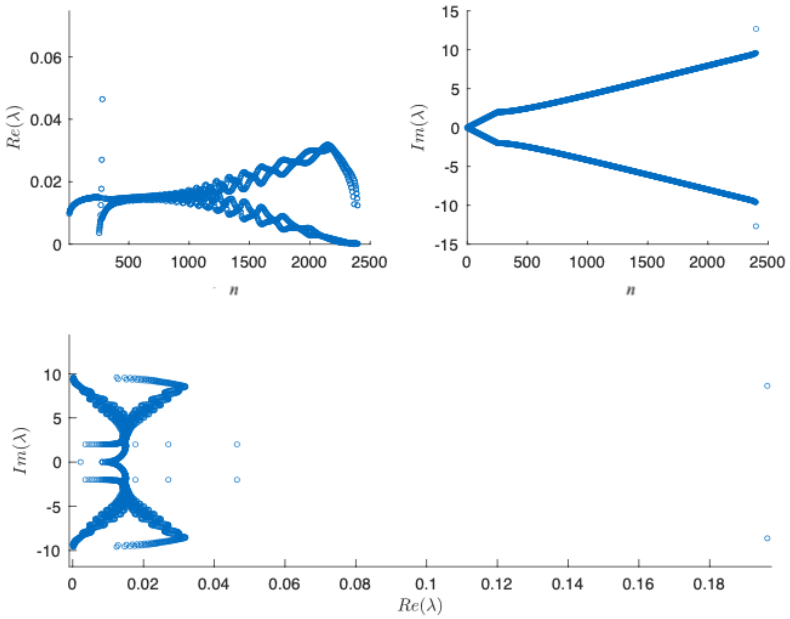

Figure 4.8: The sine series expansion evaluation of the eigenvalues of $\mathcal{JL}_m$ (4.69) with $m = 2$.

The numerical solutions are shown in Figs. 4.7–4.6, with the eigenvalues of the radially symmetric perturbations shown in Fig. 4.4. Fig. 4.4 depicts the imaginary part (top left), and the real part (top right) with the real versus imaginary parts of the spectrum plotted on the same axes in the bottom figure. In the case $m = 0$ the highest real part of the eigenvalues is ~ 0.02, which means that the exponential growth of the solution is proportional to $e^{0.02t}$ with oscillations facilitated by the imaginary part of the spectrum. During the process of experimenting with different values of the total number of modes N I found that the maximum value of the real part of the spectrum can be lowered by increasing the number of nodes N, and thus a number smaller than 0.02 might be obtained with a high-performance computer. In the case of angular perturbations, that is, the case $m = \{\pm 1, \pm 2\}$ it can be seen that the real part of the eigenvalues in Figs. 4.7–4.5 and 4.6–4.8 require higher accuracy. In particular, the choice $N = 600$ is insufficient to provide a full description of the real eigenvalues, this is can be seen in the plot of $Im(\lambda)$ and $Re(\lambda)$ in the aforementioned figures where the plot does not show a well-defined closed curve. By "well-defined" I mean that the plot does not have too much noise. The imaginary part of the spectrum behaves as expected from the continuous spectrum of eigenvalues obtained in section 4.6.1 to be $\lambda_{1,2} = \pm ik$ and $\lambda_{3,4} = \pm i\sqrt{k^2 + 4}$– the entire imaginary axis is covered from $-\infty$ to ∞, with the spectrum consisting of two branches with one of the branches having a gap between -2 and 2.

4.8 Eigenvalues by Chebyshev spectral method

The approximation of derivatives via Chebyshev spectral collocation methods is more advantageous over the sine series expansion above since one need not solve any integrals iteratively and spectral methods (Chebyshev) give a higher accuracy for a smaller number of nodes N. The error associated with spectral differentiation, both Fourier and Chebyshev are of order $\mathcal{O}(10^{-15})$. The major drawback with regards to the Chebyshev collocation is that the differentiation matrix $\mathcal{D}_N^{(1)}$, with the superscript (1) denoting the order of the derivative and N denoting an $N \times N$ matrix, possesses a large number of spurious eigenvalues or outliers [40]. These outliers possess a noticeable nonzero real part which grows proportional to N. For this particular problem, the Chebyshev spectral method is advantageous over the Fourier spectral method because they handle fixed boundary conditions better. The Chebyshev spectral differentiation matrix is formally defined as (see Ref.s [50, 51])

$$\begin{aligned}
(\mathcal{D}_N^{(1)})_{00} =& \frac{2N^2+1}{6}, \\
(\mathcal{D}_N^{(1)})_{NN} =& -\frac{2N^2+1}{6} \\
(\mathcal{D}_N^{(1)})_{jj} =& \frac{-r_j}{2(1-r_j^2)},\ j \in \{1,\dots,N-1\} \\
(\mathcal{D}_N^{(1)})_{ij} =& \frac{c_i}{c_j}\frac{(-1)^{i+j}}{(r_i-r_j)},\ i \neq j,
\end{aligned} \tag{4.83}$$

with $i, j \in \{1, \dots, N-1\}$ and

$$c_i = \begin{cases} 2 & if \quad i = 0 \ or \ N \\ 1 & otherwise \end{cases},$$

and the radial coordinate discretised as

$$r_j = L\cos\left(\frac{j\pi}{N}\right), \qquad j \in \{1,\dots,N-1\}. \tag{4.84}$$

The multiplication by a factor of L in (4.84) is to account for the fact that Chebyshev differentiation matrices are defined on the interval $[-1, 1]$ and thus to cover the interval of interest, $[-L, L]$ one must introduce the factor L.

4.8.1 Results

Numerical solutions in this section were calculated for $L = 150$ and $N = 3000$ so that $\mathcal{JL}_m$ (4.69) becomes a $4N \times 4N = 6000 \times 6000$ matrix. The amount of time spent evaluating the eigenvalues of $\mathcal{JL}_m$ is ~ 18.7 minutes. This of course is a huge improvement compared to several hours spent in solving systems of equations in (4.79).

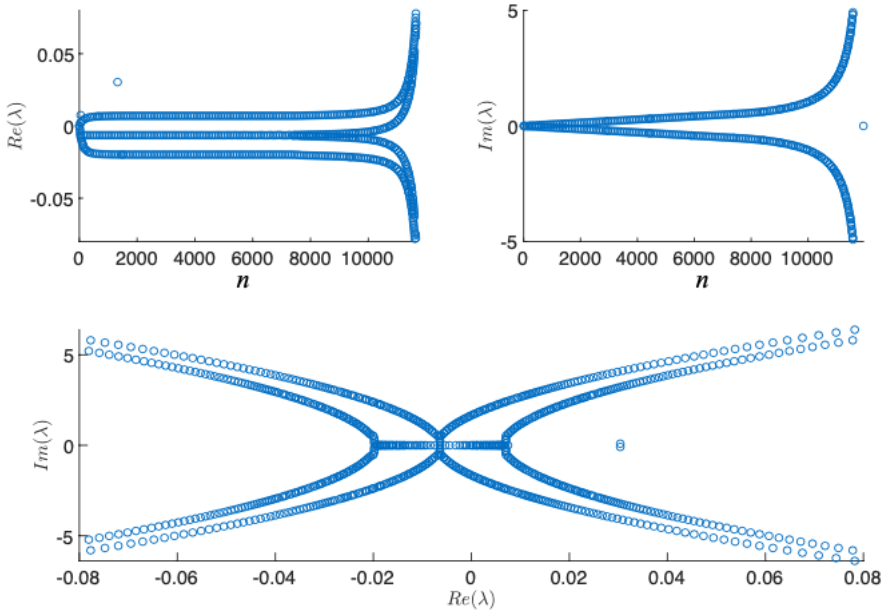

Figure 4.9: The numerical solution to the eigenvalue problem (4.67) via Chebyshev spectral collocation. The solution is computed for the radially symmetric ($m = 0$) perturbations about a single vortex solution.

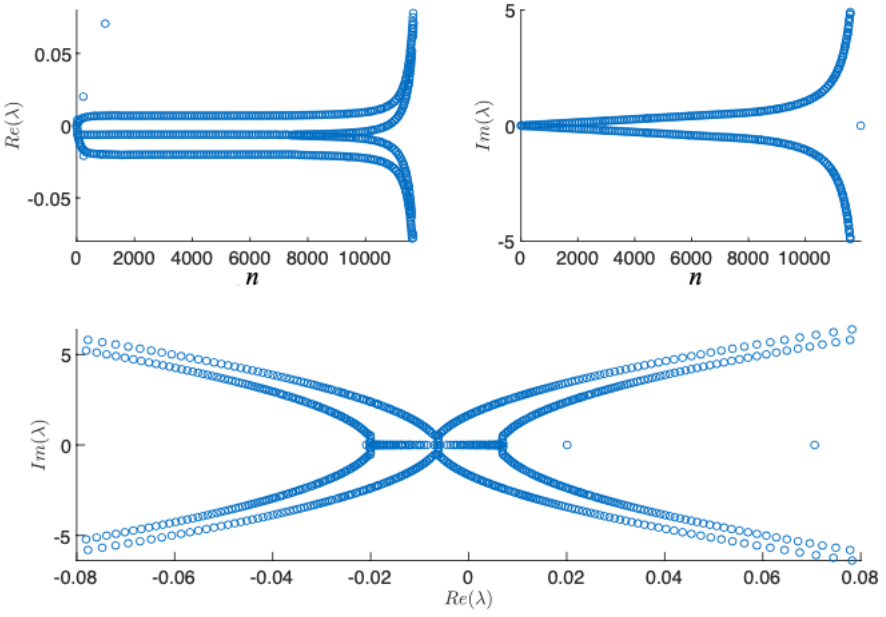

Figure 4.10: The numerical solution to the eigenvalue problems (4.67) via Chebyshev spectral collocation. The eigenvalues are computed for the single vortex with angular perturbation $m = -1$.

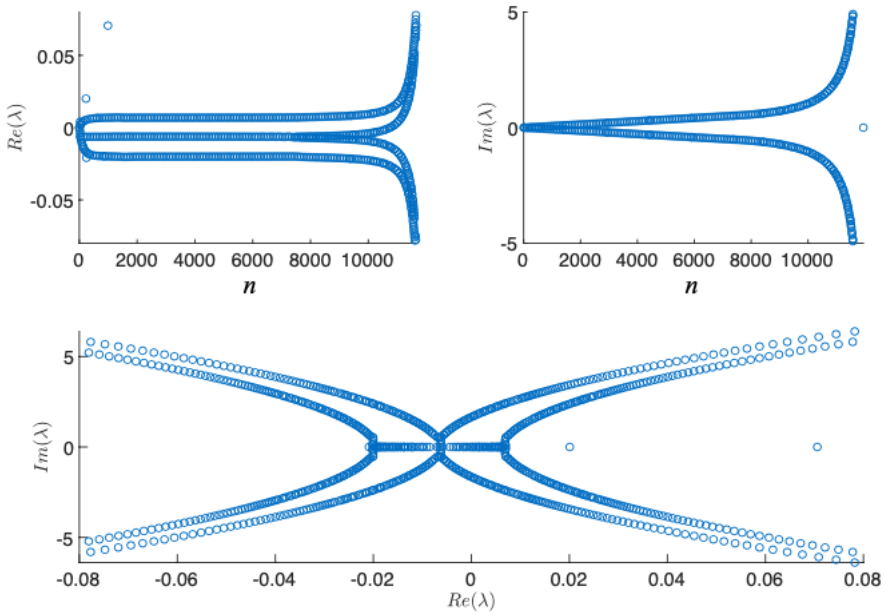

Figure 4.11: The numerical solution to the eigenvalue problems (4.67) via Chebyshev spectral collocation. The eigenvalues are computed for the single vortex with angular perturbation $m = 1$.

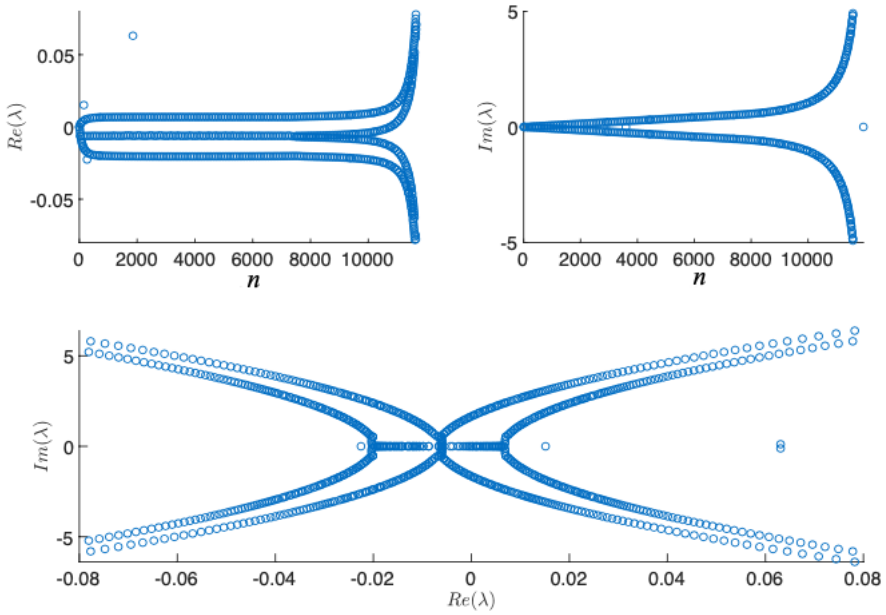

Figure 4.12: The numerical solution to the eigenvalue problems (4.67) via Chebyshev spectral collocation. The eigenvalues are computed for the single vortex with angular perturbation $m = -2$.

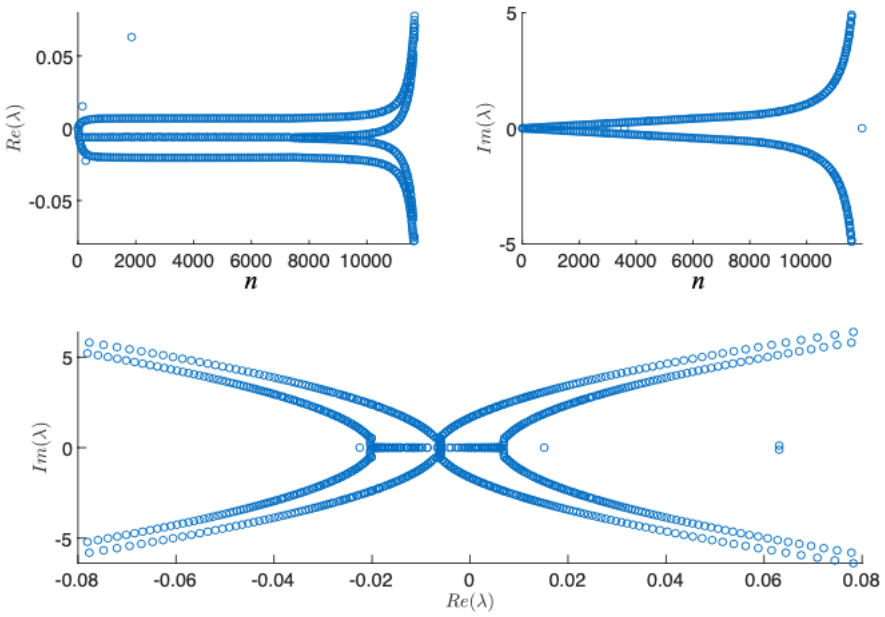

Figure 4.13: The numerical solution to the eigenvalue problems (4.67) via Chebyshev spectral collocation. The eigenvalues are computed for the single vortex with angular perturbation $m = 2$.

The first noticeable thing in the real part of λ in Fig. 4.9 are the outliers located towards $4N \sim 6000$. These are due to the nature of the differentiation matrix (4.83) where the collocation points (4.84) are concentrated at the endpoints. Neglecting these aforementioned outliers we can observe that the real part of λ has about two discrete eigenvalues just below $4N = 1000$, and the real part of λ also has a maximum of ~ 0.006 (neglecting the outliers) and a minimum of ~ -0.006, with several real eigenvalues located at zero. The eigenvalues on the line $\lambda \approx 0$ and $\lambda \approx -0.006$ do not present any problems since both give stable vortices, with $\lambda \approx 0$ giving pure imaginary eigenvalues and $\lambda \approx -0.006$ giving solutions that decay at a slow exponential rate. Real eigenvalues located on the line $\lambda \approx 0.006$, however, result in solutions growing proportional to $e^{0.006t}$. The exponential growth of $e^{0.006t}$ is small enough to imply that the radially symmetric perturbations about the single vortex are stable as $r \to \infty$. The imaginary part of the spectrum of λ in Fig. 4.9 shows that the entire imaginary axis is covered, with a gap between -2 and 2 as predicted by the continuous spectrum.

Angular perturbations with $m = \{\pm 1, \pm 2\}$ are shown in Figs. 4.12–4.10 and Figs. 4.11–4.13 where the result of nonzero m is a shift on a few of the discrete eigenvalues in the real part of λ. In the case $m = \pm 1$, we can see in Fig. 4.10 and Fig. 4.11 that the two discrete real eigenvalues have been shifted slightly upward from their original position shown in Fig. 4.9. The case $m = \pm 2$ results in more of these discrete real eigenvalues shifted upwards, Fig. 4.12 and Fig. 4.13 show three of these discrete eigenvalues having been shifted from their original position in Fig. 4.9. The imaginary part of λ for all $m \in \{\pm 1, \pm 2\}$ is unaltered with the spectrum consisting of a gap between 2 and -2.

There are noticeable differences between the eigenvalues obtained using the sine series expansion and the Chebyshev spectral method. The main difference besides computation time is the quality of the plots of the real part of λ. Under angular perturbations real part of λ in the sine series expansion eigenvalues contains a lot of noise, that is the plot of $Re(\lambda)$ versus $n = 4N$ does not show a well-defined curve. In the case where the Chebysehv differentiation matrices are used to obtain eigenvalues, it is clear in the figures presented such is not the case, that is, the figures show a well-defined curve when $Re(\lambda)$ is plotted against n. The one drawback associated with Chebyshev differentiation matrices is the spurious eigenvalues that grow with the size of N. Putting these differences aside, we can conclude from the eigenvalues obtained via Chebyshev differentiation matrices that the eigenvalues of $\mathcal{J}\mathcal{L}_m$ are stable since the exponential growth for all $m \in \{0, \pm 1, \pm 2\}$ are is small enough to not result in instabilities.

4.9 The Soler model

The Soler model is a nonlinear Dirac-type equation with a scaler self-interaction potential of the form $\left(\bar{\psi}\psi\right)^2$. The standard *tardyonic* Lagrangian density of the Soler model is

$$\mathscr{L} = \bar{\psi}\left(i\gamma^\mu\partial_\mu - m\right)\psi + \frac{1}{2}\left(\bar{\psi}\psi\right)^2, \qquad 0 \leq \mu \leq 2, \tag{4.85}$$

with the coupling constant usually taken to be one in natural units. In $(2+1)$ dimensions Soler nonlinearity coincides with the Thirring nonlinearity. This can be see as follows:

$$J_\mu J^\mu = \left(\psi^\dagger\psi\right)^2 - \left(\psi^\dagger\sigma^1\psi\right)^2 - \left(\psi^\dagger\sigma^2\psi\right)^2 = \left(\bar{\psi}\psi\right),$$

where we have used the identity

$$\left(\psi^\dagger\psi\right)^2 = \sum_{j=1}^{3}\left(\psi^\dagger\sigma^j\psi\right)^2, \tag{4.86}$$

valid for any $\psi \in \mathbb{C}^2$ [40]. In the *tachyonic* case, however, the Soler Lagrangian density turns out to coincide with the equation with the massive Thirring Lagrangian because of the equality of the γ^5 matrix with the 2×2 identity matrix. Because of this equality, the Soler model presented here is deemed to be non-Lagrangian. Therefore, the $(2+1)$ dimensional tachyonic Soler model is of the form

$$\begin{aligned} u_t + (\partial_x + i\partial_y)v - u\left(|u|^2 - |v|^2\right) = 0, \\ v_t + (\partial_x - i\partial_y)u - v\left(|u|^2 - |v|^2\right) = 0, \end{aligned} \tag{4.87}$$

or

$$\begin{aligned} u_t + \bar{\partial}v - u\left(|u|^2 - |v|^2\right) = 0, \\ v_t + \partial u - v\left(|u|^2 - |v|^2\right) = 0, \end{aligned} \tag{4.88}$$

with $\partial = \partial_z$, $\bar{\partial} = \partial_{\bar{z}}$ and $z = (x + iy)/2$. The Dirac γ matrices are chosen as $\gamma^0 = \sigma^3$, $\gamma^1 = i\sigma^2$ and $\gamma^2 = -i\sigma^1$. This model is analogous to a generalisation of the spinor extension of the complex sine-Gordon model (4.42). To put this into perspective, consider a slight modification of (4.87):

$$\begin{aligned} u_t + (\partial_x + i\partial_y)v - mu - u\left(A_{11}|u|^2 - A_{12}|v|^2\right) = 0, \\ v_t + (\partial_x - i\partial_y)u + mv - v\left(A_{21}|u|^2 - A_{22}|v|^2\right) = 0, \end{aligned} \tag{4.89}$$

where A_{ij} are real constants, $i, j = \{1, 2\}$ and m is the mass which is not to be confused with the angular momentum number is the study of vortex stability in section 4.6. Equation (4.42) can be obtained by letting $m = 1$, $A_{11} = A_{22} = 0$ and $A_{12} = A_{21} = 1$, which of course admits vortex solutions. The model in question (4.87) is obtained by letting $m = 0$ an and $A_{ij} = 1$, $i, j = \{1, 2\}$. The choice $m = 0$ is to avoid the complex roots in the constant background dispersion relation. It remains to be found whether this version of the Soler model admits stationary vortex solutions. Since this model is *tachyonic* this means that its zero background dispersion relation has complex roots and thus cannot have any physical interpretation. To revert this to physics, as in the case of the complex sine-Gordon model, the dispersion relation is best considered in a nonvanishing background. As in the case of the complex sine-Gordon, the system in question (4.87) admits a constant solution of the form $u = 1$ and $v = e^{i\alpha}$. Expanding (4.87) around this solution yields

$$\begin{aligned} \delta\dot{u} + (\partial_x + i\partial_y)\,\delta v + \left(\delta\bar{u} + \delta u - \left(e^{i\alpha}\delta\bar{v} + e^{-i\alpha}\delta v\right)\right) = 0, \\ \delta\dot{v} + (\partial_x - i\partial_y)\,\delta u - e^{i\alpha}\left(\delta\bar{u} + \delta u - \left(e^{i\alpha}\delta\bar{v} + e^{-i\alpha}\delta v\right)\right) = 0. \end{aligned} \tag{4.90}$$

Letting $\delta u = a + ib$, $\delta v = p + iq$ and splitting the resulting equations into the real and imaginary parts yields

$$\dot{a} + \partial_x p - \partial_y q - 2a + 2(p\cos\alpha + q\sin\alpha) = 0, \tag{4.91}$$

$$\dot{b} + \partial_x q + \partial_y p = 0, \tag{4.92}$$

$$\dot{p} + \partial_x a + \partial_y b - 2a\cos\alpha + 2p\sin^2\alpha + \sin 2\alpha = 0, \tag{4.93}$$

$$\dot{q} + \partial_x b - \partial_y - 2a\sin\alpha + p\sin 2\alpha + 2q\sin^2\alpha = 0 \tag{4.94}$$

To find the dispersion relation of the Soler model we consider waves of the form $(a, b, p, q)^T = (A, B, P, Q)^T e^{i(\omega t - \mathbf{k}\cdot\mathbf{x})}$. Substituting into (4.91)–(4.94) results in a system of linear equations

$$e^{i(\omega t - \mathbf{k}\cdot\mathbf{x})}\begin{pmatrix} i\omega - 2 & 0 & -ik_1 + 2\cos\alpha & ik_2 + 2\sin\alpha \\ 0 & i\omega & -ik_2 & -ik_1 \\ -ik_1 - 2\cos\alpha & -ik_2 & i\omega + 2\cos^2\alpha & \sin 2\alpha \\ ik_2 - 2\sin\alpha & -ik_1 & \sin 2\alpha & i\omega + 2\sin^2\alpha \end{pmatrix}\begin{pmatrix} A \\ B \\ P \\ Q \end{pmatrix} = \begin{pmatrix} 0 \\ 0 \\ 0 \\ 0 \end{pmatrix}. \tag{4.95}$$

Similarly, the above equation has a solution when its determinant is zero, that is

$$\omega^4 - 2\omega^2|\mathbf{k}|^2 + |\mathbf{k}|^4 = 0. \tag{4.96}$$

or

$$\left(\omega^2 - |\mathbf{k}|^2\right)^2 = 0, \tag{4.97}$$

this quantity is always positive, implying that its roots are always real. On the contrary, the choice $m = 0$, $A_{11} = A_{12} = 1$, and $A_{21} = A_{22} = -1$ yields another Soler-type equation whose nonvanishing background dispersion relation takes the form

$$\omega^2 + 4i\omega - |\mathbf{k}|^2 + 4i\left(k_1 \sin\alpha - k_1 \cos\alpha\right) = 0. \tag{4.98}$$

This equation of course has complex valued roots, which implies that this particular choice of A_{ij} does not produce a system with a physical interpretation.

4.9.1 Stationary vortices in the Soler model

To search for stationary vortex solutions we set the time derivatives to zero and write (4.87) in polar coordinates:

$$\begin{aligned} e^{-i\theta}\left(\partial_r - i\frac{\partial_\theta}{r}\right)v - u\left(|u|^2 - |v|^2\right) = 0, \\ e^{i\theta}\left(\partial_r + i\frac{\partial_\theta}{r}\right)u - v\left(|u|^2 - |v|^2\right) = 0. \end{aligned} \tag{4.99}$$

We are looking for solutions of the form

$$u = f_n(r)e^{in\theta}, \qquad v = g_{n-1}(r)e^{i(n-1)\theta}, \tag{4.100}$$

where the f_n and g_{n-1} are real valued functions of the radial coordinate r and n is the vorticity. Substituting solution (4.100) into (4.99) yields

$$\frac{dg_{n-1}}{dr} - \frac{n-1}{r}g_{n-1} - f_n\left(f_n^2 - g_{n-1}^2\right) = 0, \tag{4.101}$$

$$\frac{df_n}{dr} + \frac{n}{r}f_n - g_{n-1}\left(f_n^2 - g_{n-1}^2\right) = 0, \tag{4.102}$$

The single vortex equations are obtained by setting the vorticity to unity ($n = 1$) in the above system, that is

$$\frac{dg}{dr} - f\left(f^2 - g^2\right) = 0, \tag{4.103}$$

$$\frac{df}{dr} + \frac{1}{r}f - g\left(f^2 - g^2\right) = 0. \tag{4.104}$$

The numerical solution to the single vortex differential equations (4.103)–(4.104) is sought by a nonlinear shooting method for two-point boundary value problems where a nonlinear boundary value problem is converted into a series of initial value problems. This method is fully described in the eleventh chapter of Ref. [52]. The boundary conditions utilised in the search for a single vortex solution are $f(r) \to 0$ as $r \to 0$ and $f \to 1$ as $r \to \infty$ or $g'(r) \to 0$ as $r \to 0$ and $g'(r) \to 0$ as $r \to \infty$. Figure 4.14 shows the output obtained from the nonlinear shooting method, with both f and g growing for large values of r and thus suggesting that this version of the Soler model (4.87) does not admit topological vortex solutions.

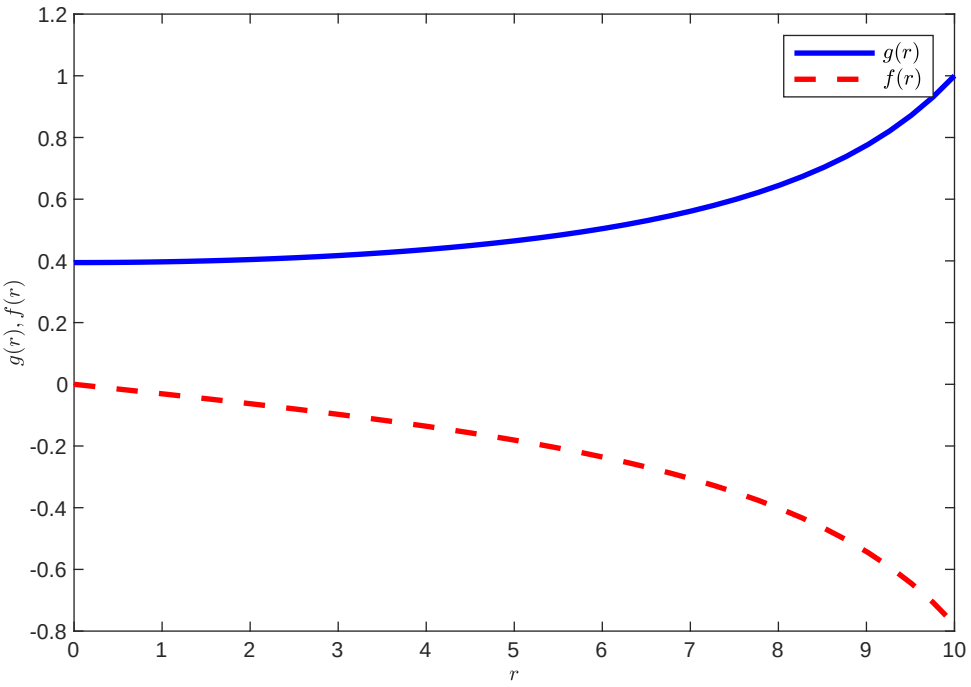

Figure 4.14: The numerical solution of single vortex ordinary differential equation (4.103)–(4.104) obtained via a nonlinear shooting method with boundary conditions $f(r) \to 0$ as $r \to 0$ and $f \to 1$ as $r \to \infty$. The solution is computed on the interval $r \in [0, 10]$.

4.9.2 The standard Soler model

The standard Soler model, that is, the Soler model associated with the *tardyonic* Dirac equation has been reported to admit stationary vortex solutions by Cuevas-Maraver *et al* [40]. The authours of Ref. [40] present a nonlinear Dirac equation with a generalised Soler-type nonlinearity with a Lagrangian density of the form:

$$\mathscr{L} = \bar{\psi}\left(i\gamma^{\mu}\partial_{\mu} - m\right)\psi + \frac{1}{2}\frac{\left(\bar{\psi}\psi\right)^{k+1}}{k+1}, \qquad \mu = 0, 1, 2 \text{ and } k \in \mathbb{N}. \tag{4.105}$$

The choice $\gamma^0 = \sigma^3$, $\gamma^1 = i\sigma^2$ and $\gamma^2 = -i\sigma^1$, with $k = 1$ and $m = 1$ yields a massive $(2+1)$ dimensional nonlinear Dirac equation of the form:

$$\begin{aligned} i\partial_t u + \left(i\partial_x + \partial_y\right)v - u + \left(|u|^2 - |v|^2\right)u = 0, \\ i\partial_t v + \left(i\partial_x - \partial_y\right)u + v - \left(|u|^2 - |v|^2\right)v = 0. \end{aligned} \tag{4.106}$$

The polar coordinate version of (4.106) is

$$\begin{aligned} i\partial_t u + e^{-i\theta}\left(i\partial_r + \frac{\partial_\theta}{r}\right)v - u + \left(|u|^2 - |v|^2\right)u = 0, \\ i\partial_t v + e^{i\theta}\left(i\partial_r - \frac{\partial_\theta}{r}\right)u + v - \left(|u|^2 - |v|^2\right)v = 0. \end{aligned} \tag{4.107}$$

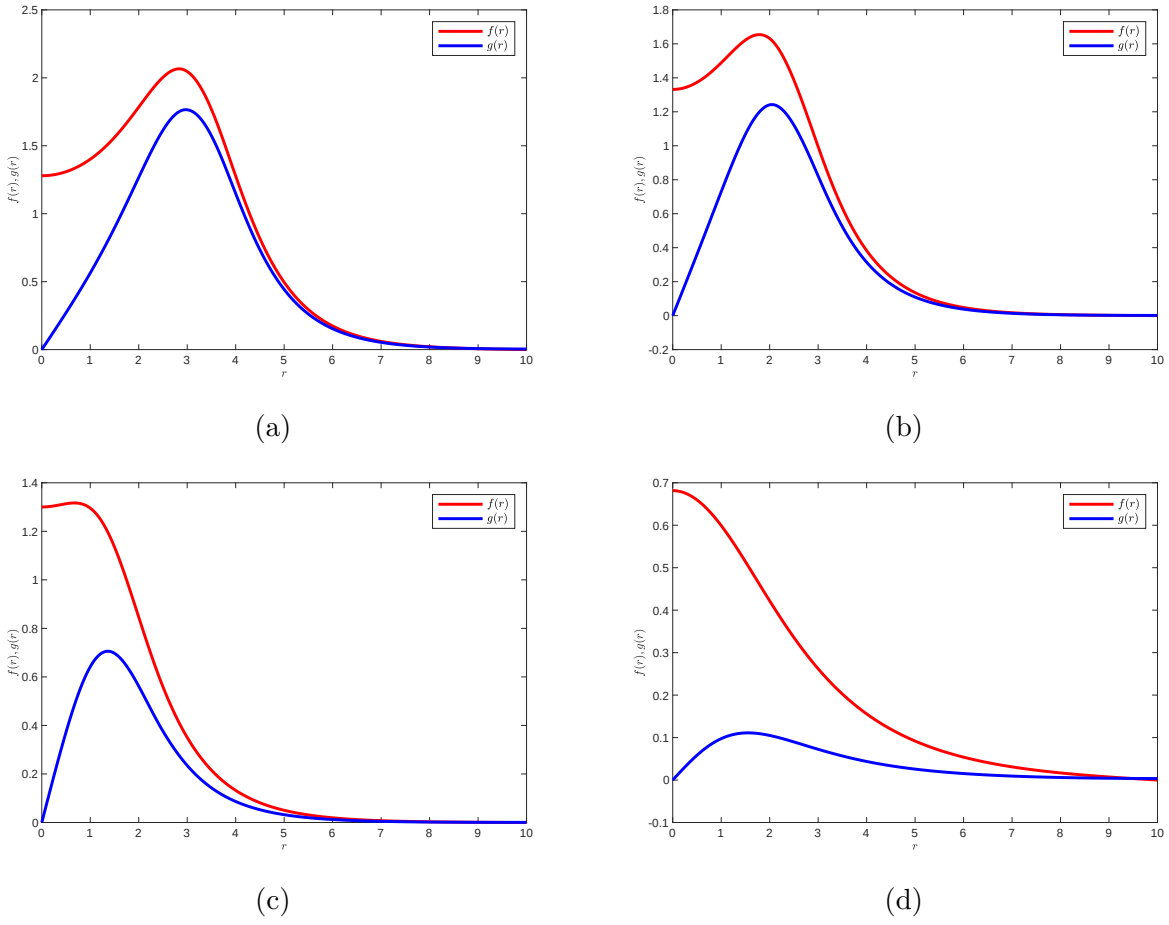

(a) (b)

(c) (d)

Figure 4.15: The numerical solution of the vortex differential equation (4.109) via the shooting method. The solution is computed for several values of the frequency omega, namely, (a) $\omega = 0.2$, (b) $\omega = 0.3$, (c) $\omega = 0.5$ and (d) $\omega = 0.9$. The solution is computed with vorticity $n = 1$.

Substituting a solution ansatz $\psi(t, x) = e^{-i\omega t}\phi(r)$, with

$$\phi(r) = \begin{pmatrix} g(r)e^{in\theta} \\ if(r)e^{i(n+1)\theta} \end{pmatrix} \tag{4.108}$$

gives a system of nonlinear vortex ordinary differential equations

$$\begin{aligned} \omega g - \left(\partial_r + \frac{n+1}{r}\right) f - f + \left(g^2 - f^2\right) g = 0, \\ \omega f + \left(\partial_r - \frac{n}{r}\right) g + f - \left(g^2 - f^2\right) f = 0. \end{aligned} \tag{4.109}$$

Equation (4.109) is a nonlinear differential equation whose solutions are solitary wave structures, that is localised waves whose localisation shifts towards the origin for large values of the frequency ω. Fig 4.15 depicts this phenomenon in the $n = 1$ case– the spinors begin with localisation at $r = 3$ for $\omega = 0.2$ and move closer and closer to the origin as ω grows closer to

one. These images agree with those of Cuevas-Maraver *et al* [40]– these solitary waveforms were also obtained in the context of photonic graphene with Kerr-like nonlinearities in Ref. [53]. The authors of Ref. [40] report that solutions of higher vorticity are unstable and split into lower vortex charge configurations to preserve the overall vorticity. The spectral stability of (4.106) was computed and it showed that the $n = 1$ vortices are unstable that is the eigenvalues associated with the perturbation of (4.106) have dependency on the real and imaginary values. It was also observed that in the case of $n = 1$ vortices one of the spinor components split into structures without angular dependence whereas the other split into structures with angular dependence – this is what preserves the vorticity across both spinor components [40].

4.10 Nonlinear Dirac equation in photonic graphene

The tight binding approximation of the photonic graphene Hamiltonian, that is, an array of laser beams organised in a hexagonal lattice, near the Dirac points corresponds to the massless Dirac equation as shown in chapter 1. Thus, in optics, the nonlinear extension of the Dirac-like Hamiltonian obtained in (1.40) involves adding a Kerr nonlinearity, which is cubic-type nonlinearity where the spinor components are decoupled with the nonlinearity. Due to this decoupling of spinor components with the nonlinearity, the $(2+1)$ dimensional nonlinear Dirac equation with Kerr nonlinear is not Lorentz invariant as already shown by Haddad and Carr [35]. This model is presented in Refs. [35, 10, 36] as:

$$\begin{aligned} i\partial_t\psi_1 &= -i\partial_x\psi_2 - \partial_y\psi_2 + \left(M - g|\psi_1|^2\right)\psi_1, \\ i\partial_t\psi_2 &= -i\partial_x\psi_1 + \partial_y\psi_1 - \left(M + g|\psi_2|^2\right)\psi_2. \end{aligned} \tag{4.110}$$

4.10.1 Topological edge states

This model is known to have topological edge states since it is the $(2+1)$ dimensional extension of the $(1+1)$ dimensional nonlinear lattice model, the nonlinear Su-Schrieffer-Heeger-Model. The edge states are obtained by restricting oneself to a single axis and thus reducing the problem to a $(1+1)$ dimensional problem. A one dimensional reduction of system (4.110) is performed by letting $\psi_1(x,y,t) = b(y,t)e^{ikx}$ and $\psi_2(x,y,t) = a(y,t)e^{ikx}$:

$$\begin{aligned} i\partial_t a &= \partial_y b + kb - \left(M + g|a|^2\right)a, \\ i\partial_t b &= -\partial_y a + ka + \left(M - g|b|^2\right)b. \end{aligned} \tag{4.111}$$

The system (4.111) is a (1+1) dimensional nonlinear Dirac equation is written in a non-standard form. To write (4.111) in the standard Dirac gamma matrix representation (spinor) we make the following change of variables

$$u = \frac{b + ia}{2\delta}, \qquad v = \frac{b - ia}{2\gamma}, \tag{4.112}$$

and

$$a = i(\gamma v - \delta u), \qquad b = \delta u + \gamma v. \tag{4.113}$$

Using (4.112)-(4.113) we can turn (4.111) into spinor equations as follows:

$$\begin{aligned} i\left(\partial_t u-\partial_y u\right) &= \frac{1}{2\delta}\left\{i\partial_t b-\partial_t a-i\partial_y b+\partial_y a\right\} \\ &= \frac{1}{2\delta}\left\{ka+Mb-g|b|^2b+ikb+Ma-ig|a|^2a\right\}, \end{aligned}$$

substituting (4.113) into the above equation yields

$$\begin{aligned} i\left(\partial_t u-\partial_y u\right) =& \frac{1}{2\delta}\left\{2i\gamma kv+2\gamma Mv-g|\delta u+\gamma v|^2(\delta u+\gamma v)+g|i(\gamma v-\delta u)|^2(\gamma v-\delta u)\right\} \\ =& \frac{1}{2}\left\{2(M+ik)v-g|v-u|^2(v-u)+g|i(u+v)|^2(u+v)\right\} \\ =& \frac{1}{2}\left\{2(M+ik)v+g\left(|u|^2+|v|^2+uv^*+vu^*\right)(u+v)\right\} \\ & -\frac{1}{2}\left\{g\left(|u|^2+|v|^2-(uv^*+vu^*)\right)(v-u)\right\} \\ =& \frac{1}{\delta}\left\{\gamma\left(M+ik\right)v-g\delta\left(\delta^2|u|^2+\gamma^2|v|^2\right)u-g\gamma^2\delta\left(u^*v+v^*u\right)v\right\}, \end{aligned}$$

setting $\delta=-1$ and $\gamma=1$ gives

$$i\left(\partial_t u-\partial_y u\right) = -\left\{\left(M+ik\right)+g\left(uv^*+vu^*\right)v+g\left(|u|^2+|v|^2\right)u\right\}.$$

Similarly, we can use (4.112) to write

$$\begin{aligned} i\left(\partial_t v+\partial_y v\right) &= \frac{1}{2\gamma}\left\{i\partial_t b+\partial_t a+i\partial_y b+\partial_y a\right\} \\ &= \frac{1}{2\gamma}\left\{ka+Mb-ikb+iMa-g|b|^2b+ig|a|^2a\right\} \\ &= \frac{1}{2\gamma}\left\{\left(M+ik\right)u-2g\delta^2\gamma\left(u^*v+v^*u\right)u-2g\gamma\left(|u|^2+|v|^2\right)v\right\}, \end{aligned}$$

similarly, setting $\delta=-1$ and $\gamma=1$ gives

$$i\left(\partial_t v+\partial_y v\right) = \left\{-\left(M-ik\right)u-g\left(uv^*+vu^*\right)u-g\left(|u|^2+|v|^2\right)v\right\}.$$

The nonlinear Dirac equation in the representation using standard Dirac matrices becomes

$$\begin{aligned} &i\left(\partial_t u-\partial_y u\right)+\left(M+ik\right)v+\mathcal{F}(u,v)v+\mathcal{G}(u,v)u=0, \\ &i\left(\partial_t v+\partial_y v\right)+\left(M-ik\right)v+\mathcal{F}(u,v)u+\mathcal{G}(u,v)v=0, \end{aligned} \tag{4.114}$$

where

$$\mathcal{F}(u,v)=g\left(uv^*+vu^*\right),\ \mathcal{G}(u,v)=g\left(|u|^2+|v|^2\right). \tag{4.115}$$

Equation (4.114) is a $(1+1)$ dimensional nonlinear Dirac equation writen usnig the standard choice of γ-matrices. The newly transformed nonlinear Dirac equation is not Lorentz invariant because of the term $\mathcal{G}(u,v)$ which does not transform like a spinor, see appendix

A.4. The solution to (4.114) has been obtained by Smirnova *et al* [10] by search for soltions proportional to $e^{-i\omega t}$ and applying the Lorentz transformation $\tau = \gamma(t - vy)$, $\xi = \gamma(y - vt)$ with $\gamma = \frac{1}{\sqrt{1-v^2}}$. The solution takes the form

$$\begin{pmatrix} u \\ v \end{pmatrix} = \sqrt{2\rho_s(\xi)} e^{-i\omega t} \begin{pmatrix} \cos\alpha_s(\xi) \\ -\sin\alpha_s(\xi) \end{pmatrix}, \tag{4.116}$$

where ρ_s is the intensity and α_s is the spin angle. These take the form

$$\alpha_n(\xi) = \arctan\left(\frac{\Omega-\omega}{\sqrt{\Omega^2-\omega^2}}\tanh\sqrt{\Omega^2-\omega^2}\xi\right),\ \alpha_s = \alpha_n - \frac{\delta}{2}, \tag{4.117}$$

$$\rho_s(\xi) = \frac{2(\Omega\cos 2\alpha_n - \omega)}{\mathscr{B} + \mathscr{A}\cos^2 2\alpha_s}, \tag{4.118}$$

with coefficients $\mathscr{A} = \gamma(1+v)$, $\mathscr{B} = \gamma/(1-v)$, $\Omega = \sqrt{k^2+M^2}$ and $\delta = \arctan\frac{k}{M_0}$.

4.10.2 Stationary vortex solutions

To find the vortex solution of (4.110) it is useful to cast it into its polar coordinate form as follows:

$$\begin{aligned} i\partial_t\psi_1 =& -e^{-i\theta}\left(i\partial_r + \frac{1}{r}\partial_\theta\right)\psi_2 + \left(M - |\psi_1|^2\right)\psi_1, \\ i\partial_t\psi_2 =& -e^{i\theta}\left(i\partial_r - \frac{1}{r}\partial_\theta\right)\psi_1 - \left(M + |\psi_2|^2\right)\psi_2. \end{aligned} \tag{4.119}$$

The vortex ansatz in the case of the nonlinear Dirac equation with Kerr nonlinearity is takes the form

$$\begin{pmatrix} \psi_1 \\ \psi_2 \end{pmatrix} = \begin{pmatrix} fe^{in\theta} \\ ige^{i(n+1)\theta} \end{pmatrix} e^{-i\omega t}, \tag{4.120}$$

where $n = 0, \pm1, \pm2, \ldots$ is the azimuthal number or simply vorticity. Solutions of the form (4.120) can be interpreted as radially symmetric two-dimensional bulk solitons. Substituting this ansatz into (4.119) yields a system of spinor ordinary differential equations

$$\begin{aligned} \frac{dg}{dr} + \frac{n+1}{r}g + (M - \omega - f^2)f =& 0, \\ \frac{df}{dr} - \frac{n}{r}f + (M + \omega + g^2)g =& 0. \end{aligned} \tag{4.121}$$

The numerical solution for this system and its stability analysis has been presented in Ref. [36]. Here I present my own numerical solutions via the nonlinear shooting method. These are shown in Fig.4.16 where the vorticity is fixed to $n = 1$ and the numerical solution is computed for several values of ω, namely $\omega = 0.3$, $\omega = 0.5$, $\omega = 0.7$ and $\omega = 0.9$, with $M = 1$ and boundary conditions on $g(r)$ are $g(0) = 0$ and $g(\infty) = 0$. On the other hand, the boundary conditions on $f(r)$ are such that $f(\infty) = 0$, with the best possible starting value of $f(0)$ being computed with Newton's method or *MATLAB*'s root finder `fsolve()` . These solutions are stable for values of ω above the critical angular frequency $\omega_c > 0.338$ [36]. The effect of ω on the radial solution is shown in Fig. 4.16 where the amplitude of the localised spinors decreases with an increase in omega, with the width of the localised solutions widening. The radial solution starts with a localisation near the origin when $\omega = 0.3$, the localisation then moves further away from the origin with a rise in ω.

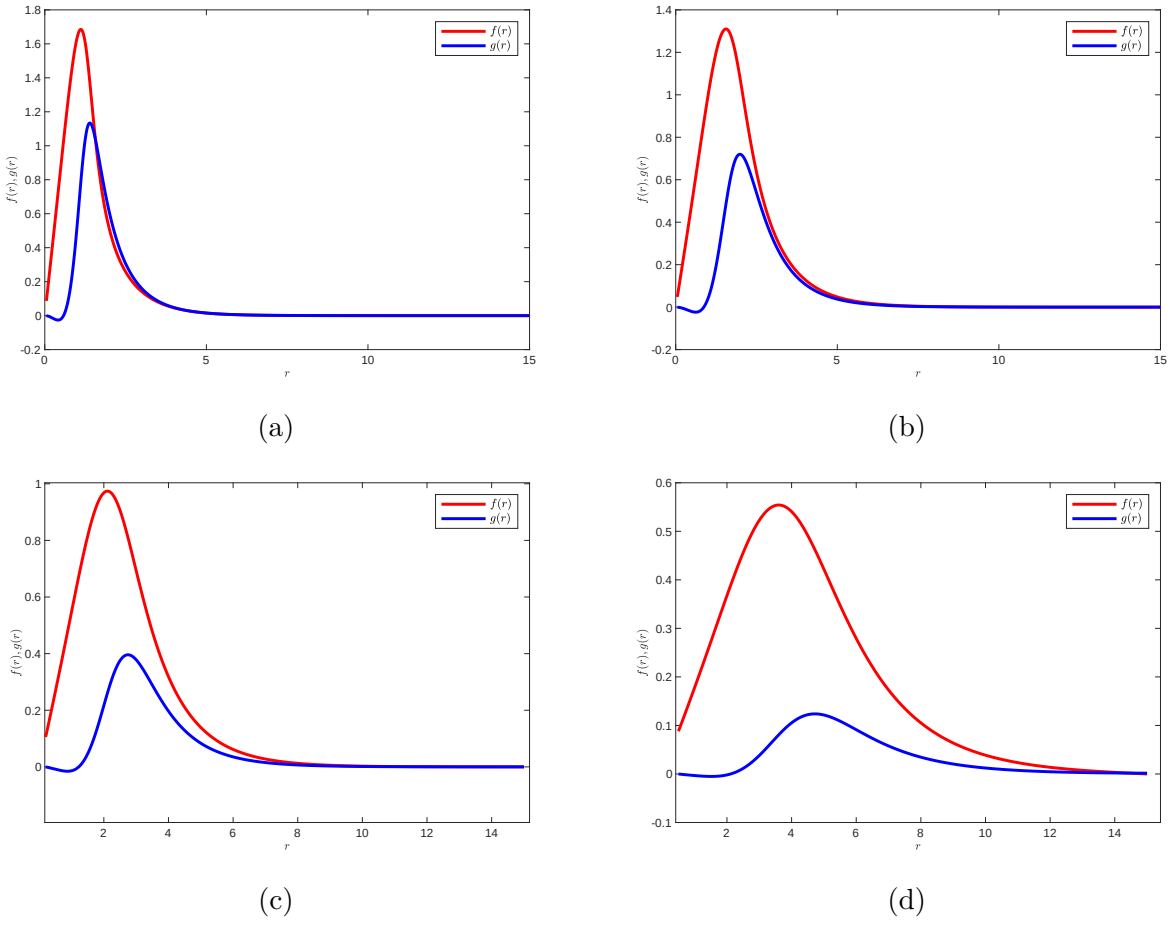

(a) (b)

(c) (d)

Figure 4.16: The numerical solution of the nonlinear vortex differential equation (4.119) via the shooting method. The solution is computed for several values of the frequency ω, namely, (a) $\omega = 0.3$, (b) $\omega = 0.5$, (c) $\omega = 0.7$ and (d) $\omega = 0.9$. The solution is computed with vorticity $n = 1$ and $M = 1$.

4.11 The Soler model in 3+1 dimensions

In the case of $(3+1)$ dimensions, it is convenient to consider the Soler model in spherical coordinates, that is, consider 4-spinor solitary waves in the form of the Wakano Ansatz [54]:

$$\psi(t,\mathbf{r}) = \begin{pmatrix} v(r,\omega)\begin{pmatrix}1\\0\end{pmatrix} \\ iu(r,\omega)\begin{pmatrix}\cos\theta\\ e^{i\phi}\sin\theta\end{pmatrix}\end{pmatrix} e^{-i\omega t}, \tag{4.122}$$

where u and v are real-valued functions satisfying a nonlinear system of ordinary equations

$$\begin{aligned}\left(\partial_r + \frac{2}{r}\right)u + \left(1-\left(v^2-u^2\right)\right)v - \omega v &= 0,\\ \partial_r v + \left(1-\left(v^2-u^2\right)\right)u - \omega u &= 0.\end{aligned} \tag{4.123}$$

We can go ahead and make the changes $u = \sqrt{\frac{1+\omega}{2}}U$, $v = \sqrt{\frac{1+\omega}{2}}V$, with $r = \frac{\rho}{1+\omega}$ (see equation eleven in Ref. [41]) so that (4.123) becomes

$$\begin{aligned}\partial_\rho V + U + U(U^2-V^2) &= 0,\\ \partial_\rho U + \frac{2}{\rho}U + \kappa V + V(U^2-V^2) &= 0,\end{aligned} \tag{4.124}$$

with $\kappa = \frac{1-\omega}{1+\omega}$ for positives values of ω and $0<\kappa<1$. The numerical solution of (4.124) is depicted in Fig. 4.17– these numerical solutions agree with those obtained in Ref. [41]. To obtain the images in Fig. 4.17 it is convenient to discretise the re-scaled radial coordinate ρ via Chebyshev discretisation, i.e.

$$\rho_j = L\cos\left(\frac{j\pi}{N}\right), \qquad j\in\{0,1,\ldots,N\}, \tag{4.125}$$

where L is the length of the interval. Chebyshev collocation points are proffered over equispaced grid points since these generate instabilities in the shooting method. Figure 4.17a the localisation of one of the spinor components (shown in blue) is centered at the origin when $\kappa = 0.1$. The increase in κ shifts the center of the localisation of both spinor components towards the midpoint of the interval. This is shown clearly in Figs. 4.17c–4.17d.
The stability of these numerical numerical solutions are studied by considering a perturbation of solutions (4.122), that is,

$$\psi(t,\mathbf{r}) = \begin{pmatrix} (v(r,\omega)+p(t,r)+iq(t,r))\begin{pmatrix}1\\0\end{pmatrix} \\ i(u(r,\omega)+a(t,r)+ib(t,r))\begin{pmatrix}\cos\theta\\ e^{i\theta}\sin\theta\end{pmatrix}\end{pmatrix} e^{-i\omega t}, \tag{4.126}$$

substituting the perturbed Wakano ansatz into (4.123) yields an eigenvalue problem of the form [40]:

$$\partial_t\Phi(t,r) = \mathcal{L}_\omega\Phi(t,r), \tag{4.127}$$

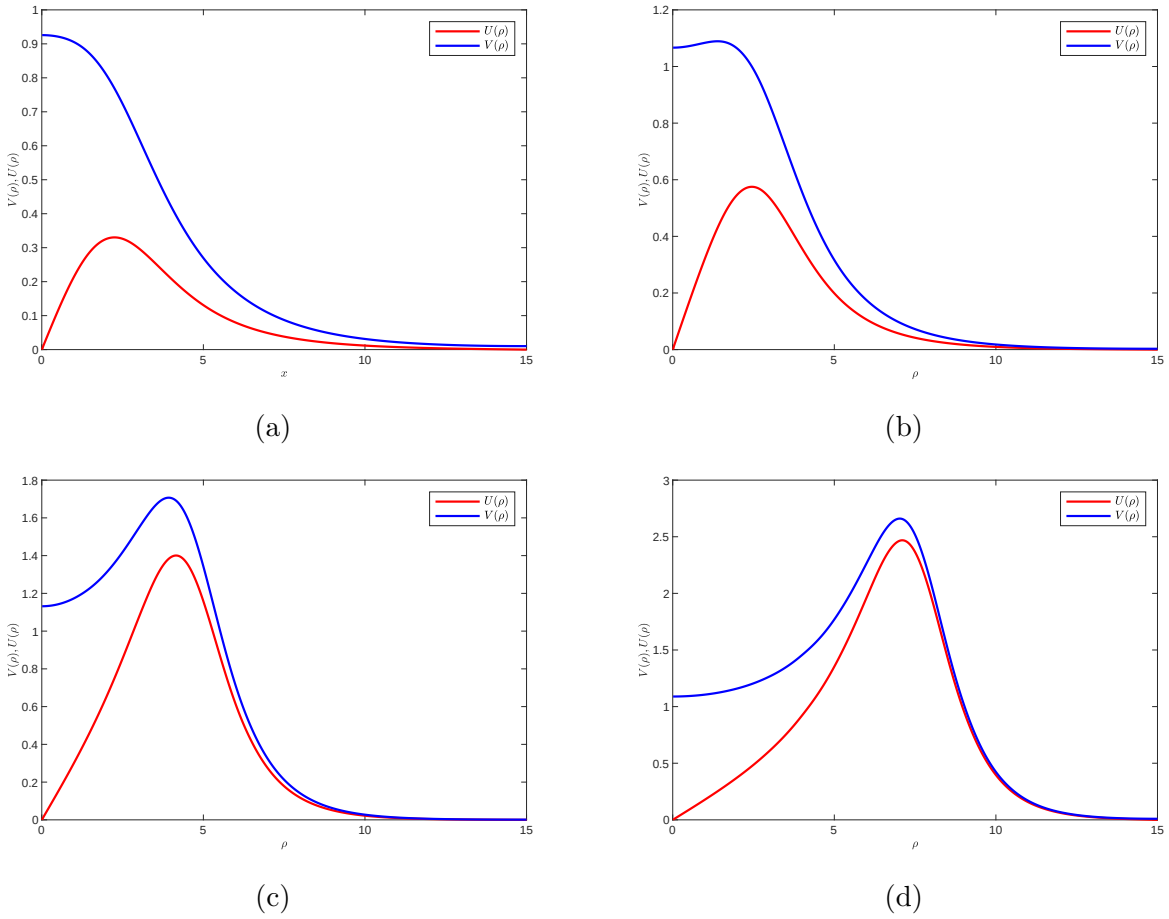

Figure 4.17: The numericla solution to the $(3+1)$ dimensional Soler model with: (a)$\kappa = 0.1$, (b) $\kappa = 0.2$, (c) $\kappa = 0.5$ and (d) $\kappa = 0.7$. The solution is computed by the shooting method with Chebyshev collocation points on the interval $\rho \in [0, 15]$.

where $\Phi(r,t) = (a,b,p,q)^T$ and

$$\mathcal{L}_\omega = \begin{pmatrix} 0 & L_- \\ -L_+ & 0 \end{pmatrix}, \tag{4.128}$$

with

$$L = \begin{pmatrix} v^2 - u^2 - \omega & \partial_r + \frac{2}{r} \\ -\partial_r & -v^2 + u^2 - \omega \end{pmatrix}, \qquad L_+ = L_- - 2\begin{pmatrix} v^2 & -uv \\ -uv & u^2 \end{pmatrix}. \tag{4.129}$$

The eigenvalues of (4.128) are not presented here since that is beyond the scope of this thesis.

Chapter 5

Conclusions

In this thesis, we studied planar Dirac models, namely the $(2+1)$ dimensional extension of the (2+0) dimensional sine-Gordon equation. We did so by arguing in the introductory chapter that planar Dirac models coincide with two-dimensional materials like graphene i.e. both real graphene composed of carbon atoms and photonic graphene and bosonic gases arranged in a hexagonal lattice[35]. We showed that the tight binding Hamiltonian of atoms arranged in a hexagonal lattice structure reduces to a Dirac-like Hamiltonian in $(2+1)$ dimensions (1.40). We also discussed that graphene, for example, is a two-dimensional generalisation of the one-dimensional lattice model called the Su-Schrieffer-Heeger model. The tight binding Hamiltonian of the Su-Schrieffer-Heeger model also reduces to a Dirac-like Hamiltonian in (1+1) dimensions. These models, the Su-Schrieffer-Heeger and graphene have been shown to admit topological solitons under consideration of cubic nonlinearity like the Kerr nonlinearity.

The second chapter formally introduced the Dirac equation and its properties, beginning with the Klein-Gordon equation. We showed that the Klein-Gordon equation failed as a candidate to describe the quantum dynamics of an electron. This was because the time derivative appeared in second derivatives. This fact leads to the Klein-Gordon equation not being able to produce a positive definite probability density which solves the continuity equation. We then introduced Dirac's proposition for dealing with the challenge of the lack of a positive definite probability density function. The proposition was an equation composed of matrices that multiplied the derivatives, these matrices obeyed a particular algebraic structure that retained the hermiticity of the Hamiltonian and ensured the existence of a positive definite probability density function which solves the continuity equation.

The third chapter looked at formulating the Lorentz invariance of the Dirac equation. We transformed the Dirac equation through the transformation $\psi(x) \mapsto S(\Lambda)\psi(x)$ and observed that for the Dirac equation to be invariant under Lorentz transformations the matrix $S(\Lambda)$ must satisfy the relation stated in equation (3.8). Such a matrix satisfying (3.8) was found to take the form of matrix exponential in (3.47).

In the last chapter considered nonlinear Dirac equations in $(1+1)$, $(2+1)$ and $(3+1)$ dimensions and the stationary wave solutions with them. These include the massive Thirring model in $(1+1)$ dimensions, and the $(1+1)$ dimensional Soler model, with both possessing

stable solitary wave solutions. Two-dimensional models include the euclidean version of the massive Thirring in $(2+0)$ dimensions which turned out to correspond to the nonlinear *tachyonic* Dirac equation since its linear part reduces to the imaginary mass Klein-Gordon equation. This model was shown to admit stationary vortex solutions which were obtained analytically in terms of modified Bessel functions in Ref. [3, 4].

The $(2+1)$ extension of the euclidean version of the massive Thirring model was presented in section 4.5.1 with a perturbation of the stationary single vortex solution studied. The perturbed vortex solution leads to a linearised eigenvalue problem (4.67) where λ's are the eigenvalues of $\mathcal{JL}$. The eigenvalues of $\mathcal{JL}$ for vorticity $n = 1$ were calculated using the sine series expansion and via Chebyshev differentiation matrices. Chebyshev differentiation matrices proved to be the most effective since there were no integrals that need to be approximated in order the find the eigenvalues of $\mathcal{JL}$. The eigenvalues of radially symmetric perturbations about the single vortex solutions were found to have a nonzero real part of order 10^{-3} implying that the single vortex solution is stable since 10^{-3} not to result in rapidly growing solutions.

The angular perturbations of the single vortex solutions only resulted in a few discrete real eigenvalues being lifted from their original position. Imaginary eigenvalues, however, were found to agree with the continuous spectrum of eigenvalues obtained in section 4.6.1, where the entire real line was covered, with the spectrum consisting of a gap between -2 and 2. The real part of the spectrum of eigenvalues associated with angular perturbations was found to be nonzero but small enough to not result in instabilities.

The $(2+1)$ dimensional *tachyonic* Soler model was also introduced and it was shown that although this model possesses a dispersion relation with complex roots when studied in a zero background, it model can be reverted to physics by studying it from a nonvanishing background. This particular version of the Soler model was also shown to not admit vortex solutions as shown in Fig. 4.14 where the spinor components were growing for large r instead of approaching the vacuum value as $r \to \infty$. Contrary to the *tachyonic* Soler model, the *tardyonic* Soler model, however, does admit vortex solutions. These are radially symmetric waves that vanish exponentially as $r \to \infty$ with a localisation whose centre shifts towards the origin as ω is raised, where $0 < \omega < 1$. The stability of these vortices was presented by Cuevas-Maraver *et al* in Ref. [40].

We also looked at a photonic graphene model, that is, a planar nonlinear Dirac model with Kerr nonlinearity. The model also admits vortex solutions which are obtainable numerically via the shooting method, see Fig. 4.16. Moreover, the photonic graphene model also possesses topological solitons closely related to those of the nonlinear Su-Schrieffer-Heeger model with Kerr nonlinearity. This was demonstrated in the work of Smirnova *et al* where the photonic graphene model is reduced to one dimension through consideration of waves of the form: $\psi_1(x,y,t) = b(y,t)e^{ikx}$ and $\psi_2(x,y,t) = a(y,t)e^{ikx}$. This is equivalent to ignoring the x axis and only studying waves that propagate along the y axis.

Lastly, we looked at the $(3+1)$ dimensional *tardyonic* Soler model and obtained its solitary

wave solutions numerical via the shooting method with the Chebyshev collocation method. The solitary waves of the three-dimensional Soler model have a similar shape to those of the planar Soler model with the difference being that the centre of the localisation in the three-dimensional case shifts away from the origin towards the centre of the interval $[0, 15]$ as κ is raised whereas those of the planar Soler model move towards the origin as one raises ω. We can also observe that the effect of raising κ on the amplitude of solitary waves of the three-dimensional Soler model is that the amplitude raises with an increase in κ compared to the decrease in the solitary wave amplitude in the planar Soler model as one raised ω. The numerical results obtained in Fig. 4.17 agree with those of [41].

Appendix A

Appendices

A.1 Products of Pauli matrices

The product of Paul matrices is given as

$$\sigma_j \sigma_k = \delta_j kI + i\epsilon_{jkl}\sigma_l, \tag{A.1}$$

and

$$\sigma_j^* \sigma_k = \delta_j kI + i\epsilon_{jkl}\sigma_l. \tag{A.2}$$

A.2 Weyl (or spinor) representation

Alternatively, the Dirac equation can be written in another matrix representation which still obeys the Clifford algebra. Such a representation is the Weyl or spinor representation which is given by

$$\beta_W = \begin{pmatrix} 0 & I_{N/2} \\ I_{N/2} & 0 \end{pmatrix}, \qquad \alpha_W^i \begin{pmatrix} \sigma_i & 0 \\ 0 & -\sigma_i \end{pmatrix}, \tag{A.3}$$

with the matrix that maps the Weyl spinors back to the standard representation being

$$T_W = \frac{1}{\sqrt{2}} \begin{pmatrix} I_{N/2} & iI_{N/2} \\ iI_{N/2} & I_{N/2} \end{pmatrix}. \tag{A.4}$$

A.3 Dirac matrix algebraic relations in (3+1) dimensions

The form of the Dirac matrices α^j and β was presented in the second chapter. In this appendix, we are going to show that the relations involving α^j and β indeed hold in the $(3+1)$-dimensional case.

(i) Firstly, we begin with :

$$\alpha^j \alpha^k + \alpha^k \alpha^j = 2\delta^{jk} I_4,$$

focusing on the left-hand side (LHS)

$$\begin{pmatrix} 0 & \sigma_j^* \\ \sigma_j & 0 \end{pmatrix}\begin{pmatrix} 0 & \sigma_k^* \\ \sigma_k & 0 \end{pmatrix} + \begin{pmatrix} 0 & \sigma_k^* \\ \sigma_k & 0 \end{pmatrix}\begin{pmatrix} 0 & \sigma_j^* \\ \sigma_j & 0 \end{pmatrix} = \begin{pmatrix} \sigma_j^*\sigma_k + \sigma_k^*\sigma_j & 0 \\ 0 & \sigma_j\sigma_k + \sigma_k\sigma_j \end{pmatrix}.$$

Using (2.28) and the property of Pauli matrices the LHS becomes

$$\begin{pmatrix} 2\delta_{jk}I_2 & 0 \\ 0 & 2\delta_{jk}I_2 \end{pmatrix},$$

which equals the right hand side (RHS).

(ii) Secondly:

$$\alpha^j\beta + \beta\alpha^j = 0$$

carrying out the expression we get

$$\begin{pmatrix} 0 & \sigma_j^* \\ \sigma_j & 0 \end{pmatrix}\begin{pmatrix} I_4 & 0 \\ 0 & -I_4 \end{pmatrix} + \begin{pmatrix} I_4 & 0 \\ 0 & -I_4 \end{pmatrix}\begin{pmatrix} 0 & \sigma_j^* \\ \sigma_j & 0 \end{pmatrix}$$
$$\begin{pmatrix} 0 & -\sigma_j^* \\ \sigma^j & 0 \end{pmatrix} + \begin{pmatrix} 0 & \sigma_j^* \\ -\sigma_j & 0 \end{pmatrix} = \begin{pmatrix} 0 & 0 \\ 0 & 0 \end{pmatrix}.$$

(iii) Lastly:

$$\alpha^{j\,2} = \beta^2 = I_4,$$

it is obvious to note that $\beta^2 = I_4$, what remain now is the LHS. Carrying this out we find that

$$\alpha^{j\,2} = \begin{pmatrix} \sigma_j^*\sigma_k & 0 \\ 0 & \sigma_j\sigma_k \end{pmatrix},$$

where the product in the first and last entry is given as

$$\sigma_j\sigma_k = \delta_{jk}I_2 + i\varepsilon_{jkl}\sigma_l, \qquad \sigma_j^*\sigma_k = \delta_j kI + i\epsilon_{jkl}\sigma_l, \tag{A.5}$$

See A.1 for proof of the second equation in (A.5). It is clear that the only nonzero case occurs when $j = k$, and thus the desired product becomes

$$\alpha^{j\,2} = I_4,$$

a 4×4 identity matrix.

A.4 Lorentz invariance of (1+1) dimensional reduction of the nonlinear Dirac equation with Kerr nonlinearity

The linear Dirac equation is said to be Lorentz invariant under the transformation

$$x \mapsto \Lambda^{\mu}_{\nu} x, \qquad \psi(x) \mapsto S(\Lambda)\psi(x), \qquad \psi(x) \in \mathbb{C}^N,\ x \in \mathbb{R} \times \mathbb{R}^n, \tag{A.6}$$

if $S(\Lambda)$, an $N \times N$ matrix of Lorentz transformations satisfies the relation

$$S(\Lambda)^{-1}\gamma^{\nu}S(\Lambda) = \Lambda^{\nu}_{\mu}\gamma^{\mu}. \tag{A.7}$$

The matrix $S(\Lambda)$ in the third chapter was found to be $S(\Lambda) = e^{-\frac{i}{4}\sigma_{\mu\nu}\omega^{\mu\nu}}$, with the Lorentz transformation being $\Lambda^{\mu}_{\nu} = e^{\omega^{\mu}_{\nu}}$. Substituting this into (A.7) gives

$$e^{-s\rho(\omega)}\gamma^{\nu}e^{s\rho(\omega)} = (e^{s\omega})^{\nu}_{\mu}\gamma^{\nu}, \qquad s \in \mathbb{R} \tag{A.8}$$

where we have called $\rho(\omega) = -\frac{i}{4}\sigma_{\mu\nu}\omega^{\mu\nu}$ and introduced a scaling factor s. The quantity $\sigma_{\mu\nu}$ is an $N \times N$ matrix for each pair of μ and ν.

To check whether the nonlinear Dirac equation is Lorentz invariant it is useful to write (4.114) in covariant form. To do this we let $\psi(x) = \psi(y,t) = (u,v)^T$ and $f(M,k) = (M+ik, M-ik)^T$ and write (4.114) as

$$i\partial_t\psi + \sigma_2\partial_y\psi + \sigma_1 f\psi + \mathcal{F}\sigma_1\psi + \mathcal{G}\psi = 0,$$

multiplying by σ^1 from the left gives

$$i\gamma^{\mu}\partial_{\mu}\psi + f\psi + \mathcal{F}\psi + \mathcal{G}\sigma_1\psi = 0, \qquad \mu = \{0,1\},\ \psi(x) \in \mathbb{C}^2,\ x \in \mathbb{R} \times \mathbb{R} \tag{A.9}$$

with $\gamma^{\mu}\partial_{\mu} = \gamma^0\partial_0 + \gamma^1\partial_1$, where $\partial_0 = \partial_t$, $\partial_1 = \partial_y$ and $\gamma^0 = \sigma_1$, $\gamma^1 = \sigma_3$.

Having written the nonlinear Dirac equation in covariant form, we can substitute (A.6) into (A.9) to obtain

$$i\gamma^{\mu}\partial_{\mu}e^{s\rho(\omega)}\psi\left(e^{s\omega}x\right) + fe^{s\rho(\omega)}\psi\left(e^{s\omega}x\right) + \tilde{\mathcal{F}}e^{s\rho(\omega)}\psi(e^{s\omega}x) + \tilde{\mathcal{G}}\sigma_1 e^{s\rho(\omega)}\psi(e^{s\omega}x) = 0, \tag{A.10}$$

letting $z = e^{s\omega}x$ yields

$$\gamma^{\mu}e^{s\rho(\omega)}\partial_{\mu}\psi\left(z\right) + fe^{s\rho(\omega)}\psi\left(z\right) + \tilde{\mathcal{F}}e^{s\rho(\omega)}\psi(z) + \tilde{\mathcal{G}}\sigma_1 e^{s\rho(\omega)}\psi(z) = 0. \tag{A.11}$$

The nonlinear terms of (A.11) remain to be checked as to whether they are invariant or not. Setting the nonlinearity to zero in (A.11) results in the invariance of the linear Dirac equation in $(1+1)$ dimensions, that is the structure of the equation

$$i\gamma^{\nu}\partial_{\nu}\psi(z) + f\psi(z) = 0, \qquad \nu = \{0,1\} \tag{A.12}$$

where $(e^{s\omega})^{\mu}_{\nu}\,\partial_{\mu} := \partial_{\nu}$, is not affected by Lorentz transformations.

To check for the invariance of the nonlinear terms of (4.111) we look for what is known as the Lorentz scalar, which is a function which is Lorentz invariant. To do this, let us begin with the function

$$\psi^{\dagger}\psi = |u|^2 + |v|^2, \tag{A.13}$$

where $\psi^{\dagger}$ is the hermitian adjoint of a spinor. The Lorentz transformation of (A.13) is

$$\psi^{\dagger}\psi \longrightarrow S^{\dagger}\psi^{\dagger}S\psi = \psi^{\dagger}S^{\dagger}S\psi,$$

since $S^{\dagger}S \neq I$, where I is a 2×2 indentity matrix, the quantity $\psi^{\dagger}\psi$ is not a Lorentz scalar and thus not invariant. From this calculation, we conclude that the term $\mathcal{G}$ in (4.114) is not invariant under Lorentz transformations.

What now remains is to check the invariance of $\mathcal{F}$. To do this we construct what is known as the *adjoint spinor* as follows

$$\bar{\psi} = \psi^{\dagger}\gamma^0, \tag{A.14}$$

where $\gamma^0 = \sigma^1$ in the standard choice of Dirac matrices. The Lorentz transformation of a scalar $\bar{\psi}\psi = uv^* + vu^*$ is

$$\bar{\psi}\psi \longrightarrow S^{\dagger}\psi^{\dagger}\gamma^0 S\psi = \psi^{\dagger}S^{\dagger}\gamma^0 S\psi = \psi^{\dagger}\gamma^0\psi = \bar{\psi}\psi,$$

where we have used the fact that $S^{\dagger}\gamma^0 S = \gamma^0$. The implication of this calculation is that the scalar $\bar{\psi}\psi$ is a Lorentz scalar and thus Lorentz invariant.

A.5 MATLAB Codes

A.5.1 Code used for solving the massive Thirring model in (1+1) dimensions:

```
function [usol, vsol] = soliton_thirring(x)
global gamma vel
r1 = ((1+gamma)/(1-gamma)).^0.25;
r0 = ((1-gamma)/(1+gamma)).^0.25;
kappa = sqrt(1-gamma^2);
alpha = pi/4;
beta = atanh(vel)/2;
veloc = 1./sqrt(1-vel.^2);
a = cosh((kappa*x)/(sqrt(1-vel^2)-1i*alpha)) ...
    ./cosh((kappa*x)/(sqrt(1-vel^2)+1i*alpha));
usol = r0*kappa*((a).^(1+gamma)).*sech(kappa*x*veloc - 1i*alpha
   );
vsol = r1*kappa*((1./a).^(1-gamma)).*sech(kappa*x*veloc + 1i*
   alpha);
end

function [tdata, udata, vdata] = Thirring_Dirac_Solution(N,dt,
   tmax, u,v,uold, vold)
global gamma
%% matching the thirring mode using Pseudosopectral method with
    centered
%% difference for time integration.
%% The right-hand side functions
fu = @(u,v) (1 - gamma)*v + abs(v).*abs(v).*u;
fv = @(u,v) (1 + gamma)*u + abs(u).*abs(u).*v;
tplot = 0.15; clf;
plotgap = round(tplot/dt); dt = tplot/plotgap;
nplots = round(tmax/tplot);
%% Time-Stepping scheme
udata  = [u; zeros(nplots, N)]; vdata =  [v; zeros(nplots, N)];
t =0;  tdata = t;
%% main loop
for i = 1:nplots
  for n = 1:plotgap
    t = t + dt;
    %% moving to the fourier space
    uhat = fft(u); vhat = fft(v);

    %% calculating the derivative on the fourier space
    kk = 1i*[0:N/2-1 0 -N/2+1:-1]; % fourier modes
```

```
    what_u = kk.*uhat; what_v = kk.*vhat;    % derivative in
       the fourier space

    % moving back to the physical space
    wu = ifft(what_u);
    wv = ifft(what_v);

    %% updating the solution
    unew =  uold + 2*dt*wu + 2*1i*dt*fu(u,v);
    vnew =  vold - 2*dt*wv + 2*1i*dt*fv(u,v);
    uold = u; vold = v; u= unew; v = vnew;
  end
  udata(i+1,:)=u; vdata(i+1,:) =v;  tdata = [tdata; t];
end

%% solving the thirring model
clear all; close all; clc
% initial parameters
global gamma vel
N = 2^9 ; L = 20; h = 2*pi/N; x = h*(1:N); x = L/pi*(x-pi);
dt = h/10;
% varying parameters of the solitons
gamma = 0.01;  vel = 0.8; tmax = 8;
%% The solitons t = 0
[u, v] = soliton_thirring(x);
[uold, vold] = soliton_thirring(x-dt);
%% the calculation
t0 = cputime;
[tdata, udata, vdata] = Thirring_Dirac_Solution(N,dt,tmax, u,v,
   uold, vold);
tf = cputime -t0        %% runtime of the code
udata = udata'; vdata = vdata';
%% plots
%[XX, TT] = meshgrid(x,tdata);
figure(1)
surf(tdata, x, abs(udata), 'FaceColor','interp','EdgeColor','
   none');
view([10 70]);
set(gca,'FontSize',15)
axis([0 tmax -L L ])
xlabel('$t$', 'Interpreter', 'latex');
ylabel('$x$', 'Interpreter', 'latex');
zlabel('$ u(x,t)$', 'Interpreter', 'latex');
figure(2)
surf(tdata, x, abs(vdata), 'FaceColor','interp','EdgeColor','
```

```
   none');
view([10 70]);
set(gca,'FontSize',15)
axis([0 tmax -L L])
xlabel('$t$', 'Interpreter', 'latex');
ylabel('$x$', 'Interpreter', 'latex');
zlabel('$v(x,t)$', 'Interpreter', 'latex');
```

A.5.2 Code used for computing the eigenvalues using sines series expansion:

```
N = 300;R = 100;%m=0;
%These are the integral matrices to be populated
S = zeros(N, N);I= zeros(N, N);V = zeros(N, N);II = zeros(N, N)
   ;
%x = linspace(0,R);
g = @(x) besseli(1, x)./besseli(0, x);
%Populate the S,I, V matrices
eps = 0.001;
for i=1:N
    for j =1:N
        S(i, j) = integral(@(x)(g(x).^2 - 1).*sin(pi*x*i/R).*
           sin(pi*x*j/R), eps, R);
        V(i, j) = integral(@(x)g(x).*sin(pi*x*i/R).*sin(pi*x*j/
           R), eps, R);
        I(i, j) = integral(@(x)(1./x).*sin(pi*x*i/R).*sin(pi*x*
           j/R), eps, R);
        II(i,j) = integral(@(x)sin(pi*x*i/R).*sin(pi*x*j/R),
           eps, R);
    end
end
%% Define the L operator whose eigenvalues we seek.
for m=-2:1:2
    L = -(2/R).*[S, zeros(N, N), II + I + 2 * V, -m * I;
     zeros(N, N), S,  II, I + 2 * V - m * I;
     II - 2 * V, m * I, zeros(N, N), zeros(N, N);
     m * I, II, zeros(N, N), zeros(N, N)];


    eigs = eig(L);
    h = figure;
    tiledlayout(2, 2)
    nexttile
    scatter(linspace(0, 4*N , 4*N), real(eigs));
```

```
    nexttile
    scatter(linspace(0, 4*N , 4*N), imag(eigs));
    nexttile([1 2])
    scatter(real(eigs), imag(eigs))
    saveas(h, sprintf('FIG%d.pdf',m))

end
```

A.5.3 Code used for finding the eigenvalues using Chebyshev spectral method:

```
function [x,D] = cheb(N)
  if N==0, D=0; x=1; return, end
  x = cos(pi*(0:N)/N+1)';
  c = [2; ones(N-1,1); 2].*(-1).^(0:N)';
  X = repmat(x,1,N+1);
  dX = X-X';
  D = (c*(1./c)')./(dX+(eye(N+1)));
  D = D - diag(sum(D'));
end
x, D = cheb(N);
L = -(2/R).*[D-2.*g, m./x, zeros(N, N),  zeros(N, N);
     m./x, D, zeros(N, N), zeros(N, N);
    -(1-g.^2),zeros(N, N),D+1./x + 2.*g, -m./x;
     zeros(N, N), -(1-g.^2), -m./x, D + 1./x];
eigs = eig(L);
```

A.5.4 Code for the shooting method:

This code can be adopted to each of the ODEs solved in this thesis.

```
%shooting_fzero1.m,
clc;clear;close;format shortE; format compact
global span alpha beta
span=[10e-9;100];% Interval
alpha=0; beta=1;
for i=1:2
if i==1, u = 1.0; else, u=1.5 ;end  % Trial value
odes=@(x,y) [(1/x)*y(1) + y(2)*(y(2).^2-y(1).^2);...
                y(2)*(y(2).^2-y(1).^2)];
w = fzero(@res_fzero1,u); [X,Y] = ode45(odes,span,[alpha  w]);
X;Y; plot(X,Y(:,1), 'r',X,Y(:,2), 'b--','linewidth',2);hold on;
end
xlabel('$r$', 'Interpreter', 'latex');
```

```
ylabel('$g(r)(r),\f(r)$', 'Interpreter', 'latex');
legend('$f(r)$', '$g(r)$', 'Interpreter', 'latex');
function r = res_fzero1(u) % Boundary residuals.
global  span alpha  beta
odes=@(x,y) [(1/x)*y(1) + y(2)*(y(2).^2-y(1).^2);...
                y(2)*(y(2).^2-y(1).^2)];
[~, Y] = ode45(odes,span,[alpha  u]);
r= Y(end,1)-beta; end
```

Bibliography

[1] Castro Neto, A. H., Guinea, F., Peres, N. M. R., Novoselov, K. S. & Geim, A. K. The electronic properties of graphene. *Rev. Mod. Phys.* **81**, 109–162 (2009). URL https://link.aps.org/doi/10.1103/RevModPhys.81.109.

[2] Barashenkov, I. V. & Getmanov, B. S. Multisoliton solutions in the scheme for unified description of integrable relativistic massive fields. non-degenerate $sl(2,\mathbb{C})$ case. *Communications in Mathematical Physics* **112**, 423–446 (1987). URL https://doi.org/10.1007/BF01218485.

[3] Barashenkov, I. & Pelinovsky, D. Exact vortex solutions of the complex sine-gordon theory on the plane. *Physics Letters B* **436**, 117–124 (1998). URL https://www.sciencedirect.com/science/article/pii/S0370269398008417.

[4] Barashenkov, I. V., Shchesnovich, V. S. & Adams, R. M. Noncoaxial multivortices in the complex sine-gordon theory on the plane. *Nonlinearity* **15**, 2121 (2002). URL https://dx.doi.org/10.1088/0951-7715/15/6/317.

[5] Smirnova, D., Leykam, D., Chong, Y. & Kivshar, Y. Nonlinear topological photonics. *Applied Physics Reviews* **7**, 021306 (2020). URL https://doi.org/10.1063/1.5142397. https://doi.org/10.1063/1.5142397.

[6] Hasan, M. Z. & Kane, C. L. Colloquium: Topological insulators. *Rev. Mod. Phys.* **82**, 3045–3067 (2010). URL https://link.aps.org/doi/10.1103/RevModPhys.82.3045.

[7] Ozawa, T. *et al.* Topological photonics. *Rev. Mod. Phys.* **91**, 015006 (2019). URL https://link.aps.org/doi/10.1103/RevModPhys.91.015006.

[8] Xie, B.-Y. *et al.* Photonics meets topology. *Opt. Express* **26**, 24531–24550 (2018). URL https://opg.optica.org/oe/abstract.cfm?URI=oe-26-19-24531.

[9] Su, W. P., Schrieffer, J. R. & Heeger, A. J. Solitons in polyacetylene. *Phys. Rev. Lett.* **42**, 1698–1701 (1979). URL https://link.aps.org/doi/10.1103/PhysRevLett.42.1698.

[10] Smirnova, D. A., Smirnov, L. A., Leykam, D. & Kivshar, Y. S. Topological edge states and gap solitons in the nonlinear dirac model. *Laser & Photonics Reviews* **13**, 1900223 (2019). URL https://onlinelibrary.wiley.com/doi/abs/10.1002/lpor.201900223. https://onlinelibrary.wiley.com/doi/pdf/10.1002/lpor.201900223.

[11] Ozawa, T. *et al.* Topological photonics. *Rev. Mod. Phys.* **91**, 015006 (2019). URL https://link.aps.org/doi/10.1103/RevModPhys.91.015006.

[12] McCann, E. Electronic properties of monolayer and bilayer graphene. In *Graphene Nanoelectronics*, 237–275 (Springer Berlin Heidelberg, 2011). URL https://doi.org/10.1007%2F978-3-642-22984-8_8.

[13] Zhen, Z. & Zhu, H. 1 - structure and properties of graphene. In Zhu, H., Xu, Z., Xie, D. & Fang, Y. (eds.) *Graphene*, 1–12 (Academic Press, 2018). URL https://www.sciencedirect.com/science/article/pii/B978012812651600001X.

[14] Lima, W., Araújo, F., Da Costa, D., Sena, S. & Pereira, J. Tight-binding model in first and second quantization for band structure calculations. *Brazilian Journal of Physics* **52** (2022).

[15] Saito, R., Dresselhaus, G. & Dresselhaus, M. S. *Physical Properties of Carbon Nanotubes* (PUBLISHED BY IMPERIAL COLLEGE PRESS AND DISTRIBUTED BY WORLD SCIENTIFIC PUBLISHING CO., 1998). URL https://www.worldscientific.com/doi/abs/10.1142/p080. https://www.worldscientific.com/doi/pdf/10.1142/p080.

[16] Arbunich, J. & Sparber, C. Rigorous derivation of nonlinear dirac equations for wave propagation in honeycomb structures (2016). URL https://arxiv.org/abs/1610.08542.

[17] Dirac, P. A. M. & Fowler, R. H. The quantum theory of the electron. *Proceedings of the Royal Society of London. Series A, Containing Papers of a Mathematical and Physical Character* **117**, 610–624 (1928). URL https://royalsocietypublishing.org/doi/abs/10.1098/rspa.1928.0023. https://royalsocietypublishing.org/doi/pdf/10.1098/rspa.1928.0023.

[18] Dirac, P. A. M. & Fowler, R. H. The quantum theory of the electron. *Proceedings of the Royal Society of London. Series A, Containing Papers of a Mathematical and Physical Character* **117**, 610–624 (1928). URL https://royalsocietypublishing.org/doi/abs/10.1098/rspa.1928.0023. https://royalsocietypublishing.org/doi/pdf/10.1098/rspa.1928.0023.

[19] Cuevas-Maraver, J. *et al.* Solitary waves in the nonlinear dirac equation. *Nonlinear Systems, Vol. 1* 89–143 (2018). URL http://dx.doi.org/10.1007/978-3-319-66766-9_4.

[20] Boussaid, N. *et al.* Spectral stability and instability of solitary waves of the dirac equation with concentrated nonlinearity (2020). URL https://arxiv.org/abs/2006.03345.

[21] Alexeeva, N., Barashenkov, I. & Saxena, A. Spinor solitons and their pt-symmetric offspring. *Annals of Physics* **403**, 198–223 (2019). URL https://www.sciencedirect.com/science/article/pii/S0003491618302951.

[22] Jentschura, U. Dirac hamiltonian with imaginary mass and induced helicity—dependence by indefinite metric. *Journal of Modern Physics* **3**, 887–894 (2012).

[23] Jentschura, U. D. & Wundt, B. J. Pseudo-hermitian quantum dynamics of tachyonic spin-1/2 particles. *Journal of Physics A: Mathematical and Theoretical* **45**, 444017 (2012). URL https://doi.org/10.1088/1751-8113/45/44/444017.

[24] Jentschura, U.D. & Wundt, B.J. Localizability of tachyonic particles and neutrinoless double beta decay. *Eur. Phys. J. C* **72**, 1894 (2012). URL https://doi.org/10.1140/epjc/s10052-012-1894-4.

[25] Feinberg, G. Possibility of faster-than-light particles. *Phys. Rev.* **159**, 1089–1105 (1967). URL https://link.aps.org/doi/10.1103/PhysRev.159.1089.

[26] Bandukwala, J. & Shay, D. Theory of free, spin-½ tachyons. *Phys. Rev. D* **9**, 889–895 (1974). URL https://link.aps.org/doi/10.1103/PhysRevD.9.889.

[27] Jentschura, U. D. & Wundt, B. J. Localizability of tachyonic particles and neutrinoless double beta decay. *The European Physical Journal C* **72**, 1894 (2012).

[28] Chodos, A., Hauser, A. I. & Alan Kostelecký, V. The neutrino as a tachyon. *Physics Letters B* **150**, 431–435 (1985). URL https://www.sciencedirect.com/science/article/pii/0370269385904605.

[29] Chang, T. A new dirac-type equation for tachyonic neutrinos (2000). URL https://arxiv.org/abs/hep-th/0011087.

[30] Chang, T. Parity violation and a preferred frame (2002). URL https://arxiv.org/abs/quant-ph/0204002.

[31] Miri, M.-A., Aceves, A. B., Kottos, T., Kovanis, V. & Christodoulides, D. N. Bragg solitons in nonlinear $\mathcal{PT}$-symmetric periodic potentials. *Phys. Rev. A* **86**, 033801 (2012). URL https://link.aps.org/doi/10.1103/PhysRevA.86.033801.

[32] Cuevas-Maraver, J. *et al.* Solitary waves in the nonlinear dirac equation. In *Understanding Complex Systems*, 89–143 (Springer International Publishing, 2018). URL https://doi.org/10.1007%2F978-3-319-66766-9_4.

[33] Thirring, W. A soluble relativistic field theory. *Annals of Physics* **3**, 91–112 (1958).

[34] E.A.Kuznetsov, A. On the complete integrability of the two-dimensional classical thirring model. *Theoret. and Math. Phys.* **30**, 303–314 (1977).

[35] Haddad, L. & Carr, L. The nonlinear dirac equation in bose–einstein condensates: Foundation and symmetries. *Physica D: Nonlinear Phenomena* **238**, 1413–1421 (2009). URL https://www.sciencedirect.com/science/article/pii/S0167278909000372. Nonlinear Phenomena in Degenerate Quantum Gases.

[36] Cuevas-Maraver, J., Kevrekidis, P. G., Aceves, A. B. & Saxena, A. Solitary waves in a two-dimensional nonlinear dirac equation: from discrete to continuum. *Journal of Physics A: Mathematical and Theoretical* **50**, 495207 (2017). URL https://dx.doi.org/10.1088/1751-8121/aa8e36.

[37] Ma, Y.-P. & Susanto, H. Topological edge solitons and their stability in a nonlinear su-schrieffer-heeger model. *Phys. Rev. E* **104**, 054206 (2021). URL https://link.aps.org/doi/10.1103/PhysRevE.104.054206.

[38] Lee, S. Y., Kuo, T. K. & Gavrielides, A. Exact localized solutions of two-dimensional field theories of massive fermions with fermi interactions. *Phys. Rev. D* **12**, 2249–2253 (1975). URL https://link.aps.org/doi/10.1103/PhysRevD.12.2249.

[39] Mertens, F. G., Quintero, N. R., Cooper, F., Khare, A. & Saxena, A. Nonlinear dirac equation solitary waves in external fields. *Phys. Rev. E* **86**, 046602 (2012). URL https://link.aps.org/doi/10.1103/PhysRevE.86.046602.

[40] Cuevas–Maraver, J., Kevrekidis, P. G., Saxena, A., Comech, A. & Lan, R. Stability of solitary waves and vortices in a 2d nonlinear dirac model. *Physical Review Letters* **116** (2016). URL http://dx.doi.org/10.1103/PhysRevLett.116.214101.

[41] Soler, M. Classical, stable, nonlinear spinor field with positive rest energy. *Phys. Rev. D* **1**, 2766–2769 (1970). URL https://link.aps.org/doi/10.1103/PhysRevD.1.2766.

[42] Thirring, W. E. A soluble relativistic field theory. *Annals of Physics* **3**, 91–112 (1958). URL https://www.sciencedirect.com/science/article/pii/0003491658900150.

[43] Aceves, A. & Wabnitz, S. Self-induced transparency solitons in nonlinear refractive periodic media. *Physics Letters A* **141**, 37–42 (1989). URL https://www.sciencedirect.com/science/article/pii/0375960189904416.

[44] Destri, C. & De Vega, H. Light-cone lattice approach to fermionic theories in 2d: The massive thirring model. *Nuclear Physics B* **290**, 363–391 (1987). URL https://www.sciencedirect.com/science/article/pii/0550321387901933.

[45] Berkolaiko, G. & Comech, A. On spectral stability of solitary waves of nonlinear dirac equation on a line (2009).

[46] Lund, F. Example of a relativistic, completely integrable, hamiltonian system. *Phys. Rev. Lett.* **38**, 1175–1178 (1977). URL https://link.aps.org/doi/10.1103/PhysRevLett.38.1175.

[47] Lund, F. & Regge, T. Unified approach to strings and vortices with soliton solutions. *Phys. Rev. D* **14**, 1524–1535 (1976). URL https://link.aps.org/doi/10.1103/PhysRevD.14.1524.

[48] Park, Q.-H. & Shin, H. J. Effective field theory for coherent optical pulse propagation (1996). URL https://arxiv.org/abs/hep-th/9605052.

[49] Barashenkov, I. V., Getmanov, B. S. & Kovtun, V. E. The unified approach to integrable relativistic equations: Soliton solutions over nonvanishing backgrounds. i. *Journal of Mathematical Physics* **34**, 3039–3053 (1993). URL https://doi.org/10.1063/1.530403. https://doi.org/10.1063/1.530403.

[50] Trefethen, L. N. *Spectral methods in MATLAB*. Software, environments, tools (Society for Industrial and Applied Mathematics, Philadelphia, PA, 2000).

[51] Herring, G., Carr, L. D., Carretero-González, R., Kevrekidis, P. G. & Frantzeskakis, D. J. Radially symmetric nonlinear states of harmonically trapped bose-einstein condensates. *Phys. Rev. A* **77**, 023625 (2008). URL https://link.aps.org/doi/10.1103/PhysRevA.77.023625.

[52] Rosen, D., Burden, R. L., Faires, J. D. & Reynolds, A. C. Numerical analysis. *The American mathematical monthly* **87**, 231– (1980).

[53] Poddubny, A. N. & Smirnova, D. A. Ring dirac solitons in nonlinear topological systems. *Phys. Rev. A* **98**, 013827 (2018). URL https://link.aps.org/doi/10.1103/PhysRevA.98.013827.

[54] Wakano, M. Intensely Localized Solutions of the Classical Dirac-Maxwell Field Equations. *Progress of Theoretical Physics* **35**, 1117–1141 (1966). URL https://doi.org/10.1143/PTP.35.1117. https://academic.oup.com/ptp/article-pdf/35/6/1117/5329288/35-6-1117.pdf.